Cell

Tetherin Inhibits HIV-1 Release by Directly Tethering Virions to Cells

David Perez-Caballero,[1,2] Trinity Zang,[1,2,3] Alaleh Ebrahimi,[1,2] Matthew W. McNatt,[1,2] Devon A. Gregory,[4] Marc C. Johnson,[4] and Paul D. Bieniasz[1,2,3,*]
[1]Aaron Diamond AIDS Research Center
[2]Laboratory of Retrovirology
The Rockefeller University, New York, NY 10016, USA
[3]Howard Hughes Medical Institute, Aaron Diamond AIDS Research Center, New York, NY 10016, USA
[4]Department of Molecular Microbiology and Immunology, University of Missouri School of Medicine, Columbia, MO 65211, USA
*Correspondence: pbienias@adarc.org
DOI 10.1016/j.cell.2009.08.039

SUMMARY

Tetherin is an interferon-induced protein whose expression blocks the release of HIV-1 and other enveloped viral particles. The underlying mechanism by which tetherin functions and whether it directly or indirectly causes virion retention are unknown. Here, we elucidate the mechanism by which tetherin exerts its antiviral activity. We demonstrate, through mutational analyses and domain replacement experiments, that tetherin configuration rather than primary sequence is critical for antiviral activity. These findings allowed the design of a completely artificial protein, lacking sequence homology with native tetherin, that nevertheless mimicked its antiviral activity. We further show that tetherin is incorporated into HIV-1 particles as a parallel homodimer using either of its two membrane anchors. These results indicate that tetherin functions autonomously and directly and that infiltration of virion envelopes by one or both of tetherin's membrane anchors is necessary, and likely sufficient, to tether enveloped virus particles that bud through the plasma membrane.

INTRODUCTION

Eukaryotic cells have evolved various mechanisms of defense against viral infections. Indeed, many components of the type I interferon (IFN)-induced innate immune system are thought to directly inhibit the replication of various viruses. However, while >900 genes are known to be induced by type-1 IFN (http://www.lerner.ccf.org/labs/williams/isgd.cgi), the mechanisms by which IFN-induced gene products inhibit virus replication are known for only a few (Samuel, 2001). Recently, we and others identified an IFN-induced protein, termed tetherin (also referred to as BST-2 or CD317), whose expression can cause inhibition of HIV-1 particle release from infected cells (Neil et al., 2008; Van Damme et al., 2008). Notably, HIV-1 encodes an accessory protein, Vpu, that counteracts tetherin activity. It is not known how tetherin expression causes the retention of viral particles, but the retained viral particles are mature and have lipid bilayers that are discontinuous with host cell membranes (Neil et al., 2006, 2007). While particles accumulate both in endosomes and at the plasma membrane, endosomal accumulation is the result of internalization of virions that were initially trapped at the cell surface and is not required for their retention. Indeed, the virions can be released from cell surfaces by protease treatment, indicating that tetherin either forms or induces protein-based tethers that cause virion entrapment (Neil et al., 2006, 2008). This mechanism of virion retention is distinct from that found in "late-domain" mutants, where viral proteins fail to recruit the ESCRT machinery and the virion lipid envelope remains continuous with the host cell plasma membrane (Morita and Sundquist, 2004).

Tetherin is a type II single-pass transmembrane protein with a highly unusual arrangement, encoding both a transmembrane anchor toward its N terminus and a putative glycophosphatidylinositol (GPI) lipid anchor at its C terminus (Kupzig et al., 2003). These membrane anchors are linked by an extracellular domain that is predicted to form a coiled coil. What role each domain plays and how this topology impacts the biological activity of tetherin is unknown. In principle, the tetherin protein itself could be necessary and sufficient to assemble into protease-sensitive tethers that retain virions on the surface of infected cells. Alternatively, it is possible that tetherin is a component of the protease-sensitive tethers, but requires specific virion or cellular interacting components to induce tethering. A third possibility is that tetherin is not directly involved in tethering at all and instead is a signaling molecule, sensor or inducer, that triggers the expression of some other set of factors that are responsible for tethering. In this regard, a recent report identified a second protein, CAML, whose expression has the same consequence as tetherin expression, namely retention of HIV-1 particles (Varthakavi et al., 2008). It is difficult to reconcile these findings, unless one protein induces the expression of another that is actually responsible for tethering.

Tetherin expression induces retention of virus-like particles (VLPs) assembled using the structural proteins of a range of enveloped viruses (Jouvenet et al., 2009; Kaletsky et al., 2009; Sakuma et al., 2009). Moreover, tetherin colocalizes with retroviral Gag puncta at the plasma membrane (Jouvenet et al., 2009; Neil et al., 2008). This is consistent with the notion that it

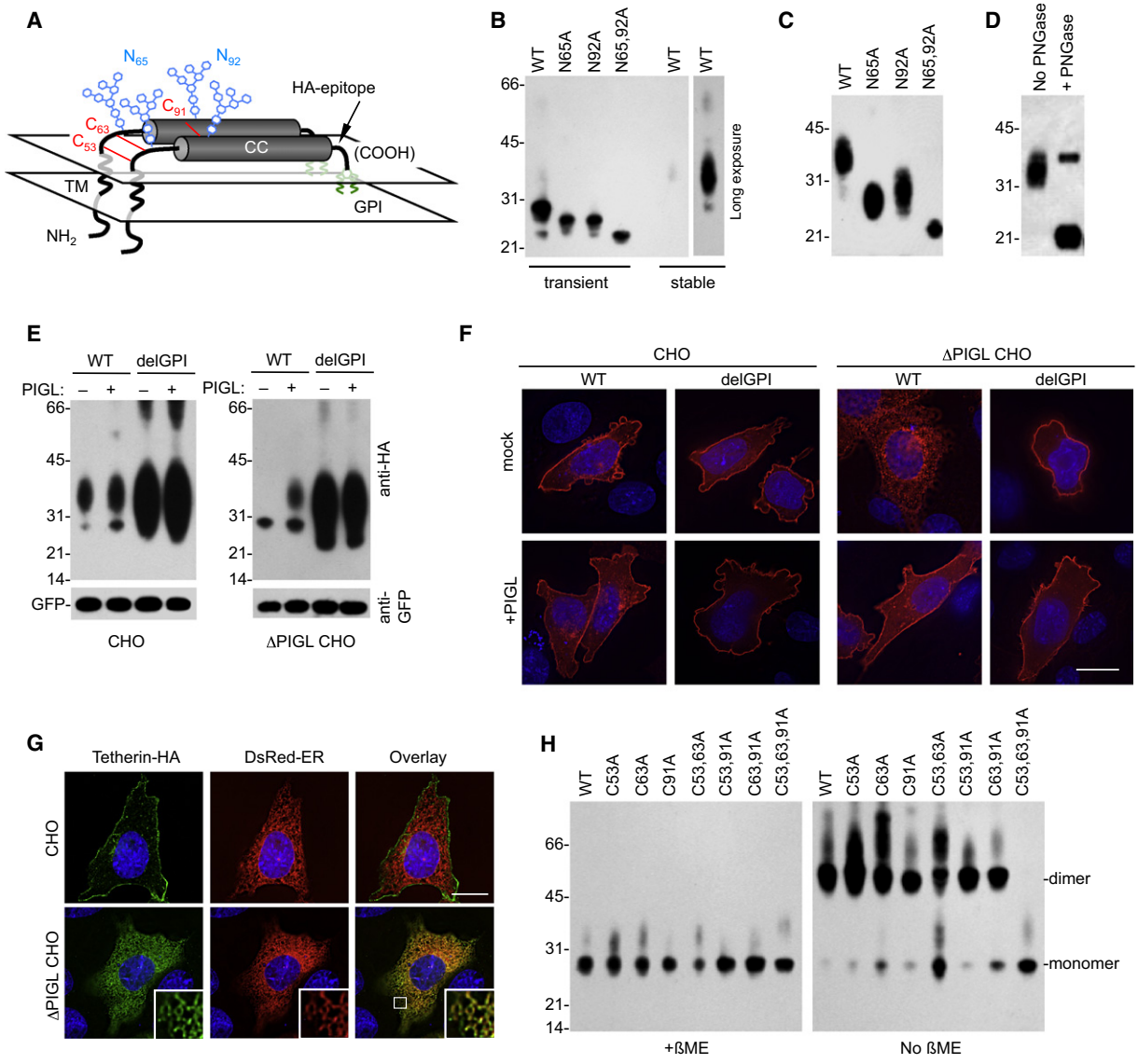

Figure 1. Schematic Representation of Tetherin and Analysis of Posttranslational Modifications

(A) Schematic representation of the tetherin dimer, indicating the transmembrane (TM) and coiled-coil (CC) domains as well as glycophosphatidylinositol (GPI, green), glycosylation (blue), and disulfide bond (red) modifications. A tetherin derivative that incorporated an extracellular HA tag was used throughout, unless otherwise indicated.

(B) Western blot analysis (anti-HA) of 293T cells transiently transfected with 200 ng of plasmids expressing WT tetherin and variants bearing mutations at putative glycosylation sites. Additionally, lysates of 293T cells stably expressing WT tetherin were run on the same gel. A longer exposure of this lane is also shown.

(C) Western blot analysis (anti-HA) of 293T cells stably transduced with LHCX-based retroviral vectors expressing WT tetherin and tetherin variants bearing mutations at putative glycosylation sites.

(D) Western blot analysis (anti-HA) of tetherin following deglycosylation. Lysates of 293T cells stably expressing HA tagged tetherin were incubated in the presence or absence of peptide-N-glycosidase-F (PNGase), as described in the Supplemental Experimental Procedures, prior to analysis.

(E) Western blot analysis (anti-HA) of parental (CHO) and PIGL-defective (ΔPIGL CHO) cells transfected with plasmids (200 ng) expressing WT or delGPI tetherin in the absence (–) or presence (+) of 100 ng of a plasmid expressing rat PIGL. A GFP expression plasmid (100 ng) was cotransfected, and blots were probed with anti-GFP (lower panel) verify equal transfection efficiency and gel loading.

(F) Immunofluorescence analysis (anti-HA, red) of parental (CHO) and PIGL-defective (ΔPIGL CHO) cells transfected with plasmids expressing WT or delGPI tetherin in the absence (mock) or presence (+PIGL) of a plasmid expressing rat PIGL. Cells were transfected as in (E) and nuclei were stained with DAPI (blue). The scale bar represents 10 μm.

(G) Immunofluorescence analysis (anti-HA; green) of parental (CHO) and PIGL-defective (ΔPIGL CHO) cells transfected with plasmids expressing WT tetherin and an ER-localized DsRed2 fluorescent protein. Cells were transfected as in (E) and nuclei were stained with DAPI (blue). The scale bar represents 10 μm. The inset shows an expanded portion of the image indicated by the white square in the lower-right image. For (F) and (G), at least 50 cells were inspected and all exhibited similar patterns of tetherin localization.

may be directly involved in tethering nascent virions. However, there is currently no direct evidence that tetherin is directly responsible for virion tethering.

Here, we show that tetherin is indeed directly responsible, and likely sufficient, for tethering of nascent enveloped virions to infected cell surfaces. First, we delineate features of tetherin that are required for antiviral activity and show that while the overall configuration of tetherin is important, there is little specific sequence requirement for antiviral activity. These findings allowed the design of a completely artificial tetherin protein, assembled from fragments of heterologous proteins. Despite lacking significant sequence homology to natural tetherins, this artificial tetherin causes tethering of two widely divergent enveloped viruses (HIV-1 and Ebola virus). We also show that either the transmembrane domain or the GPI modified C terminus can drive insertion of tetherin into the lipid envelope of HIV-1 particles as a parallel homodimer. Together, these results strongly suggest the dual membrane anchors, configured as they are in tetherin proteins, are directly responsible, and likely sufficient, to cause retention of enveloped virions that bud through the plasma membrane.

RESULTS

A putative topology of tetherin is depicted schematically in Figure 1A. To determine the accuracy of this configuration and its role in antiviral activity, point mutations and deletions were introduced at various positions. These mutations targeted residues that are putatively involved in disulfide bond formation or glycosylation. Alternatively, major features of tetherin were deleted or replaced with heterologous protein domains.

Role of Tetherin Configuration and Posttranslational Modifications in Antiviral Activity

Tetherin migrates as a number of species upon SDS-PAGE analysis, presumably due to heterogeneity in posttranslational modifications (Goffinet et al., 2009; Kaletsky et al., 2009; McNatt et al., 2009; Miyagi et al., 2009; Neil et al., 2007). When transiently overexpressed in 293T cells, human tetherin that is untagged or bears an HA epitope insertion at residue 154 in the extracellular domain (Figure 1A) migrates primarily as an ~28 kDa species, sometimes accompanied by a higher molecular weight smear of ~32–38 kDa (Figure 1B). Conversely, when stably expressed at lower levels, in the identical cell type, only the ~32–38 kDa smear is observed (Figures 1B and 1C). This suggests that the addition of complex carbohydrates to tetherin occurs more slowly than translation under conditions of transient expression in 293T cells. Individual mutation of each of the two putative N-linked glycosylation sites (N65A and N92A) reduced the molecular weight of ~28 kDa transiently expressed and the ~32–38 kDa stably expressed tetherin by a few kilodaltons, while mutation at both positions reduced the apparent molecular weight of both transiently and stably expressed tetherin to ~21 kDa (Figures 1B and 1C). Treatment of the stably expressed ~32–38 kDa tetherin protein with peptide-N-glycosidase-F reduced its molecular weight to a similar degree as did mutation of both glycosylation sites (Figure 1D).

A second posttranslational modification of tetherin that is thought to occur is the addition of a GPI anchor at its C terminus (Kupzig et al., 2003). To confirm that tetherin is indeed modified in this way, and to determine its effect on tetherin trafficking and maturation, we used a CHO-derived cell line lacking PIGL, an ER-resident enzyme required for the addition of GPI anchors. Proteins that harbor a GPI modification signal as their only membrane anchor are inserted into ER membrane but remain trapped there in the absence of PIGL (Nakamura et al., 1997). It was not known whether the same restriction would apply to tetherin, which also encodes a transmembrane domain and cytoplasmic tail. Nonetheless, removal of the GPI modification signal (e.g., in tetherin delGPI) should allow escape from this block, if it occurs.

In CHO cells, both WT and delGPI tetherin forms were expressed at significantly lower levels than in transiently transfected 293T cells and, presumably as a consequence of this, appeared primarily in their fully glycosylated ~32–38 kDa forms (Figure 1E). They localized primarily at the plasma membrane (Figure 1F). Conversely, in PIGL-defective CHO cells, WT tetherin was expressed in its incompletely glycosylated (28 kDa) form (Figure 1E), adopted a thread-like intracellular distribution and was localized primarily in the ER (Figures 1F and 1G). Reconstitution of the PIGL defect, by transient expression of rat PIGL, allowed WT tetherin to achieve mature glycosylation and reach the plasma membrane (Figures 1E and 1F). Removal of the signal for GPI modification from tetherin (in delGPI) enhanced expression but, more importantly, abolished the requirement for PIGL in completing tetherin glycosylation and transport to the cell surface (Figures 1E and 1F).

Tetherin forms disulfide-linked dimers (Ohtomo et al., 1999), but which of the three available cysteines that are present in the tetherin extracellular domain participate in intra- or intermolecular bond formation is not known. A triple cysteine mutant (C53,63,91A) abolished the ability of tetherin to form β-mercaptoethanol-sensitive dimers, while mutations at individual cysteines or at any combination of two of the three cysteines did not (Figure 1H). Thus, all three cysteines form disulfide bonds with an orthologous cysteine in a tetherin dimer. Overall, the aforementioned experiments indicate that the tetherin molecule is configured, in schematic terms, approximately as depicted in Figure 1A.

To determine the importance of this configuration for the antiviral activity of tetherin, 293T cells were transfected with HIV-1(WT) or HIV-1(delVpu) proviral plasmids, along with varying amounts of plasmids expressing WT or one of a panel of mutant tetherin proteins (Figure 2A). Virion release was evaluated using infectious particle and western blot assays. As expected, the release of HIV-1(WT) was only slightly affected by human tetherin, while the release of HIV-1 (delVpu) was strongly inhibited (Figures 2B and 2C).

(H) Western blot analysis (anti-HA) of 293T cells transiently transfected with 200 ng of plasmids expressing WT tetherin or tetherin variants bearing mutations at the indicated cysteine residues. Samples were untreated or treated with β-mercaptoethanol (β-ME) prior to analysis. Numbers to the left of (B), (C), (D), (E), and (H) represent the positions and sizes (in kDa) of molecular weight markers.

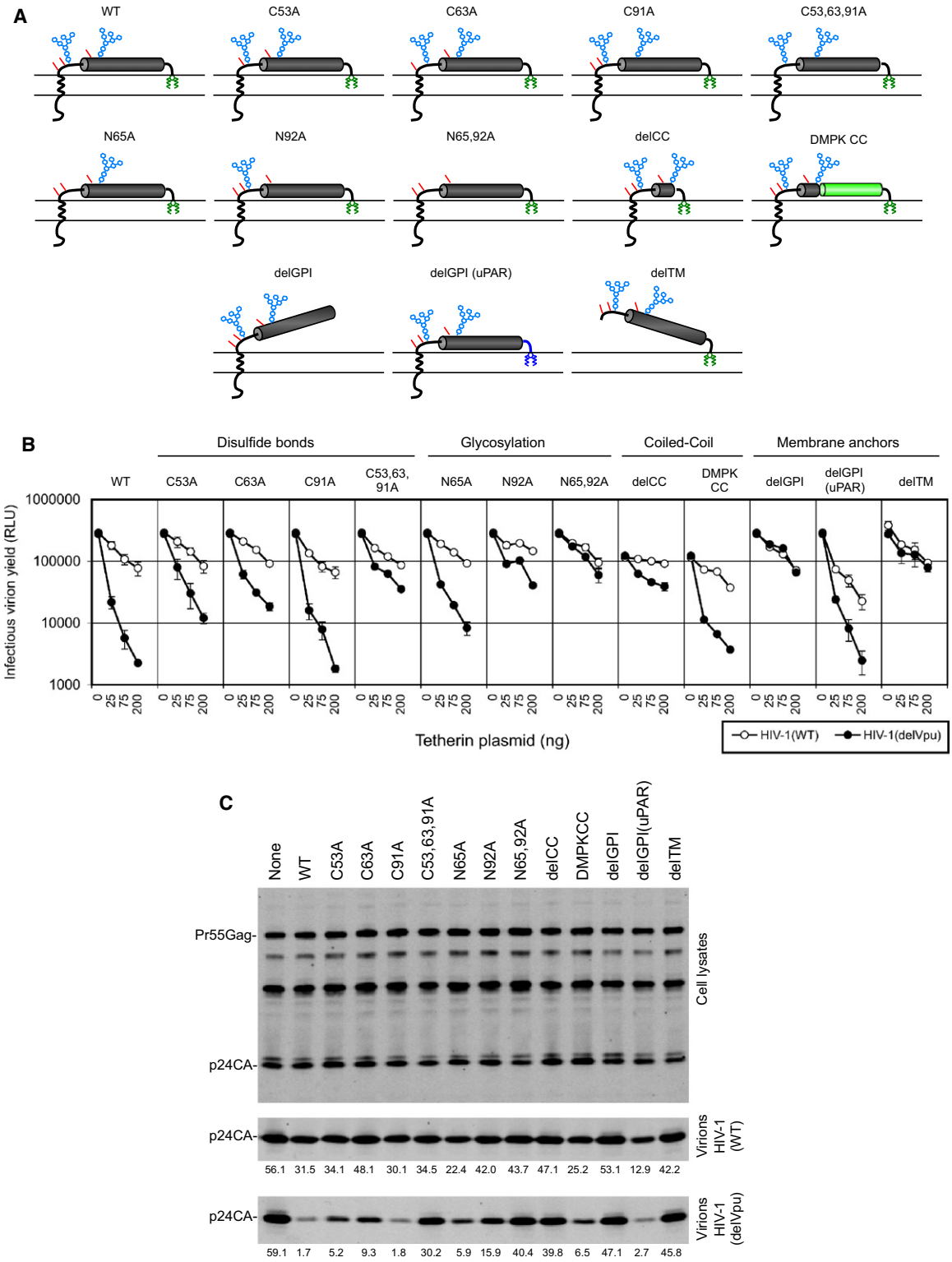

Figure 2. Tetherin Features Required for Antiviral Activity

(A) Schematic representation of the tetherin mutants panel, indicating the positions of GPI (green), glycosylation (blue), and disulfide bond (red) modifications. The tetherin proteins bore point mutations at cysteine residues involved in disulfide bonding (C53, C63, and/or C91) or N-linked glycosylation sites (N65 and/or N92). Alternatively, the tetherin coiled-coil was deleted (delCC) or replaced with a coiled-coil from dystrophia myotonica protein kinase (DMPK CC). The membrane anchors were removed (delGPI and delTM) or replaced by the C-terminal GPI modification signal from urokinase plasminogen activator receptor [delGPI(uPAR)].

In general, tetherin mutations affecting disulfide bonding or glycosylation had variable effects on antiviral activity. Disruption of individual intermolecular disulfide bonds by mutation of cysteine residues (C53A, C63A, or C91A) was quite well tolerated. The C53A and C63A mutations reduced but did not eliminate antiviral activity, while the C91A mutation had no effect (Figures 2B and 2C). Mutation of all three cysteines (C53,63,91A) dramatically reduced tetherin activity without inhibiting cell surface expression (see Figure S1, available online), suggesting that disulfide bond-mediated maintenance or stabilization of tetherin conformation was important for activity. Nonetheless, no individual disulfide bond was essential and even mutation of all three cysteine residues resulted in a tetherin protein that retained weak activity (Figure 2B).

Analysis of tetherin glycosylation site mutants revealed that the N65A mutation had rather small effects on tetherin activity while the N92A mutation markedly impaired activity (Figures 2B and 2C). The N65,92A double mutant was almost completely inactive. However, this mutant was less well expressed at the cell surface than WT and other mutant tetherins (Figure S1) and a secreted form of tetherin (delTM/delGPI), lacking both membrane anchors, was dependent on glycosylation for efficient secretion (Figure S2). These results suggested that glycosylation was required for the correct transport, and perhaps folding of the tetherin molecule, rather than playing a specific role in tethering activity, although the latter possibility could not be excluded.

A prominent feature of tetherin protein is a coiled coil that incorporates the majority of the extracellular protein sequence. Deletion of the bulk of the coiled-coil domain (in delCC) strongly inhibited antiviral activity, although a low residual level of Vpu-reversible particle release inhibition was observed (Figures 2B and 2C). The delCC protein was also well expressed at the cell surface (Figure S1) and formed disulfide linked homodimers (data not shown), demonstrating that the coiled coil is important for reasons other than dimer formation.

A mutant tetherin protein, named delTM, that lacked the N-terminal transmembrane domain and was retained in the cell membrane only by its GPI anchor (Figure 2A) did not block particle release (Figures 2B and 2C). Similarly, removal of the GPI anchor signal from tetherin (delGPI) also abolished antiviral activity. Despite their inactivity, these truncated proteins were well expressed at the cell surface (Figure S1). Thus, the major structural features of tetherin, namely N- and C-terminal membrane anchors positioned at either end of a coiled-coil domain were required for antiviral activity.

Notably, the reintroduction of a heterologous coiled coil from a constitutively dimeric cytoplasmic protein, dystrophia myotonica protein kinase (DMPK), into the poorly active delCC tetherin protein (Figure 2A) substantially restored activity (Figures 2B and 2C). Similarly, appending the delGPI tetherin protein with a C-terminal sequence from a heterologous GPI-linked protein, urokinase plasminogen activator receptor (uPAR), fully rescued activity (Figures 2B and 2C). These reintroduced protein domains exhibited little, if any, sequence homology with tetherin. Thus, the presence of these structural features appeared more important for activity than did their specific primary sequence.

An Artificial Tetherin-like Protein Assembled from Heterologous Protein Domains Has Virion-Tethering Activity

Because critically important features of the tetherin molecule could be functionally replaced by heterologous protein domains, we attempted to construct a completely artificial tetherin-like protein (art-tetherin). This designed protein incorporated domains from proteins that were ''tetherin-like'' based on size, topology, and posttranslational modifications but were otherwise unrelated and lacked sequence homology with tetherin (Figure 3A). The N terminus of art-tetherin consisted of a fragment of the N terminus of transferrin receptor (TfR) comprising the membrane proximal ~20 amino acid residues of its cytoplasmic tail (residues 43–62), the transmembrane domain (residues 63–88), and part of the extracellular stalk (residues 89–121). Like tetherin, TfR is a dimeric type-II transmembrane protein, and the extracellular portion incorporated into art-tetherin contains two cysteines that form intermolecular disulfide bonds. This TfR-derived N terminus was linked to the ~75 residue coiled coil from the cytoplasmic dimeric protein DMPK. An HA epitope tag was inserted immediately C-terminal to the DMPK coiled coil for detection purposes and the C terminus of art-tetherin was from uPAR, including a signal for GPI modification (Figure 3A).

The art-tetherin protein was well expressed in 293T cells and formed β-mercaptoethanol-sensitive dimers (Figure 3B). Immunofluorescence (Figure 3C) and FACS (Figure S3) analyses revealed that art-tetherin was expressed at the plasma membrane, as well as at intracellular locations, adopting a distribution that resembled that of native tetherin (Figure 3C).

Strikingly, art-tetherin potently inhibited the release of extracellular HIV-1 particles (Figures 3D and 3E). Inhibition occurred without effects on Gag protein expression (Figure 3D). As expected, art-tetherin was not antagonized by HIV-1 Vpu, unlike native tetherin. The mechanism by which art-tetherin inhibited particle release mimicked that of native tetherin. Specifically, mutant forms of art-tetherin that lacked either the N-terminal transmembrane domain or the C-terminal GPI anchor were devoid of antiviral activity (Figures 3E and 3F), indicating that both membrane anchors were essential for art-tetherin function. Moreover, when particle release was inhibited by either art-tetherin or native tetherin, particles could be recovered from cell surfaces by subtilisin treatment (Figure 3G). Scanning electron

(B and C) Effect of WT and mutant tetherin proteins on HIV-1 release. 293T cells were transfected with HIV-1(WT) or HIV-1(delVpu) proviral plasmids and increasing amounts of plasmids expressing WT or mutant tetherin proteins (0, 25, 75, and 200 ng for each). Infectious virion yield, measured using TZM-Bl indicator cells, is given in relative light units (RLU). Error bars indicate the range of duplicate determinations and are representative of two to five experiments for each tetherin mutant.

(C) Quantitative western blot analysis (LICOR, anti-p24) of 293T cells and corresponding virions after transfection with HIV-1(WT) or HIV-1(delVpu) proviral plasmids and 50 ng of the WT and mutant tetherin plasmids. Numbers below each lane indicate the amounts of p24 in virion pellets, in arbitrary units, and are representative of three experiments.

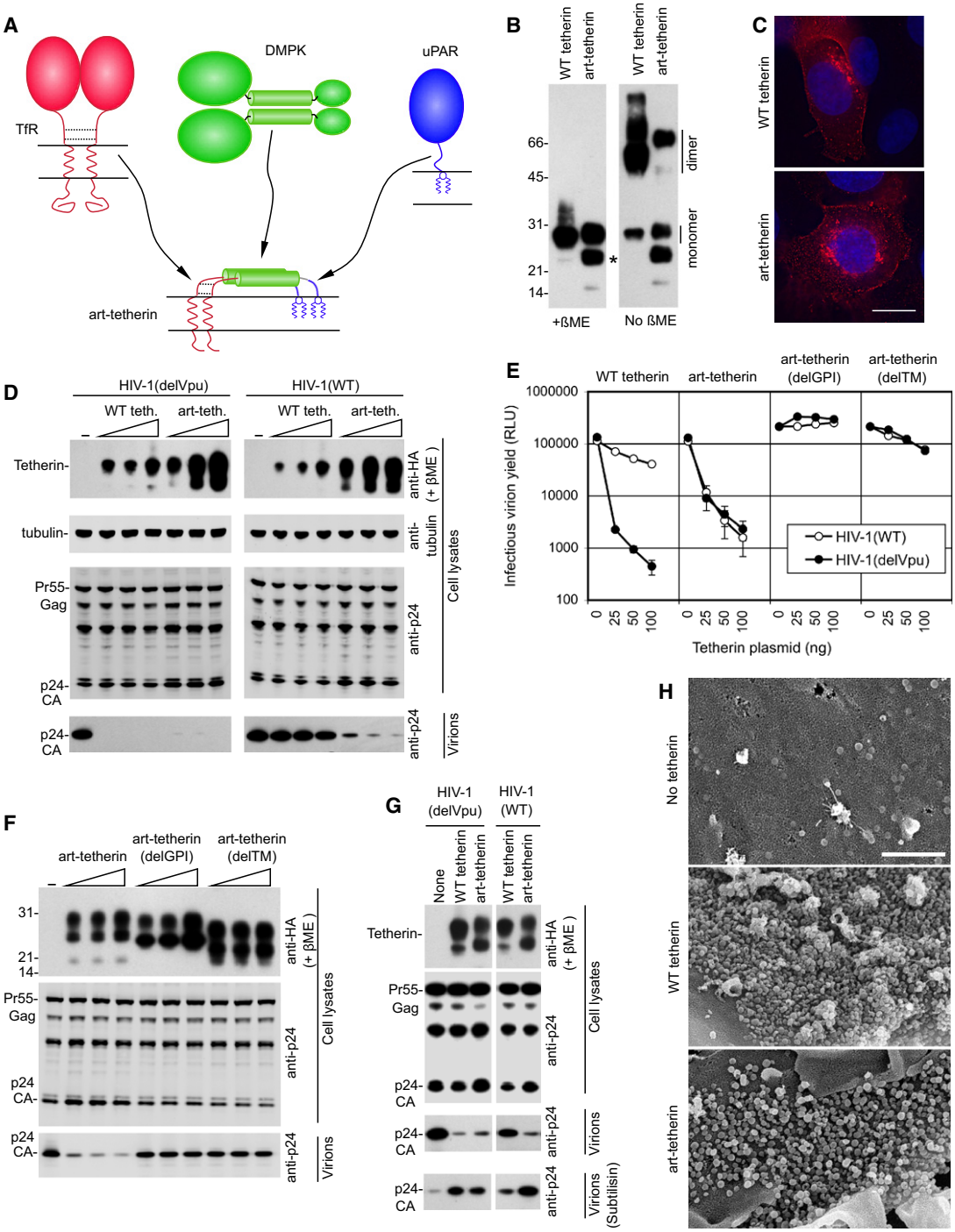

Figure 3. An Artificial Tetherin-like Protein Has Potent Antiviral Activity

(A) Design of an artificial tetherin (art-tetherin) protein using domains of similar configuration from the transferrin receptor (TfR), dystrophia myotonica protein kinase (DMPK), and urokinase plasminogen activator receptor (uPAR). An HA epitope tag was inserted between the DMPK and uPAR domains.

(B) Western blot analysis (anti-HA) of 293T cells transfected with plasmids expressing WT tetherin or art-tetherin and subjected to SDS-PAGE in the absence or presence of β-mercaptoethanol. A presumed degradation product from art-tetherin is indicated by an asterisk.

(C) Immunofluorescence analysis (anti-HA, red) of HT1080 cells transfected with plasmids expressing WT tetherin or art-tetherin. Nuclei were stained with DAPI (blue) and the images are representative of at least 50 cells that were inspected for each expressed protein. The scale bar represents 10 μm.

(D) Western blot analysis (anti-HA and anti-tubulin [upper panels] and anti-p24 [lower panels]) of cell lysates and corresponding released virions following transfection of 293T cells with HIV-1(WT) or HIV-1(delVpu) proviral plasmids and increasing amounts (0 ng, 25 ng, 50 ng, or 100 ng) of plasmids expressing WT tetherin or art-tetherin.

microscopic (EM) analysis revealed that art-tetherin, like WT tetherin, induced the accumulation of HIV-1 particles on cell surfaces (Figure 3H). Art-tetherin also inhibited the release of VLPs assembled using the Ebola VP40 protein, although it appeared somewhat less potent than native tetherin (Figure S4). Overall, the fact that it proved rather straightforward to design an active artificial tetherin that has no significant sequence homology to native tetherin makes it unlikely that tetherin functions through indirect mechanisms or requires specifically associated cofactors.

Tetherin Incorporation into HIV-1 Particles

If tetherin acts directly, and without cofactors, to block the release of virion particles, then a possible mechanism of action could involve incorporation of one or both of the membrane anchors into virion membranes. Thereafter, the other membrane anchor, or one of a pair of molecules in a tetherin dimer, could remain embedded in the host cell membrane. This would inevitably result in the formation of a tether, composed of the tetherin protein itself.

To determine whether tetherin is incorporated into virion envelopes, we employed both biochemical and EM assays. Transmission EM analysis of HT1080 cells expressing tetherin-HA and infected with either HIV-1(WT) or HIV-1(delVpu) revealed that only HIV-1(delVpu) infection resulted in significant numbers of virions tethered at the cell surface. Immunogold labeling of cell surfaces with anti-HA antibodies revealed that tetherin-HA was frequently associated with virions (Figure 4A).

WT tetherin blocked HIV-1 particle release and, therefore, it was difficult to determine whether it was incorporated into virions using western blot assays (Figure 4B). Indeed, if a given virion incorporated molecules that cause tethering it would be unlikely to be released. Therefore, we generated HIV-1(delVpu) particles in the presence of inactive tetherin mutants. Deletion of either one of the two of the tetherin membrane anchors (in the delTM and delGPI mutants) resulted in proteins that did not impair virion release but were efficiently incorporated into virions (Figure 4B). Importantly, the apparent incorporation of tetherin into pelleted virions was specific, because no pelletable tetherin was observed in the absence of virion production (Figure 4B). Other poorly, but partly, active tetherin mutants, for example (C53,63,91A), that retained both membrane anchors were also incorporated into particles, albeit at significantly reduced levels compared to delGPI (Figure S5).

To further demonstrate that delGPI and delTM tetherin proteins were incorporated into HIV-1 particles, 293T stably expressing either delTM or delGPI tetherin proteins were infected with HIV-1(delVpu) and progeny virions purified on Optiprep gradients. Analysis of gradient fractions showed a precise concordance between those that contained virions and those that contained delGPI and delTM tetherin proteins (Figure 4C).

In contrast to the delGPI, delTM, and C53,63,91A mutant tetherin proteins, full-length tetherin was not found in virion particles when transiently expressed with HIV-1(delVpu) proviruses or in single cycle infection assays (Figures 4B and S5, and data not shown), likely because virions that encounter tetherin are not efficiently released. However, we reasoned that high levels of Gag expression and modest levels of tetherin expression might "dilute" the available cell surface tetherin among a large number of nascent particles, thereby reducing its potency and perhaps enabling its detection in released virions. Indeed, when 293T cells stably expressing HA-tagged tetherin were transiently transfected with a codon-optimized Gag expression plasmid that generates large numbers of particles, inhibition of particle release by tetherin was incomplete (Figure S6). Under these conditions, disulfide linked tetherin dimers were detected in VLPs purified on Optiprep gradients (Figure 4D). Thus tetherin was incorporated into virion particles and either of its two membrane anchors was capable of driving incorporation.

Configuration of Tetherin in Virions and Exclusion by Vpu

To determine the topology of tetherin with respect to the virion envelope, HIV-1(delVpu) virions were harvested from 293T stably expressing delGPI (HA-tagged at the N terminus) or delTM (HA-tagged at the C terminus) and purified virions were either untreated or treated with subtilisin A. Both proteins were incorporated into HIV-1(delVpu) virions as dimers (Figure 5A) and an N-terminal fragment of the delGPI tetherin protein that migrated at ~25 kDa (under nonreducing conditions) was protected from subtilisin digestion (Figure 5A). Under reducing conditions, this fragment migrated at approximately half this molecular weight (~13 kDa) (Figure 5A), strongly suggesting that delGPI is incorporated in particles as a parallel disulfide linked dimer with both N termini inside the virion particle. Conversely, the delTM tetherin protein was also incorporated in particles as a dimer but was not protected from subtilisin digestion, indicating that the entire delTM tetherin protein was on the outside of virion envelopes, anchored therein by GPI at its C terminus (Figure 5A).

We also analyzed virions trapped at the cell surface by N-terminally tagged WT tetherin (Figure 5B). In this case, virions were recovered from the cell surface by subtilisin stripping.

(E) Infectious virion release, measured using TZM-Bl indicator cells, following transfection of 293T cells with HIV-1(WT) or HIV-1(delVpu) proviral plasmids and increasing amounts (0 ng, 25 ng, 50 ng, and 100 ng) of plasmids expressing WT tetherin, art-tetherin, or art-tetherin mutants. Error bars indicate the range of duplicate determinations and are representative of two to five experiments for each protein.

(F) Western blot analysis (anti-HA [upper panels] and anti-p24 [center and lower panels]) of cell lysates and corresponding released virions following transfection of 293T cells with an HIV-1(delVpu) proviral plasmid and increasing amounts (0 ng, 25 ng, 50 ng, or 100 ng) of plasmids expressing art-tetherin and mutant derivatives. Numbers to the left of (B) and (F) represent the positions and sizes (in kDa) of molecular weight markers.

(G) Western blot analysis of 293T cells (anti-p24 and anti-HA) and virions (anti-p24) following transfection with HIV-1(WT) or HIV-1(delVpu) and plasmids expressing WT tetherin or art-tetherin. Virions that were constitutively released or released following incubation of the cells with subtilisin (bottom panels) were pelleted through sucrose prior to analysis.

(H) Scanning electron micrograph of HT1080 cells transfected with plasmids expressing HIV-1 Gag in the presence or absence of either WT or art-tetherin. Scale bar indicates 1 μm. At least ten particle-expressing cells were evaluated in each of two independent experiments and representative images are shown.

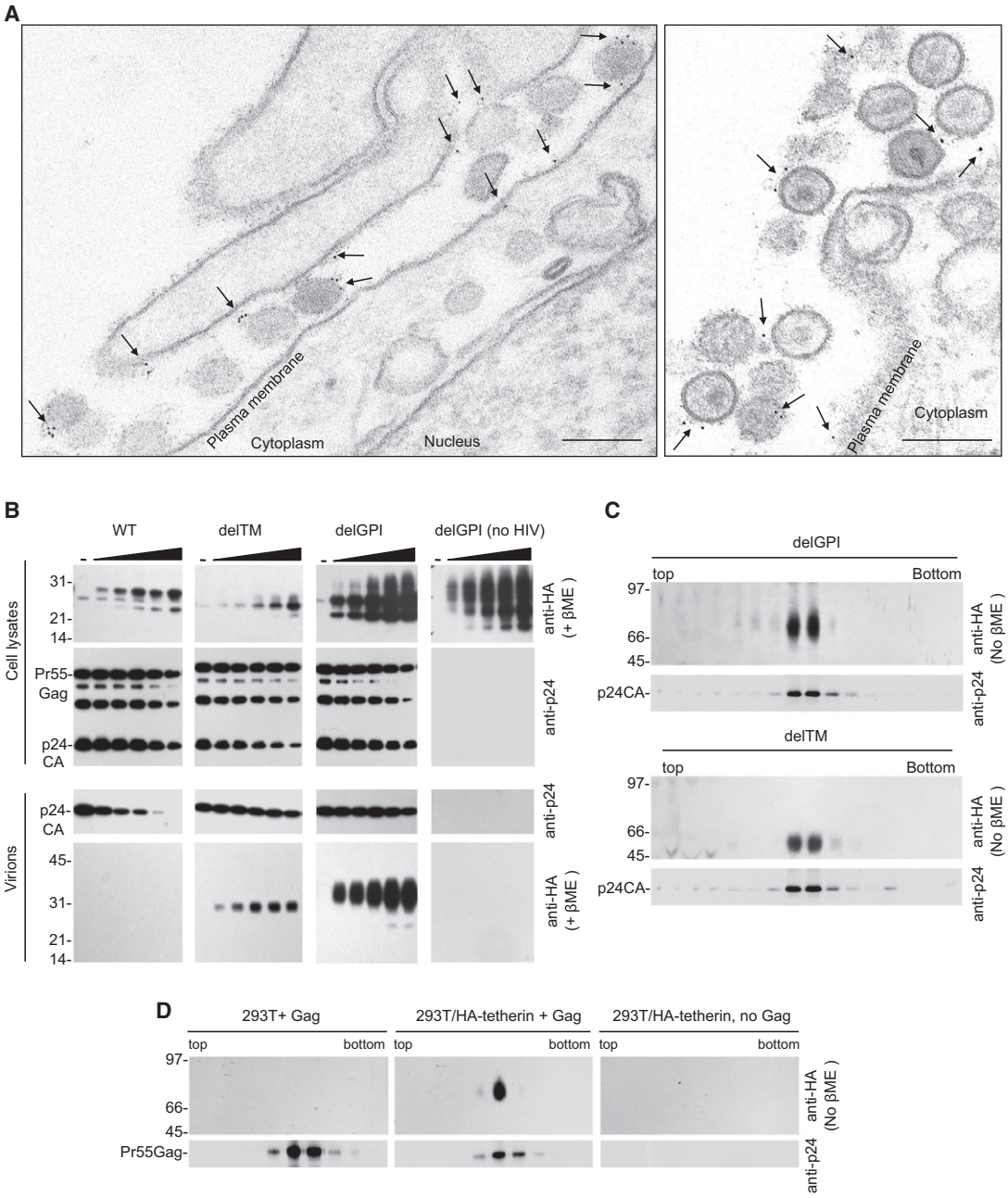

Figure 4. Incorporation of Tetherin Variants into HIV-1 Particles

(A) Transmission electron microscopic analysis of HT1080 cells stably expressing tetherin-HA and infected with HIV-1(delVpu). Infected cells were fixed and stained with anti-HA and anti-mouse IgG gold particles prior to sectioning. Scale bars represent 200 nm.

(B) Analysis of mutant tetherin incorporation into HIV-1 particles. 293T cells and corresponding released virions were harvested following transfection with HIV-1(delVpu) and increasing amounts of plasmids (0 ng, 3.125 ng, 6.25 ng, 12.5 ng, 25 ng, and 50 ng) expressing HA-tagged WT and mutant tetherin proteins. Virions were pelleted through sucrose prior to analysis. Cells and virions were subjected to western blot analysis (anti-p24 and anti-HA, as indicated).

(C) Western blot analysis (anti-p24 and anti-HA) of virions derived from HIV-1(delVpu)-infected 293T cells stably expressing delTM or delGPI tetherin proteins. Virions were purified on Optiprep gradients and 16 fractions were collected for western blot analysis of p24 and tetherin content.

(D) Analysis of WT tetherin incorporation into virions. Unmodified 293T cells (left panels) or 293T cells stably expressing full-length tetherin-HA (center panels) were transfected with a plasmid expressing codon-optimized HIV-1 Gag. VLPs were pelleted through sucrose and purified on linear (10%–30%) Optiprep gradient. Ten fractions were collected and precipitated and subjected to a western blot analysis using anti-p24 and anti-HA antibodies. As a control, mock transfected 293T cells stably expressing full-length tetherin-HA were subjected to the same procedure (right panels).

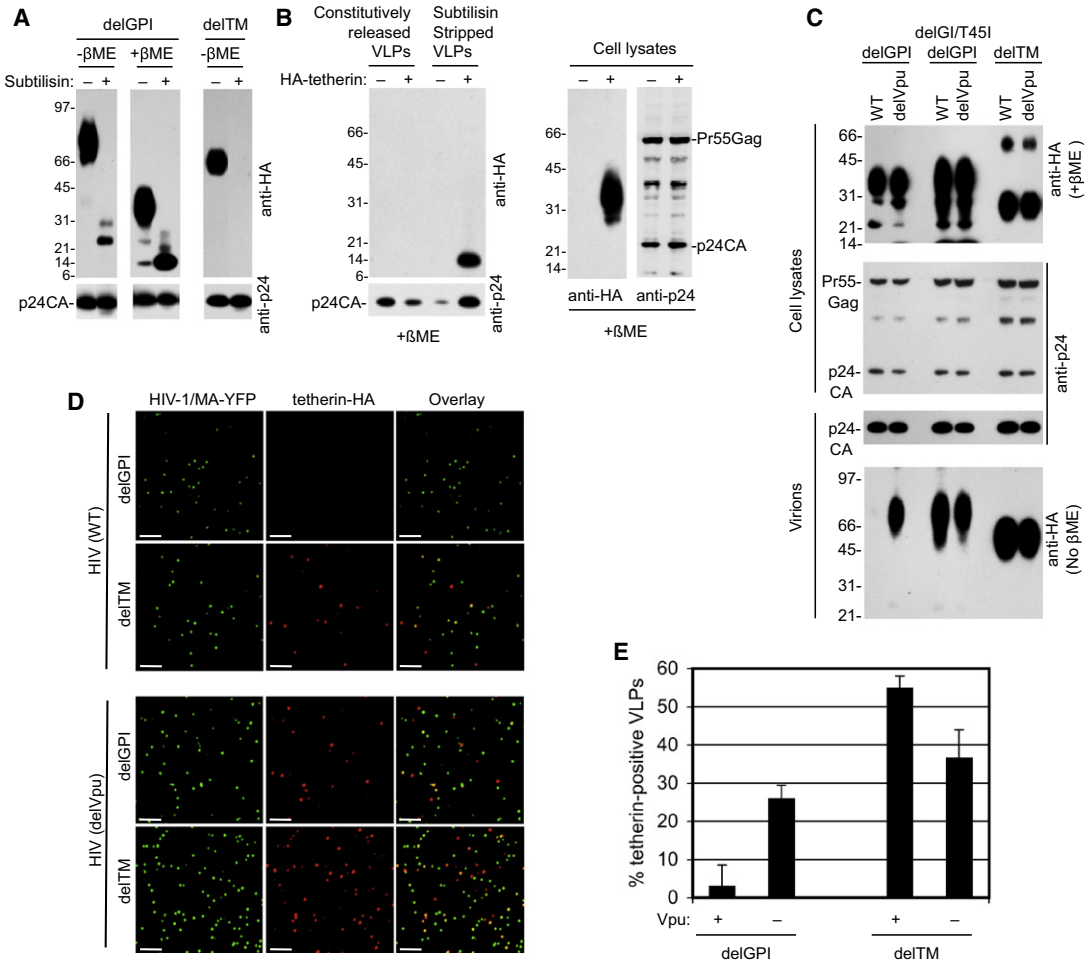

Figure 5. Configuration of Tetherin in Virions and Exclusion by Vpu

(A) Analysis of virions derived from HIV-1(delVpu)-infected 293T cells stably expressing N-terminally HA-tagged delGPI and C-terminally HA-tagged delTM tetherin proteins. Virions were pelleted through sucrose, treated with (+) or without (–) subtilisin, pelleted again through sucrose, and subjected to SDS-PAGE in the presence or absence of β-mercaptoethanol prior to western blot analysis with anti-p24 and anti-HA antibodies.

(B) Analysis of virions recovered from the surface of 293T cells stably expressing N-terminally HA-tagged WT tetherin. Cells were infected with HIV-1(delVpu) and virions that were constitutively released or released following incubation of the cells with subtilisin were pelleted through sucrose prior to analysis. Virions and corresponding cell lysates were subjected to western blot analysis with anti-p24 and anti-HA antibodies.

(C) Analysis of the effect of Vpu on virions derived from HIV-1-infected 293T cells stably expressing HA-tagged delGPI, delGI/T45I/delGPI, or delTM tetherin proteins. Cells were infected with HIV-1 (WT) or HIV-1(delVpu) and virions were pelleted through sucrose prior to analysis. Virions and corresponding cell lysates were subjected to western blot analysis with anti-p24 and anti-HA antibodies. Numbers to the left of (A), (B), and (C) represent the positions and sizes (in kDa) of molecular weight markers.

(D) Immunofluorescence analysis (anti-HA) of virions harvested from HIV-1/MA-YFP(WT)- or HIV-1/MA-YFP(delVpu)-infected 293T cells stably expressing delTM and delGPI tetherin proteins. Virions were pelleted and applied to poly-D-lysine-coated coverslips prior to analysis. Scale bars represent 2 μm. A proportion of representative fields observed in each of two experiments is shown.

(E) Quantitative analysis of tetherin incorporation into virions. The proportion of HIV-1/MA-YFP(WT) or HIV-1/MA-YFP(delVpu) virions that were positive for delTM and delGPI tetherin proteins was quantified. The mean and standard deviation of the percentage of YFP-positive virions that were positive for tetherin is shown. Three fields containing a total of at least 600 YFP-positive virions for each condition were evaluated, in each of two independent experiments.

These subtilisin-stripped virions contained an N-terminal tetherin fragment that migrated in a manner that was indistinguishable from that of fragment recovered from subtilisin-treated, constitutively released virons containing the N-terminally tagged delGPI tetherin protein. Thus, that at least some of the virions trapped at the cell surface by WT tetherin incorporated tetherin into the particles with the tetherin N terminus in the virion interior.

The HIV-1 Vpu protein antagonizes the antiviral activity of the human tetherin protein via poorly understood mechanisms. However, the differential sensitivity of human, monkey, and chimeric tetherin proteins to antagonism suggests that Vpu targets the tetherin transmembrane domain to neutralize its activity (McNatt et al., 2009). We reasoned that if tetherin incorporation into virions was relevant to its antiviral function, then

HIV-1 Vpu should be able to impair the incorporation of delGPI tetherin into viral particles.

Analysis of virions harvested from HIV-1(WT)- or HIV-1(delVpu)-infected 293T cells stably expressing delTM tetherin (anchored in membrane by the GPI modification) revealed that delTM tetherin incorporation was unaffected by Vpu (Figure 5C). In contrast, delGPI tetherin dimers (anchored in membranes by the TM domain) were efficiently incorporated into HIV-1(delVpu) but excluded from HIV-1(WT) virions (Figure 5C). Mutations in the tetherin transmembrane domain (delGI/T45I) can confer complete resistance to antagonism by Vpu (McNatt et al., 2009). Concordantly, this mutant delGPI tetherin protein was equally well incorporated into virions in the presence or absence of Vpu (Figure 5C).

To further analyze tetherin incorporation into virions and its antagonism by Vpu, 293T cells stably expressing delGPI or delTM tetherin proteins were infected with HIV-1(WT) or HIV-1(delVpu) derivatives that harbor YFP inserted into the stalk region of matrix, such that infected cells generate fluorescent virion particles (Jouvenet et al., 2006). Immunofluorescence analysis of these virions, fixed to coverslips, revealed that the HIV-1(WT) particles incorporated delTM but excluded the delGPI tetherin, whereas HIV-1(delVpu) particles incorporated both delGPI and delTM tetherin proteins (Figures 5D and 5E). Altogether, these results indicate that Vpu excludes tetherin from virions by targeting its transmembrane domain.

Tetherin Association with Budding Virions

To visualize the infiltration of nascent virions by tetherin in greater detail, we conducted scanning EM experiments with gold immunolabeling and backscatter electron detection. Virions that were in the act of, but had not completed, budding were generated in 293T cells transiently expressing either WT tetherin-HA or the delTM or delGPI mutants by simultaneously expressing HIV-1 Gag carrying a mutation in the PTAP L domain. This manipulation arrests budding before completion and enables reliable detection of nascent virion particles on cell surfaces. However, virions are retained at the cell surface whether or not they encounter tetherin during budding and regardless of whether the tetherin protein blocks release. Thus, this approach carries the disadvantage that does not allow the observation of tetherin-dependent tethering events, but the advantage that the interaction between inactive tetherin deletion mutants (delTM and delGPI) and budding particles could be observed.

The WT and delTM tetherin proteins were found to be associated with many budding virions, but there was not strong enrichment at budding sites (Figure 6A). In contrast, the delGPI tetherin protein preferentially localized at sites of particle budding. In many cases, the delGPI protein appeared to adopt a ring-like arrangement at viral budding sites (Figure 6). Overall, the full-length tetherin protein, as well as derivatives containing only one of the two membrane anchors, were able to infiltrate the envelope of budding virions, and the N-terminal domain of tetherin appears to have a particular propensity to drive localization to virion buds.

DISCUSSION

In general, the mechanisms by which IFN-induced gene products inhibit viral replication is poorly understood (Samuel,

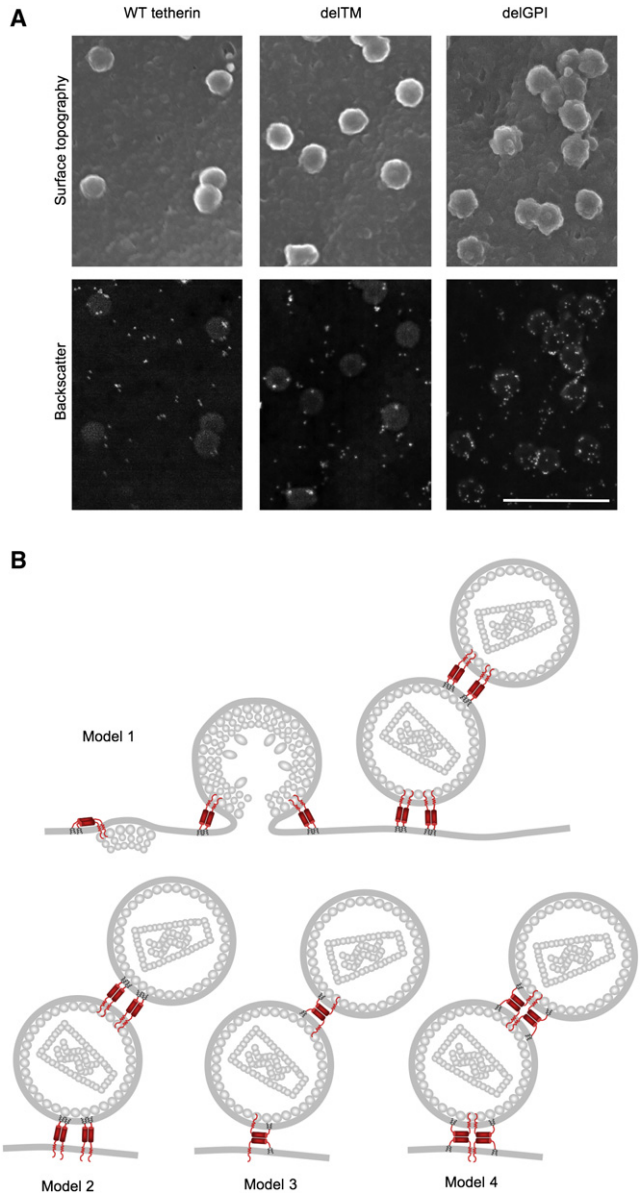

Figure 6. Scanning EM Analysis of Tetherin Interaction with Budding Virions and Models for Tetherin Incorporation

(A) Scanning electron microscopic analysis of 293T cells transiently expressing HA-tagged WT, delTM, or delGPI tetherin proteins and HIV-1 Gag bearing mutations in the PTAP L-domain sequence. Cells were fixed and stained with anti-HA primary antibody and anti-mouse IgG gold conjugate. Surface topography (upper panels) reveals virion particles, while backscatter electron detection (lower panels) reveals gold particles (white) marking the position of tetherin molecules. The scale bar represents 500 nm.

(B) Models for incorporation and virion tethering by the tetherin protein. Several stages of HIV-1 assembly are depicted for model 1, and only tethered virions are shown for models 2–4. In model 1, the TM domains of a tetherin dimer are incorporated into the virion envelope and the GPI anchors remain embedded in the host-cell membrane. In model 2, the reverse situation occurs. In model 3, only one of a pair of disulfide-linked tetherin molecules has both membrane anchors incorporated into the virion envelope. In model 4, one disulfide linked tetherin dimer incorporated into the virion envelope interacts with another dimer in the host-cell membrane via coiled-coil-based interactions.

2001). Here, we show that one such gene product, tetherin, inhibits enveloped virus release via a simple and direct mechanism. Identification of the key features of the tetherin molecule that were required for antiviral activity allowed the design of a completely artificial tetherin-like protein using domains from other proteins. Despite lacking significant sequence homology to native tetherin, the synthetic tetherin-like protein mimicked the biological activity of native tetherin. These data strongly suggest that tetherin activity does not involve interactions with specific cofactors, sensor function, signaling, or other indirect mechanisms. Rather, they suggest that tetherin itself directly tethers viral particles to cellular membranes.

Consistent with this notion, both of the tetherin membrane anchors were essential for tethering function (in both native and art-tetherin) and either of native tetherin's membrane anchors could drive incorporation into the envelope of HIV-1 particles. Because (1) all three cysteines that are situated toward the tetherin N terminus form intermolecular disulfide bonds with the corresponding residue in the tetherin homodimer and (2) the delGPI tetherin mutant was incorporated into released virions with N termini protected from externally applied protease, these data strongly suggest that tetherin bridges viral and infected cell membranes by inserting either or both its N or C termini as a parallel homodimer into the viral membrane. Based on these findings, we favor the model for tetherin incorporation shown in Figure 6B (models 1 and 2) whereby one pair of tetherin membrane anchors are incorporated into an assembling virion envelope, while the other pair remains embedded in the cell membrane. The finding that the delGPI tetherin molecule appears to have a particular propensity for localizing at sites of viral budding would tend to favor model 1. In these models, we speculate that the role of the coiled coil and homotypic disulfide bonds might be to constrain the dimer in an extended conformation, thereby maintaining distance between the two pairs of membrane anchors. This spatial separation should increase the likelihood that one pair of membrane anchors is incorporated into the virion envelope while the other remains in the cell membrane. However, there are a few possible configurations that tetherin could adopt during virion tethering that are consistent with most of the data presented in this study (Figure 6B, models 3 and 4) and it is even possible that several different configurations are used. Additionally, tetherin could form higher order complexes through interactions between dimers. Nonetheless, the key features of each of these models are (1) that tetherin itself appears necessary and sufficient to form tethers and (2) that membrane anchors in a single tetherin dimer, or higher order complex, partition into both virion and host cell membranes. Earlier findings demonstrate that tetherin causes virions to be tethered to each other, as well as to the cell surface. Obviously this can only occur if both types of tetherin membrane anchor can be incorporated into virion membranes and could result from the assembly of a virion at a site on the plasma membrane that is already occupied by a tethered virion.

Vpu caused exclusion of delGPI tetherin but not delTM tetherin from HIV-1 particles. Put another way, Vpu blocked the insertion of the tetherin transmembrane domain into virion envelopes. This effect was highly specific, as mutations in the human tetherin TM domain (delGI/T45I) that confer resistance to antagonism by Vpu (McNatt et al., 2009) also induced resistance to virion exclusion by Vpu. This suggests that exclusion of tetherin from assembling virions is central to the mechanism by which Vpu counteracts tetherin's antiviral activity, consistent with previous findings that Vpu prevented colocalization of tetherin with Gag puncta at the plasma membrane of VLP-producing cells (Jouvenet et al., 2009).

Our conclusions contrast with those of with Miyagi and colleagues who failed to detect tetherin in virions that were released from HeLa cells following agitation, and suggested that tetherin does not directly tether virions to cells (Miyagi et al., 2009). However, it is not clear how effectively agitation releases bona fide tethered viruses from cells, as HIV-1(WT) and HIV-1(delVpu) were released from cells by agitation with only moderately differing efficiencies (Miyagi et al., 2009). We were clearly able to detect full-length tetherin in constitutively released virion particles under conditions where sufficient Gag was expressed to saturate the available tetherin and allow reasonable levels of particle release. Additionally, EM analyses showed clear association of tetherin with tethered and budding HIV-1 particles. Moreover, tetherin mutants bearing only one of the two membrane anchors were efficiently inserted into the envelope of released HIV-1 virions.

The studies described herein focused primarily on HIV-1 particle release. However, while HIV-1 normally replicates in T cells and macrophages, type-1 IFN can also induce tetherin expression in a wide variety of other cell types that are not normally target cells of HIV-1, including those used in this study. Indeed, tetherin can induce essentially the same virion retention effect in a variety of cell contexts and is also capable of tethering diverse enveloped viruses (Neil et al., 2007; Jouvenet et al., 2009; Kaletsky et al., 2009; Sakuma et al., 2009).The mechanism of action elucidated herein explains how tetherin is able to inhibit the release of a variety of enveloped viruses from a variety of cells and thereby constitutes a generalized IFN-induced antiviral defense. Because this mechanism constitutes simple bridging of host and viral lipid bilayers, one can view the lipid envelope as the viral target of tetherin. Because the viral target is actually derived from the host cell, it is difficult for a virus to evade tetherin via simple mutations, as would be the case if such an inhibitor targeted a viral protein. This is likely the reason why several viruses have independently evolved *trans*-acting tetherin antagonists such as HIV-1 Vpu (Neil et al., 2008; Van Damme et al., 2008), SIV Nef (Jia et al., 2009; Zhang et al., 2009), Ebola GP (Kaletsky et al., 2009), KSHV K5 (Bartee et al., 2006), and, possibly, HIV-2 Env. The mechanism by which these antagonists counteract tetherin activity is not yet defined, although tetherin downregulation from the cell surface, proteasome-dependent degradation and possibly retention at the trans-Golgi network have been observed (Bartee et al., 2006; Dube et al., 2009; Goffinet et al., 2009; Van Damme et al., 2008). The mechanism of tetherin action described herein suggests that simply relocating tetherin such that it is excluded from sites of enveloped viral budding should be sufficient to counteract its inhibitory effect on virion release.

EXPERIMENTAL PROCEDURES

Materials

Details of the cells and plasmid constructs used in this study are given in the Supplemental Experimental Procedures.

Tetherin Activity Assays

To measure tetherin activity, 293T cells in 24 well plates were transfected using polyethylenimine (PolySciences) with 500 ng of HIV-1(WT), HIV-1(delVpu) proviral plasmids (Neil et al., 2006), or 400 ng of a plasmid expressing myc-tagged Ebola virus VP40 (Martin-Serrano et al., 2001). Tetherin expression plasmids were included at 3 to 200 ng per transfection. Cells were harvested 40 hr after transfection. Virion-containing supernatants were clarified by centrifugation and infectious HIV-1 release was determined using HeLa-TZM indicator cells as previously described (Martin-Serrano et al., 2001). The remainder of the supernatant (800 μl) was layered onto 600 μl of 20% sucrose in PBS and centrifuged at 20,000 × g for 90 min. Particle yield was determined using western blot assays (see Supplemental Experimental Procedures).

Microscopy

Fluorescence microscopy and EM assays were carried out according to standard procedures as outlined in the Supplemental Experimental Procedures.

Tetherin Incorporation Assays

To assess incorporation of transiently expressed tetherin, virions generated as described above were subjected to western blot analysis using anti-HA antibody. Alternatively, 293T cells stably expressing delGPI or delTM tetherin mutants (5×10^5 in 6 well plates) were infected with VSV-G pseudotyped HIV-1(WT) or HIV-1(delVpu) at an MOI of 1. Two days later, 2 ml of supernatant was harvested and layered on top of an 8 ml linear Optiprep gradient (10%–30%) and centrifuged at 110,000 × g for 1 hr. Sixteen gradient fractions were collected. Alternatively, 293T stably expressing tetherin-HA were plated in 10 cm dishes and transfected with 10 μg of a plasmid expressing codon-optimized Gag or a corresponding empty vector. Two days later, extracellular VLPs were pelleted through a 20% sucrose cushion at 90,000 × g for 90 min, resuspended in PBS, layered on top of a 4 ml linear Optiprep gradient (10%–30%), and centrifuged at 84,000 × g for 1 hr. Ten gradient fractions were collected. Proteins in each fraction were precipitated by adding 50 μg of BSA as a protein carrier and TCA to 10% and subjected to western blot analyses.

Subtilisin Stripping of Cells and Virions

To recover virions tethered to cell surfaces, 293T cells in 35 mm dishes were cotransfected with 1 μg of HIV-1(WT) or HIV-1(delVpu) proviral plasmids and 200 ng of WT tetherin or art-tetherin expression plasmids. Two days later, constitutively released virions were collected from supernatants. The cells were washed twice with PBS, washed once with subtilisin A buffer (10 mM Tris [pH 8.0], 1 mM $CaCl_2$, and 150 mM NaCl), and treated with 500 μl of 1 mg/ml of subtilisin A (Sigma) for 2–3 min at room temperature. Subtilisin treatment was stopped using DMEM containing 10% FCS, 5 mM PMSF, and 20 mM EGTA. The "subtilisin-strip" supernatant was layered on a 20% sucrose cushion and centrifuged at 20,000 × g for 90 min.

For subtilisin digestion of tetherin on the surface of virion particles, 293T cells stably expressing delGPI HA-tetherin or delTM tetherin-HA were infected with HIV-1(delVpu) at an MOI of 1. Two days later, virions were harvested by centrifugation through 20% sucrose. Pelleted virions were resuspended in subtilisin buffer and treated with subtilisin for 45 min at room temperature. Thereafter, subtilisin digestion was stopped as above and virions were pelleted through sucrose for a second time prior to western blot analysis.

SUPPLEMENTAL DATA

Supplemental Data include Supplemental Experimental Procedures and six figures and can be found with this article online at http://www.cell.com/supplemental/S0092-8674(09)01113-1.

ACKNOWLEDGMENTS

We thank members of the Bieniasz laboratory for helpful discussions and T. Kinoshita for PIGL-defective cells. This work was supported by National Institutes of Health grant RO1AI50111. P.D.B. is an Investigator of the Howard Hughes Medical Institute.

Received: May 16, 2009
Revised: July 25, 2009
Accepted: August 27, 2009
Published: October 29, 2009

REFERENCES

Bartee, E., McCormack, A., and Fruh, K. (2006). Quantitative membrane proteomics reveals new cellular targets of viral immune modulators. PLoS Pathog. *2*, e107.

Dube, M., Roy, B.B., Guiot-Guillain, P., Mercier, J., Binette, J., Leung, G., and Cohen, E.A. (2009). Suppression of Tetherin-restricting activity upon human immunodeficiency virus type 1 particle release correlates with localization of Vpu in the trans-Golgi network. J. Virol. *83*, 4574–4590.

Goffinet, C., Allespach, I., Homann, S., Tervo, H.M., Habermann, A., Rupp, D., Oberbremer, L., Kern, C., Tibroni, N., Welsch, S., et al. (2009). HIV-1 antagonism of CD317 is species specific and involves Vpu-mediated proteasomal degradation of the restriction factor. Cell Host Microbe *5*, 285–297.

Jia, B., Serra-Moreno, R., Neidermyer, W., Rahmberg, A., Mackey, J., Fofana, I.B., Johnson, W.E., Westmoreland, S., and Evans, D.T. (2009). Species-specific activity of SIV Nef and HIV-1 Vpu in overcoming restriction by tetherin/BST2. PLoS Pathog. *5*, e1000429.

Jouvenet, N., Neil, S.J., Bess, C., Johnson, M.C., Virgen, C.A., Simon, S.M., and Bieniasz, P.D. (2006). Plasma membrane is the site of productive HIV-1 particle assembly. PLoS Biol. *4*, e435.

Jouvenet, N., Neil, S.J., Zhadina, M., Zang, T., Kratovac, Z., Lee, Y., McNatt, M., Hatziioannou, T., and Bieniasz, P.D. (2009). Broad-spectrum inhibition of retroviral and filoviral particle release by tetherin. J. Virol. *83*, 1837–1844.

Kaletsky, R.L., Francica, J.R., Agrawal-Gamse, C., and Bates, P. (2009). Tetherin-mediated restriction of filovirus budding is antagonized by the Ebola glycoprotein. Proc. Natl. Acad. Sci. USA *106*, 2886–2891.

Kupzig, S., Korolchuk, V., Rollason, R., Sugden, A., Wilde, A., and Banting, G. (2003). Bst-2/HM1.24 is a raft-associated apical membrane protein with an unusual topology. Traffic *4*, 694–709.

Martin-Serrano, J., Zang, T., and Bieniasz, P.D. (2001). HIV-1 and Ebola virus encode small peptide motifs that recruit Tsg101 to sites of particle assembly to facilitate egress. Nat. Med. *7*, 1313–1319.

McNatt, M.W., Zang, T., Hatziioannou, T., Bartlett, M., Fofana, I.B., Johnson, W.E., Neil, S.J., and Bieniasz, P.D. (2009). Species-specific activity of HIV-1 Vpu and positive selection of tetherin transmembrane domain variants. PLoS Pathog. *5*, e1000300.

Miyagi, E., Andrew, A.J., Kao, S., and Strebel, K. (2009). Vpu enhances HIV-1 virus release in the absence of Bst-2 cell surface down-modulation and intracellular depletion. Proc. Natl. Acad. Sci. USA *106*, 2868–2873.

Morita, E., and Sundquist, W.I. (2004). Retrovirus budding. Annu. Rev. Cell Dev. Biol. *20*, 395–425. 10.1146/annurev.cellbio.20.0.10403.102350.

Nakamura, N., Inoue, N., Watanabe, R., Takahashi, M., Takeda, J., Stevens, V.L., and Kinoshita, T. (1997). Expression cloning of PIG-L, a candidate N-acetylglucosaminyl-phosphatidylinositol deacetylase. J. Biol. Chem. *272*, 15834–15840.

Neil, S.J., Eastman, S.W., Jouvenet, N., and Bieniasz, P.D. (2006). HIV-1 Vpu promotes release and prevents endocytosis of nascent retrovirus particles from the plasma membrane. PLoS Pathog. *2*, e39.

Neil, S.J., Sandrin, V., Sundquist, W.I., and Bieniasz, P.D. (2007). An interferon-alpha-induced tethering mechanism inhibits HIV-1 and Ebola virus particle release but is counteracted by the HIV-1 Vpu protein. Cell Host Microbe *2*, 193–203.

Neil, S.J., Zang, T., and Bieniasz, P.D. (2008). Tetherin inhibits retrovirus release and is antagonized by HIV-1 Vpu. Nature *451*, 425–430.

Ohtomo, T., Sugamata, Y., Ozaki, Y., Ono, K., Yoshimura, Y., Kawai, S., Koishihara, Y., Ozaki, S., Kosaka, M., Hirano, T., et al. (1999). Molecular cloning and characterization of a surface antigen preferentially overexpressed on multiple myeloma cells. Biochem. Biophys. Res. Commun. *258*, 583–591.

Sakuma, T., Noda, T., Urata, S., Kawaoka, Y., and Yasuda, J. (2009). Inhibition of Lassa and Marburg virus production by tetherin. J. Virol. *83*, 2382–2385.

Samuel, C.E. (2001). Antiviral actions of interferons. Clin. Microbiol. Rev. *14*, 778–809.

Van Damme, N., Goff, D., Katsura, C., Jorgenson, R.L., Mitchell, R., Johnson, M.C., Stephens, E.B., and Guatelli, J. (2008). The interferon-induced protein BST-2 restricts HIV-1 release and is downregulated from the cell surface by the viral Vpu protein. Cell Host Microbe *3*, 245–252.

Varthakavi, V., Heimann-Nichols, E., Smith, R.M., Sun, Y., Bram, R.J., Ali, S., Rose, J., Ding, L., and Spearman, P. (2008). Identification of calcium-modulating cyclophilin ligand as a human host restriction to HIV-1 release overcome by Vpu. Nat. Med. *14*, 641–647.

Zhang, F., Wilson, S.J., Landford, W.C., Virgen, B., Gregory, D., Johnson, M.C., Munch, J., Kirchhoff, F., Bieniasz, P.D., and Hatziioannou, T. (2009). Nef proteins from simian immunodeficiency viruses are tetherin antagonists. Cell Host Microbe *6*, 54–67.

nature immunology

Activation of innate immune antiviral responses by Nod2

Ahmed Sabbah[1], Te Hung Chang[1], Rosalinda Harnack[1], Victoria Frohlich[2], Kaoru Tominaga[2,3], Peter H Dube[1], Yan Xiang[1] & Santanu Bose[1]

Pattern-recognition receptors (PRRs), including Toll-like receptors (TLRs) and RIG-like helicase (RLH) receptors, are involved in innate immune antiviral responses. Here we show that nucleotide-binding oligomerization domain 2 (Nod2) can also function as a cytoplasmic viral PRR by triggering activation of interferon-regulatory factor 3 (IRF3) and production of interferon-β (IFN-β). After recognition of a viral ssRNA genome, Nod2 used the adaptor protein MAVS to activate IRF3. Nod2-deficient mice failed to produce interferon efficiently and showed enhanced susceptibility to virus-induced pathogenesis. Thus, the function of Nod2 as a viral PRR highlights the important function of Nod2 in host antiviral defense mechanisms.

Innate immune antiviral responses are the first line of defense against viral infection[1,2]. Interferon-α/β (IFN-α/β) serves an important function during innate antiviral responses by activating the kinase Jak–transcription factor STAT signaling pathway[3]. Virus-infected cells use pattern-recognition receptors (PRRs) to recognize pathogen-associated molecular patterns (PAMPs; in this case, virus-associated molecular patterns) and to trigger phosphorylation of the transcription factor interferon-regulatory factor 3 (IRF3), which then translocates to the nucleus to transactivate interferon genes[4]. So far two classes of viral PRRs have been identified: the Toll-like receptors (TLRs)[5] and the RIG-like helicase (RLH) receptors such as RIG-I and Mda5 (ref. 6).

A third class of PRR includes members of the nucleotide-binding domain (NBD)– and leucine-rich-region (LRR)–containing family of cytoplasmic proteins (known as NLRs); these proteins respond to bacterial PAMPs to activate the transcription factor NF-κB and mitogen-activated protein kinase pathways[7–9]. For example, the NLR Nod2 detects bacterial PAMPs, including muramyl dipeptide (MDP)[10]. However, so far, no NLRs have been reported to respond to virus-specific PAMPs and activate an antiviral response.

It has been shown that the NLR family member NLRX1 interacts with the mitochondrial antiviral signaling (MAVS) protein (also known as IPS-1, VISA or CARDIF) to negatively regulate the interferon pathway[11] and induces the formation of reactive oxygen species[12]. Thus, members of NLR family of proteins may modulate (either positively or negatively) the host antiviral apparatus. In addition, Nod2 facilitates production of human β-defensin 2 after stimulation with MDP, and human β-defensin 2 is also upregulated in human cells infected with respiratory syncytial virus (RSV), a paramyxovirus that has a negative-sense single-stranded RNA (ssRNA) genome[13,14].

Here, to investigate the involvement of NLRs in innate antiviral response, we examined the ability of various NLRs to activate IRF3 and interferon after infection with RSV, which causes severe lung disease in infants and children and elderly and immunocompromised people[15,16]. Among the various NLRs, Nod2 activated IRF3 and interferon in RSV-infected cells. Activation of Nod2 by ssRNA resulted in signaling dependent on MAVS. Both synthetic ssRNA and viral ssRNA genome were able to activate the MAVS-IRF3-interferon pathway. The important physiological function of Nod2 in antiviral defense was evident from the enhanced RSV pathogenesis, lung disease and viral susceptibility of Nod2-deficient mice. We found similar functions for Nod2 in responses to influenza A and parainfluenza viruses. Thus, our studies demonstrate a previously unknown function for Nod2 as a viral PRR important for the host defense against virus infection.

RESULTS

Induction of interferon production by ssRNA via Nod2

To study the involvement of NLR proteins in antiviral responses, we expressed various hemagglutinin (HA)-tagged human NLR proteins (such as Nod1, Nod2, IPAF, NAIP and Nod3) in 293 human embryonic kidney cells, which do not endogenously express most NLRs. We treated these cells with synthetic ssRNA and analyzed interferon production and IRF3 activation. We used ssRNA because several highly pathogenic viruses, including paramyxoviruses (RSV, Sendai virus, human parainfluenza viruses and measles virus), rhabdoviruses (rabies virus and vesicular stomatitis virus) and orthomyxoviruses (influenza viruses) have ssRNA genomes and because ssRNA activates PRRs, including TLR7, TLR8 and RIG-I (refs. 5,6). Nod2 but not Nod1 facilitated ssRNA-induced activation of IRF3 (**Fig. 1a**) and IFN-β (**Supplementary Fig. 1a**,**b**). Such activation was lacking in cells treated with CpG DNA (**Fig. 1a** and **Supplementary Fig. 1a**,**b**). Transfected 293 cells had high expression of HA-tagged Nod constructs (**Supplementary Fig. 1c**); in addition,

[1]Department of Microbiology and Immunology, [2]Department of Cellular and Structural Biology and [3]Sam and Ann Barshop Institute for Longevity and Aging Studies, The University of Texas Health Science Center at San Antonio, San Antonio, Texas, USA. Correspondence should be addressed to S.B. (bose@uthscsa.edu).

Received 20 April; accepted 15 July; Published online 23 August 2009; doi:10.1038/ni.1782

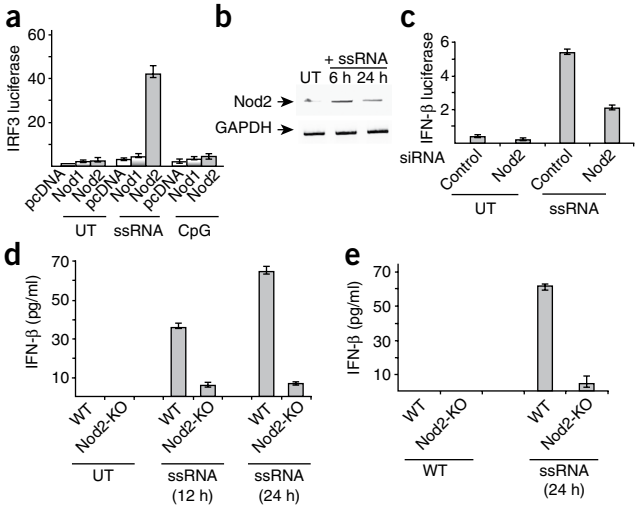

Figure 1 Activation of Nod2 by ssRNA. (**a**) Activation of an IRF3 luciferase reporter in 293 cells transfected with pcDNA, human HA-Nod1 or human HA-Nod2 and left untreated (UT) or treated for 6 h with ssRNA or CpG DNA. (**b**) RT-PCR analysis of Nod2 expression in A549 cells left untreated or stimulated with ssRNA (time, above lanes). (**c**) Activation of an IFN-β luciferase reporter in A549 cells transfected with control siRNA or Nod2-specific siRNA and left untreated or stimulated for 6 h with ssRNA. (**d**,**e**) Enzyme-linked immunosorbent assay (ELISA) of IFN-β production by wild-type (WT) and Nod2-deficient (Nod2-KO) BMMs (**d**) or MEFs (**e**) left untreated or stimulated with ssRNA (time, below graphs). Data are representative of three independent experiments (**a**,**c**–**e**; mean ± s.d.) or three experiments (**b**).

HA-Nod2 and HA-Nod1 proteins were functional, as they facilitated activation of NF-κB in 293 cells treated with MDP or γ-D-glutamyl-meso-diaminopimelic acid, respectively (**Supplementary Fig. 1d**).

To establish the physiological relevance of Nod2-mediated, ssRNA-induced activation of IRF3, we next evaluated the function of endogenous Nod2 in inducing IRF3-interferon after ssRNA treatment. For these studies we used human lung epithelial A549 cells, as these cells are permissive to most viruses that have ssRNA genomes and endogenously express various PRRs. Treatment of these cells with ssRNA resulted in higher expression of Nod2 (**Fig. 1b**); Nod1 expression remained unchanged (data not shown). Nod2-specific small interfering RNA (siRNA) diminished Nod2 expression in ssRNA-treated A549 cells (**Supplementary Fig. 2a**) and impaired ssRNA-induced activation of IRF3 and IFN-β (**Fig. 1c** and **Supplementary Fig. 2b**).

Similarly, ssRNA-induced production of IFN-β was lower in bone marrow–derived macrophages (BMMs) and mouse embryo fibroblasts (MEFs) isolated from Nod2-deficient than in those from wild-type mice (**Fig. 1d**,**e**). In contrast, wild-type and Nod2-deficient BMMs and MEFs produced similar amounts of IFN-β after treatment with poly(I:C) (double-stranded RNA that activates TLR3; **Supplementary Fig. 2c**). The ability of poly(I:C) to induce interferon (via TLR3) in both wild-type and Nod2-deficient MEFs showed that the IRF3-interferon pathway is intact in Nod2-deficient mice. Furthermore, administration of poly(I:C) *in vivo* resulted in the production of similar concentrations of IFN-β in wild-type and Nod2-deficient mice (**Supplementary Fig. 2d**). Thus, our results obtained with cell lines and primary cells demonstrate that activation of Nod2 by ssRNA results in IFN-β production.

Nod2 facilitates virus-induced interferon production

To further confirm the ability of Nod2 to launch an antiviral response, we infected 293 cells with RSV. RSV induced activation of IRF3 and IFN-β in 293 cells expressing HA-Nod2 but not in 293 cells expressing HA-Nod1 (**Fig. 2a**,**b**). Inactivation of virion particles with ultraviolet light abolished the ability of RSV to activate IRF3 in Nod2-expressing cells (**Fig. 2a**). The inability of RSV inactivated by ultraviolet light to activate IRF3 indicated that an intact viral RNA genome is essential for Nod2 activation. The direct function of viral components in Nod2 activation was further confirmed by the loss of IRF3 activation after inhibition of RSV cellular entry with an RSV-neutralizing antibody (specific for the RSV fusion protein; **Supplementary Fig. 2e**).

We established the functional importance of Nod2 in antiviral responses with the interferon-sensitive vesicular stomatitis virus (VSV). Plaque assay of VSV titers obtained from 293 cells expressing HA-Nod2 or HA-Nod1 showed that cells expressing HA-Nod2 had much lower viral titers (**Fig. 2c**). Like VSV, RSV titers were lower in Nod2-expressing cells than in Nod1-expressing cells (**Fig. 2d**). Human parainfluenza virus type 3 (ref. 17) and VSV[18] also activated IRF3 in Nod2-expressing 293 cells (**Supplementary Fig. 3a**). In contrast, vaccinia virus, a DNA virus, failed to activate IRF3 in Nod2-expressing cells (**Supplementary Fig. 3b**). These results demonstrated that like the RLH receptors RIG-I and Mda5, Nod2 can function as a cytoplasmic PRR for a viral ssRNA genome (viral ssRNA).

We next evaluated the function of endogenous Nod2 in inducing IRF3-interferon in response to RSV infection. Published studies have described IRF3 activation and IFN-β production in RSV-infected A549 cells as early as 2 h after infection[19,20]. Although uninfected A549 cells did not have detectable expression of Nod2, RSV infection resulted in higher Nod2 expression within 2 h of infection (**Fig. 3a**). RSV infection failed to induce Nod1 expression (data not shown). Nod2-specific siRNA markedly diminished Nod2 expression after RSV infection (**Supplementary Fig. 4a**) and resulted in less activation of IRF3 and IFN-β after RSV infection (**Fig. 3b** and **Supplementary Fig. 4b**). The effect was more pronounced during early time points after infection (4 h and 6 h) than later (10 h) after infection (**Fig. 3b**). This result suggests that Nod2 is critical for the early antiviral response, whereas during late time periods after infection, other PRRs (such as RIG-I) may activate the IRF3-interferon pathway.

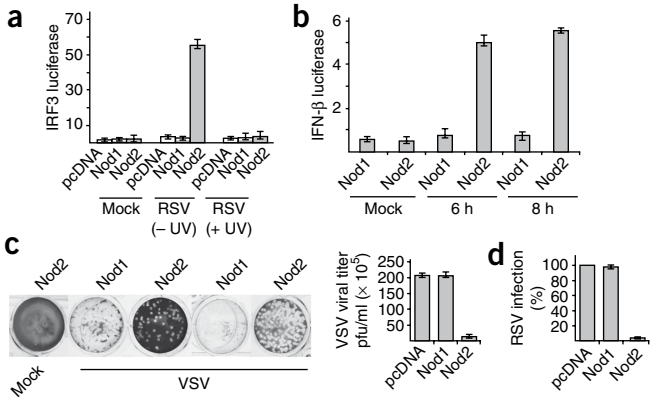

Figure 2 Activation of antiviral response by Nod2 in virus infected cells. (**a**,**b**) Activation of IRF3 (**a**) and IFN-β (**b**) luciferase reporter genes in mock-infected and RSV-infected 293 cells expressing pcDNA, HA-Nod1 or HA-Nod2. (**a**) Luciferase activity 6 h after infection in cells with (+UV) or without (–UV) treatment with ultraviolet irradiation. (**b**) Time after infection, below graph. (**c**) Plaque assay of VSV infectivity in 293 cells expressing pcDNA, HA-Nod1 or HA-Nod2, presented as crystal violet staining (left) and VSV titer (right; plaque-forming units (PFU) per ml). (**d**) RSV infectivity in 293 cells expressing pcDNA, HA-Nod1 or HA-Nod2, presented relative to viral titer in cells expressing pcDNA, set as 100%. Data are representative of three independent experiments (mean ± s.d.).

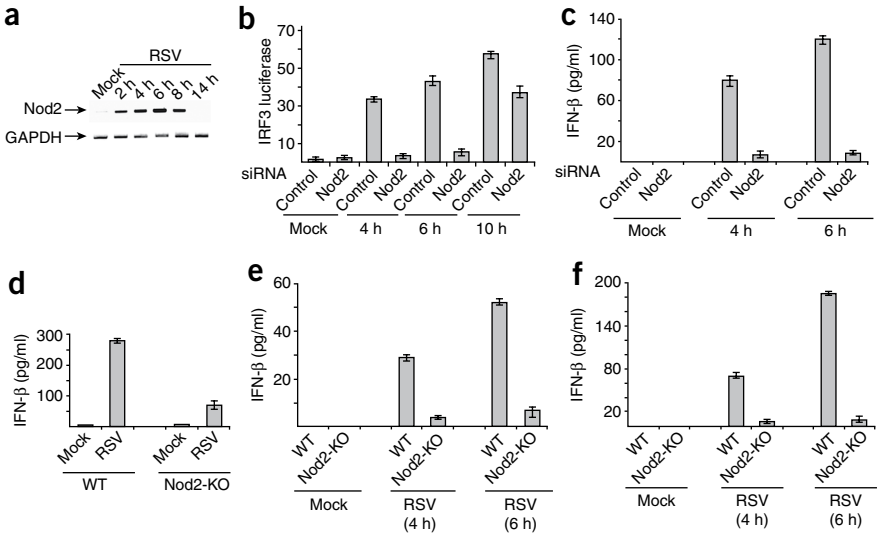

Figure 3 Nod2 is required for interferon production. (**a**) RT-PCR analysis of Nod2 expression in mock- and RSV-infected A549 cells. (**b**) Activation of an IRF3 luciferase reporter in mock- and RSV-infected A549 cells transfected with control or Nod2-specific siRNA (time after infection, below graph). (**c**) ELISA of IFN-β production by mock- and RSV-infected primary NHBE cells transfected with control or Nod2-specific siRNA. (**d**–**f**) ELISA of IFN-β production by mock- and RSV-infected alveolar macrophages (**d**), BMMs (**e**) and MEFs (**f**) isolated from wild-type or Nod2-deficient mice. Data are representative of three experiments (**a**) or three independent experiments (**b**–**f**; mean ± s.d.).

Indeed, as shown before[20], we found that RIG-I expression in A549 cells was detectable only at late time points after infection with RSV (**Supplementary Fig. 4c**). In addition, the early antiviral response was independent of RIG-I, because silencing of RIG-I had no effect in IFN-β expression during early RSV infection (**Supplementary Fig. 4d**,**e**). Like A549 cells, MEFs did not express abundant Nod2 until early time points after RSV infection, and RIG-I was undetectable until late time points after RSV infection (**Supplementary Fig. 4f**,**g**). Thus, temporal expression of Nod2 and RIG-I during early and late infection, respectively, may facilitate optimal sustained interferon production by virus-infected cells.

Next we examined the function of Nod2 in primary normal human bronchial epithelial cells (NHBE cells), as these cells constitute the main cell type infected by RSV in humans. RSV rapidly induced Nod2 expression in NHBE cells (**Supplementary Fig. 5**). Nod2 was essential for interferon production, as Nod2-specific siRNA markedly diminished IFN-β production by RSV-infected NHBE cells (**Fig. 3c**). We further established the critical function of Nod2 by demonstrating that BMMs, MEFs and alveolar macrophages derived from Nod2-deficient mice produced less IFN-β than did their wild-type counterparts after RSV infection (**Fig. 3d**–**f**). Nod2-deficient MEFs and BMMs also showed defective IFN-β production after infection with influenza A/PR/8/34 (H1N1) virus (**Supplementary Fig. 6**). Collectively these data show an important function for endogenous Nod2 in the induction of antiviral immune responses.

Nod2 interacts with viral ssRNA

We next investigated the function of viral ssRNA in Nod2 activation. Viral ssRNA genome isolated from purified RSV virion particles activated IRF3 only in Nod2-expressing cells (**Fig. 4a**). An intact ssRNA genome was required for Nod2 activation, as treatment of the viral ssRNA with RNAse abolished IRF3 activation (**Fig. 4a**). Viral ssRNA uses Nod2 for interferon production, as we found less IFN-β production after viral ssRNA treatment in MEFs and BMMs isolated from Nod2-deficient mice than in those from wild-type mice (**Fig. 4b**,**c**).

The function of viral ssRNA as an activator of Nod2 was further demonstrated by the interaction of viral ssRNA with Nod2 in a cellular milieu. We immunoprecipitated HA-Nod2 from RSV-infected 293 cells transfected with HA-Nod2 and amplified bound RNA with primers specific for either glyceraldehyde phosphate dehydrogenase (GAPDH; control) or RSV nucleocapsid protein. These experiments demonstrated association of Nod2 with viral RNA but not with control RNA (**Fig. 4d**). In a cell-free assay, we incubated HA-Nod2 bound to HA-agarose beads with RSV ssRNA genome or mRNA isolated

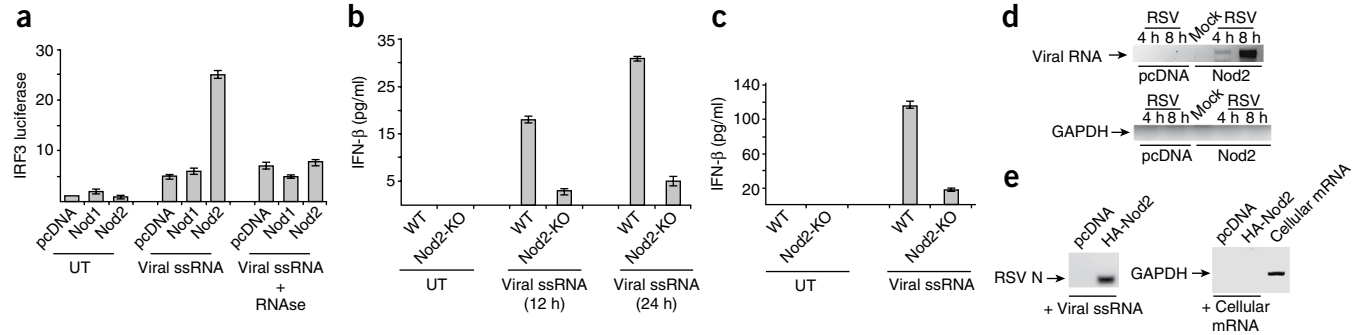

Figure 4 Activation of Nod2 by viral ssRNA. (**a**) Activation of an IRF3 luciferase reporter in 293 cells expressing pcDNA, HA-Nod1 and HA-Nod2 that were left untreated or stimulated with RSV viral ssRNA; + RNAse (below graph), viral ssRNA treated with RNAse. (**b**,**c**) ELISA of IFN-β production by wild-type or Nod2-deficient BMMs (**b**) and MEFs (**c**) left untreated or stimulated with viral ssRNA. (**d**) Association of Nod2 with RNA in 293 cells transfected with pcDNA or HA-Nod2 and then mock infected or infected with RSV; at 4 h or 8 h after infection, Nod2 was immunoprecipitated with anti-HA agarose and bound RNA was amplified with primers specific for RSV nucleocapsid protein (top) or GAPDH (bottom), followed by agarose gel electrophoresis. (**e**) Cell-free assay of HA-Nod2 bound to anti-HA agarose beads, incubated with RSV ssRNA (left) or total cellular mRNA (right); bound RNA was amplified with the primers in **d**, followed by agarose gel electrophoresis. Far right, total cellular mRNA amplified with GAPDH-specific primer (positive control). Data are representative of three independent experiments (**a**–**c**; mean ± s.d.) or two experiments (**d**,**e**).

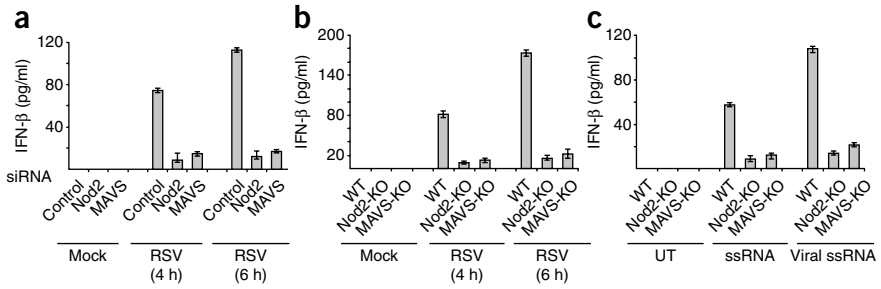

Figure 5 Function of MAVS during Nod2-mediated activation of the antiviral pathway. (**a**) ELISA of IFN-β production by mock- and RSV-infected primary NHBE cells transfected with control, Nod2-specific or MAVS-specific siRNA. (**b**) ELISA of IFN-β production by mock- and RSV-infected MEFs isolated from wild-type, Nod2-deficient or MAVS-deficient (MAVS-KO) mice. (**c**) ELISA of IFN-β production by MEFs left untreated or stimulated with synthetic ssRNA or viral (RSV) ssRNA. Data are representative of three independent experiments (mean ± s.d.).

from cells. After incubation, we amplified bound RNA with primers specific for either GAPDH or RSV nucleocapsid protein; we detected interaction of Nod2 with RSV ssRNA (**Fig. 4e**). In contrast, GAPDH mRNA (total cellular mRNA is enriched for this) did not associate with Nod2 (**Fig. 4e**). We also noted a failure of Nod1 to interact with viral ssRNA (data not shown). These results demonstrate that interaction of viral ssRNA with Nod2 results in its activation and subsequent induction of interferon production.

MAVS is required for Nod2-mediated responses

We next focused on the mechanism used by Nod2 to activate IRF3-interferon. As both RIG-I and Nod2 have caspase-recruitment domains (CARDs)[6–9], we speculated that similar to RIG-I, Nod2 may also interact with MAVS. In addition, a study has shown that the NLR family member NLRX1 interacts with mitochondria-localized MAVS through its NBD, a domain also found in Nod2 (ref. 11). The interaction of Nod2 with MAVS was essential for Nod2-mediated activation of antiviral responses, as MAVS-specific siRNA (**Supplementary Fig. 7**) and Nod2-specific siRNA (**Fig. 5a**) diminished RSV-induced production of IFN-β from infected NHBE cells to a similar extent. We obtained similar results with MEFs derived from MAVS-deficient mice infected with RSV or transfected with viral or synthetic ssRNA (**Fig. 5b**,**c**). Influenza A virus also required MAVS for interferon production, as IFN-β production by Nod2-deficient and MAVS-deficient

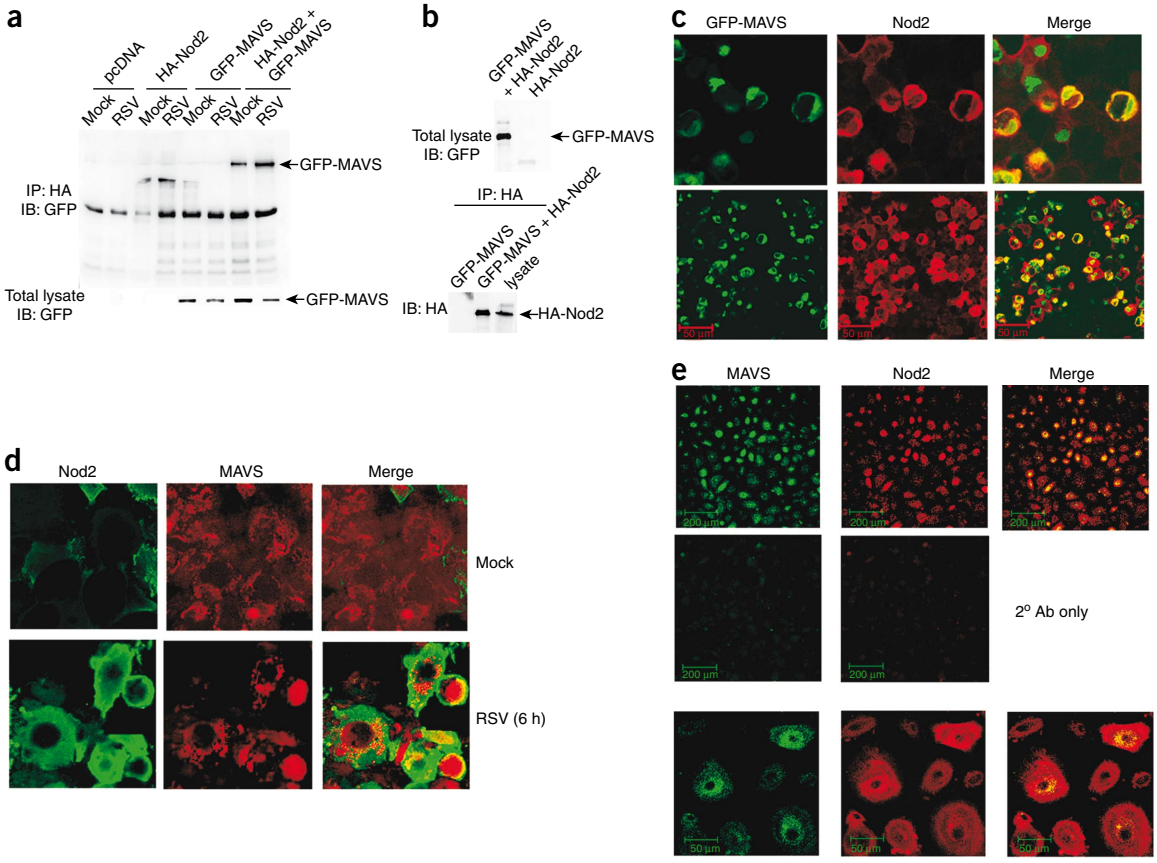

Figure 6 Interaction of MAVS with Nod2. (**a**) Immunoblot (IB) analysis of proteins immunoprecipitated (IP) with anti-HA–agarose beads from lysates of 293 cells transfected with pcDNA, HA-Nod2 and/or GFP-MAVS and mock infected or infected with RSV, probed with anti-GFP. Bottom, immunoblot analysis of 25 μg total cellular lysate with anti-GFP. (**b**) Immunoblot analysis of GFP-MAVS and HA-Nod2 in lysates (25 μg total cellular lysate protein probed with anti-GFP and anti-HA; top) and of HA-Nod2 bound to anti-HA agarose beads (bottom). (**c**) Confocal microscopy of RSV-infected (4 h) 293 cells coexpressing GFP-MAVS (green) and HA-Nod2 (red). (**d**,**e**) Confocal microscopy of mock- or RSV-infected (6 h) A549 cells (**d**) or RSV-infected (4 h) NHBE cells (**e**) stained with anti-Nod2 and anti-MAVS. Original magnification, ×40 (**c**, top row), ×20 (**c**, bottom row), ×40 (**d**), ×10 (**e**, top and middle rows) or ×40 (**e**, bottom row). Data are representative of three (**a**,**b**) or two (**c**–**e**) experiments.

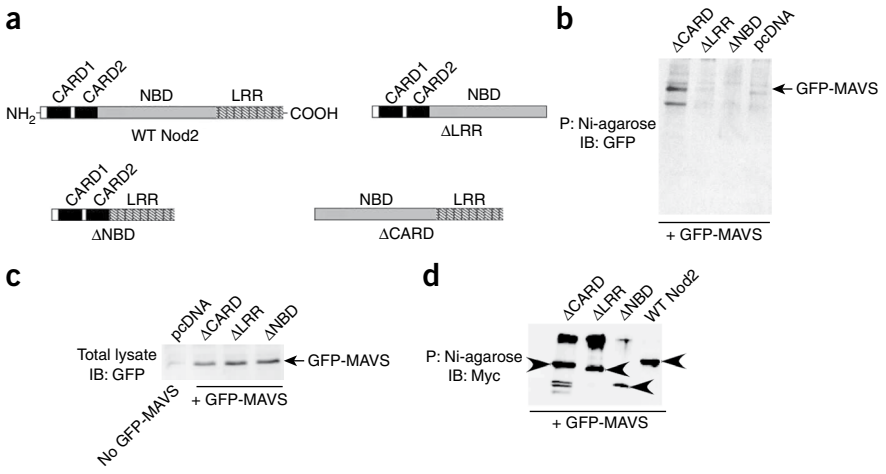

Figure 7 The NBD and LRR domains of Nod2 are essential for interaction with MAVS. (**a**) Nod2 constructs with deletion of specific domains. (**b**) Binding of Nod2 to MAVS in 293 cells expressing various His-Myc–tagged Nod2 constructs or pcDNA along with GFP-MAVS; cell lysates were incubated with nickel-agarose beads (Ni-agarose), then beads were washed and bound proteins were analyzed by immunoblot with anti-GFP. P, precipitation. (**c**) Immunoblot analysis of the expression of GFP-MAVS lysates of the cells in **b**, probed with anti-GFP. Far left, cells transfected with pcDNA only. (**d**) Immunoblot analysis of lysates of 293 cells expressing wild-type Nod2 or His-Myc–tagged Nod2 constructs along with GFP-MAVS, incubated with nickel-agarose, probed with anti-Myc to detect Nod2 constructs bound to the nickel-agarose beads. Arrowheads indicate wild-type Nod2 and deletion constructs of Nod2. Data are representative of three experiments.

MEFs was diminished to a similar extent after influenza A infection (**Supplementary Fig. 8**). These results demonstrate that MAVS is critical for virus-induced Nod2-mediated interferon production.

We next examined interaction of Nod2 with MAVS. Initially we investigated the ability of activated Nod2 to translocate to the mitochondria. Immunoblot analysis of mitochondrial extracts from RSV-infected Nod2-expressing cells showed that although approximately 6–7% of Nod2 was located in mitochondria in uninfected cells, RSV infection resulted in enrichment of Nod2 in mitochondria (40–45% of total cellular Nod2; **Supplementary Fig. 9a**,**b**). Immunofluorescence analysis also showed localization of endogenous Nod2 together with mitochondria in RSV-infected A549 cells (**Supplementary Fig. 9c**). To study the interaction of Nod2 with MAVS, we transfected 293 cells with HA-Nod2 and green fluorescent protein (GFP)-tagged MAVS. Coimmunoprecipitation analysis showed interaction of Nod2 with MAVS (**Fig. 6a**), and this interaction was enhanced after RSV infection. Cells had high expression of GFP-MAVS, as detected by immunoblot analysis of cell lysates with antibody to GFP (anti-GFP; **Fig. 6a**), and a substantial amount of HA-Nod2 was bound to the anti-HA–agarose beads used to precipitate the HA-Nod2–GFP-MAVS complex (**Fig. 6b**). In contrast to Nod2, Nod1 failed to interact with MAVS (**Supplementary Fig. 9d**). Double-labeling immunofluorescence studies with RSV-infected 293 cells expressing GFP-MAVS and HA-Nod2 confirmed the colocalization of Nod2 and MAVS (**Fig. 6c**). Similarly, RSV infection of A549 cells (**Fig. 6d**) and NHBE cells (**Fig. 6e**) enhanced the colocalization of endogenous Nod2 with endogenous MAVS. These results demonstrate that Nod2 interacts with MAVS during virus infection.

Nod2 can activate the NF-κB and mitogen-activated protein kinase pathways through the kinase RICK (also known as Rip2, CARDIAK, CCK or Ripk2)[21,22]. Bacterial products such as MDP specifically stimulate Nod2 and result in NF-κB activation via RICK. However, treatment of Nod2-expressing 293 cells with MDP did not activate IRF3 (**Supplementary Fig. 10a**). Likewise, treatment of NHBE cells and BMMs with MDP did not result in IFN-β production (**Supplementary Fig. 10b**,**c**). In addition, RICK may not be important in interferon induction by Nod2, as silencing of endogenous RICK expression did not alter Nod2-mediated production of IFN-β in RSV-infected cells (**Supplementary Fig. 11**). We also examined the efficiency of the interaction between Nod2 and MAVS relative to that of RIG-I and MAVS. Although both Nod2 and RIG-I associated with MAVS, the RIG-I–MAVS interaction was slightly more efficient than the Nod2-MAVS interaction (**Supplementary Fig. 12a**). In addition, we also noted that in RSV-infected cells, Nod2 interacted more efficiently with MAVS than with RICK (**Supplementary Fig. 12b**). However, Nod2 efficiently interacted with RICK in cells stimulated with the well-established Nod2 stimulator MDP (**Supplementary Fig. 12b**). Thus, we speculate that Nod2 uses either RICK or MAVS, depending on the stimulus (for example, MDP versus ssRNA) to activate either IRF3 or NF-κB.

In addition to IRF3, NF-κB activation is required for the expression of interferon genes. Although IRF3 alone is able to induce the transcription of interferon genes, the transactivating function of NF-κB acts synergistically with IRF3 to promote optimal interferon expression[23]. This is also true for Nod2-mediated interferon expression, as suppressing NF-κB activity in RSV-infected cells diminished interferon expression via activated Nod2 by 30–35%; as expected, expression of the NF-κB-dependent TNF gene in RSV-infected cells was diminished by 80% (**Supplementary Fig. 13**). On the basis of these results, we speculate that Nod2 activated by stimulation with viral ssRNA interacts with MAVS to induce activation of both IRF3 and NF-κB in a way similar to that of RLHs[6]. In contrast, Nod2 activated by bacterial products (such as MDP) activates NF-κB via RICK. Further detailed studies are needed to investigate the function of Nod2 in activating the NF-κB pathway during virus infection and the function of MAVS and RICK during these events.

MAVS interacts with the LRR-NBD domains of Nod2

The CARD of RIG-I promotes its association with MAVS, whereas NLRX1 uses its NBD to interact with MAVS. Thus, we next investigated the function of the NBD, CARD and LRR domains of Nod2 in MAVS association. For these studies, we generated various Nod2 deletion mutants tagged with both histidine (His) and Myc:ΔCARD (a Nod2 mutant lacking both CARDs), ΔNBD (a Nod2 mutant lacking the NBD) and ΔLRR (a Nod2 mutant lacking the LRR domain; **Fig. 7a**). We expressed these mutants in 293 cells along with GFP-MAVS. We obtained lysates of these cells and precipitated the lysates with nickel-agarose beads and, after washing the beads, analyzed the proteins bound to the beads by immunoblot with anti-GFP. Although ΔCARD was able to interact with MAVS, neither ΔNBD nor ΔLRR associated with MAVS (**Fig. 7b**). The various Nod2 mutant–expressing cells expressed similar amounts of GFP-MAVS (**Fig. 7c**). In addition, similar amounts of His-Myc–tagged Nod2 mutants were bound to the nickel-agarose beads in the experimental conditions used to study the interaction of MAVS with the Nod2 mutants (**Fig. 7d**). These results indicate that unlike RIG-I, the CARDs

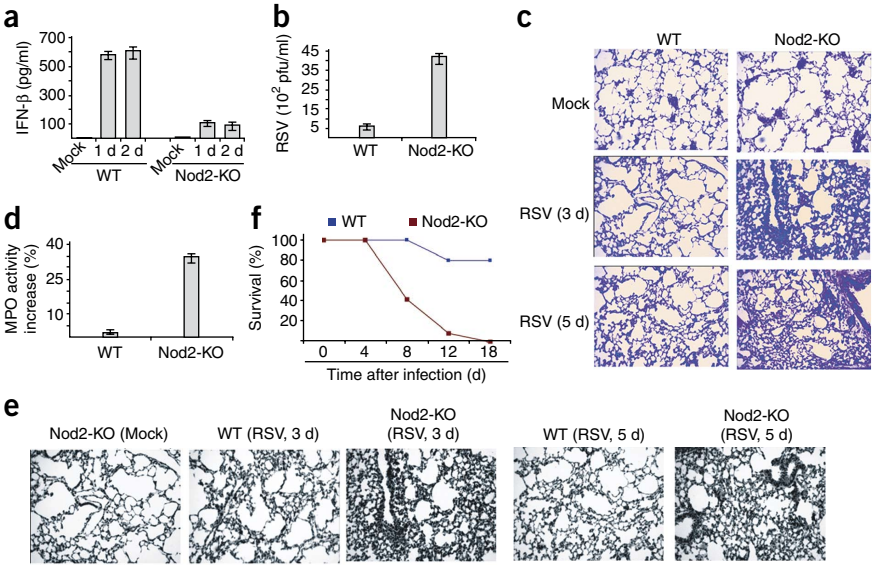

Figure 8 Nod2 is essential for host defense against viral infection. (**a**) IFN-β concentrations in BAL fluid of mock- or RSV-infected wild-type and Nod2-deficient mice ($n = 4$ mice per group). $P < 0.05$ (*t*-test for data normally distributed; Mann-Whitney rank sum test for data not normally distributed). (**b**) RSV titers in the BAL fluid of wild-type and Nod2-deficient mice at 3 d after infection. $P < 0.05$ (*t*-test for data normally distributed; Mann-Whitney rank sum test for data not normally distributed). (**c**) Hematoxylin and eosin staining of lung sections from mock- or RSV-infected wild-type and Nod2-deficient mice. Original magnification, ×10. (**d**) Neutrophil sequestration in lungs, assessed by MPO activity assay of total lung homogenates of RSV-infected wild-type and Nod2-deficient mice ($n = 5$ mice per group; 10 mice total) at 2 d after infection, presented relative to activity in mock-infected mice. $P < 0.05$. (**e**) TUNEL staining of lung sections from RSV-infected wild-type and Nod2-deficient mice. Original magnification, ×10. (**f**) Survival of wild-type and Nod2-deficient mice infected with RSV (5×10^8 PFU per mouse). $P > 0.02$, Nod2-deficient versus wild-type (Wilcoxon test). Data are representative of three (**a**,**b**,**d**) or four (**c**,**e**,**f**) experiments (mean ± s.e.m in **a**,**b**,**d**).

of Nod2 are not important for its interaction with MAVS. However, the NBD and LRR domains of Nod2 are required for the MAVS association. We further confirmed that conclusion by examining the functionality of the Nod2 mutants in activating IRF3. Infection of 293 cells transfected with either wild-type or mutant (ΔCARD, ΔNBD or ΔLRR) Nod2 constructs showed that wild-type Nod2 and ΔCARD induced IRF3 activation after infection with RSV, but neither ΔNBD nor ΔLRR did so (**Supplementary Fig. 14**).

Function of Nod2 in the host antiviral defense

Finally, we assessed the physiological function of Nod2 by infecting wild-type and Nod2-deficient mice with RSV. The mouse model of RSV infection mimics virus infection in humans, as infected mice can develop disease states resembling pneumonia[24,25]; in addition, RSV-infected mice induce a robust antiviral response in the respiratory tract characterized by production of IFN-β and expression of interferon-dependent genes such as *Mx1* during early RSV infection (within 12 h of infection)[24–30]. Moreover, RSV is sensitive to interferon in infected mice, as a dose of interferon as low as 200 units per ml inhibits RSV infection in mice by 100-fold (ref. 26). During RSV infection of the mouse respiratory tract, interferon is induced early during infection (at 12 h to 2 d after infection), but its production is lost at 3 d after infection[24–30]. This observation suggests that interferon is important in restricting the spread of RSV during early infection and that the production of interferon dictates the clinical outcome of the disease (for example, lung inflammation and apoptosis of airway cells).

We infected wild-type and Nod2-deficient mice with a sublethal dose of RSV (5×10^6 plaque-forming units per mouse, delivered by intranasal inoculation), then collected lungs and bronchoalveolar lavage (BAL) fluid at various times. We found expression of mouse Nod2 in RSV-infected lungs at 1 d after infection, and this expression was lost at 4 d after infection (**Supplementary Fig. 15a**). This result suggests an important function for Nod2 in interferon expression, as the interferon-induction kinetics correlated with the Nod2-expression kinetics[24–30]. Nod2-deficient mice had lower IFN-β production in the respiratory tract and higher viral titers than did wild-type mice (**Fig. 8a**,**b**).

It is well known that RSV causes lung disease by inducing pneumonia, a massive inflammation of the lungs[31]. A larger viral burden ultimately results in enhanced inflammation and exaggerated lung disease due to flooding of alveolar spaces with edema fluid. This occurs as a result of enhanced permeability of the epithelial barrier due to apoptosis of airway epithelial cells. RSV infection resulted in more severe lung pathology in Nod2-deficient mice, as shown by staining of lung sections with hematoxylin and eosin at 3 and 5 d after infection (**Fig. 8c**). We noted massive peribronchial lymphocytic inflammation and filling of the lumen with exudates of infiltrating neutrophils and mucus. Neutrophils constitute the main immune cells infiltrating the lung of RSV-infected mice and humans and a large number of these cells in the airway causes severe immunopathology associated with RSV clinical disease[32–34]. To examine neutrophil accumulation in the lungs, we did a myeloperoxidase (MPO) activity assay[35,36] with lung homogenates of RSV-infected wild-type and Nod2-deficient mice. Greater RSV-induced enhancement of neutrophil activity was visible in the lung tissue of Nod2-deficient mice (~35%) than in that of wild-type mice (~4%; **Fig. 8d**). The enhanced inflammation in the respiratory tract of Nod2-deficient mice was also confirmed by higher concentrations of proinflammatory cytokines and chemokines (such as tumor necrosis factor, IL-10 and RANTES) in the BAL fluid of infected Nod2-deficient than in that of wild-type mice (**Supplementary Fig. 15b–d**). A high RSV load has been associated with enhanced apoptosis of airway epithelial cells and infiltrating neutrophil granulocytes, which contributes to the development of lung lesions and injury[37]. Indeed, *in situ* apoptosis analysis of lung sections by TUNEL (terminal deoxynucleotidyl transferase–mediated dUTP nick end-labeling) showed enhanced apoptosis in the lungs of RSV-infected Nod2-deficient mice relative to that in the lungs of RSV-infected wild-type mice (**Fig. 8e**).

Notably, RSV-infected Nod2-deficient mice lost considerably more body weight and had diminished survival relative to their wild-type counterparts (**Fig. 8f** and **Supplementary Fig. 16**). We also found less IFN-β production in the BAL fluid of influenza A virus–infected Nod2-deficient mice than in that of influenza A virus–infected wild-type mice (**Supplementary Fig. 17**). These results demonstrated that Nod2 is a critical component of host antiviral defense mechanisms.

DISCUSSION

In the present study we have identified Nod2 as a viral PRR that can sense viral ssRNA to activate interferon production and antiviral defense. Like RLH receptors, Nod2 associated with MAVS to activate IRF3 and promote interferon production. The importance of Nod2 in host defense was evident from the ability of both cells of the immune response (for example, macrophages) and cells not of the immune response (for example, epithelial cells and MEFs) to use Nod2 for interferon production. The *in vivo* importance of Nod2 in antiviral responses was evident from the enhanced RSV-induced pathogenesis in infected Nod2-deficient mice.

Other PRRs, including RIG-I, may also be involved in activating an antiviral response against paramyxoviruses like RSV[20]. For some time, the *in vivo* relevance of RIG-I in antiviral function was not documented because of the embryonic death of most RIG-I-deficient mice[38]. However, one strain of RIG-I-deficient mice generated by crossing RIG-I-heterozygous mice with ICR outbred mice, followed by intercrossing of the resultant RIG-I-heterozygous mice[38], survives to adulthood. These RIG-I-deficient mice show impaired interferon production and enhanced susceptibility to two positive-sense ssRNA viruses: encephalomyocarditis virus and Japanese encephalitis virus[38]. However, no studies have been done to demonstrate the importance of RIG-I in activating the antiviral host defense apparatus against negative-sense ssRNA viruses (such as paramyxoviruses).

Uninfected mice have low Nod2 expression[39], and we have shown that its expression increased after viral infection. Our observation is similar to those of published studies demonstrating that most PRRs (such as RIG-I) have low expression but their expression is higher after pathogen invasion[40,41]. Similarly, we found that viruses mediated the induction of Nod2 in various cells. Although in our studies we noted induction of Nod2 in virus-infected MEFs, one study has reported that MDP is unable to induce Nod2 expression in wild-type MEFs; this observation may have been due to a defect in MDP transport to the cytoplasm[42]. Several other studies have shown that Nod2 expression is stimulated by various bacteria and bacterial components[40,41]. Similarly, expression of RIG-I (ref. 43) and Mda-5 (ref. 38) in uninfected, unstimulated wild-type MEFs is negligible, but treatment of cells with PAMPs results in upregulation of RIG-I expression[43]. This mechanism of restricting expression of PRRs in unstimulated cells may be critical for preventing uncontrolled inflammation.

Although Nod2 can be activated by MDP[7–10], so far no studies have demonstrated direct binding of MDP to Nod2; it is known only that lack of Nod2 expression results in loss of MDP responsiveness. Thus, MDP could directly interact with Nod2 or associate with a protein or proteins that form a complex with Nod2. In that context, the interaction of viral ssRNA with Nod2 demonstrated here could also be mediated indirectly via 'bridging' proteins. Interaction of the ssRNA genomes of viruses with RIG-I has also been noted before[44,45]. In addition to Nod2, cryopyrin (Nalp3), another NLR protein, activates the inflammasome and leads to IL-1 production after stimulation with bacterial and viral (influenza A) RNA[46–48]. Although NLRs such as cryopyrin[46–48] and NLRX1 (ref. 11) serve an important function in innate immunity by activating the inflammasome and inhibiting interferon production, respectively, no studies have determined whether other NLRs, such as Nod2, can directly contribute to antiviral responses by inducing interferon production.

Published studies have shown that transfection of Nod2 alone (in the absence of any stimulant) into wild-type MEFs results in substantial NF-κB activation[49]. However, we found that overexpression of Nod2 in 293 cells did not induce marked activation of IRF3 in the absence of external stimuli (such as RSV or synthetic or viral ssRNA). Thus, it seems that Nod2-mediated activation of IRF3 is stimulus dependent, whereas RICK activation is stimulus independent. In summary, our findings have demonstrated that in addition to RIG-I, Mda5 and TLRs, Nod2 can also function as a viral PRR and participate in inducing antiviral signaling. Distinct temporal activation of various PRRs may be needed to generate optimal antiviral responses, and various viruses may trigger the induction of different classes of PRRs.

METHODS

Methods and any associated references are available in the online version of the paper at http://www.nature.com/natureimmunology/.

Note: Supplementary information is available on the Nature Immunology website.

ACKNOWLEDGMENTS

We thank K. Li (University of Tennessee Health Science Center) for reagents; A. Garcia-Sastre (Mount Sinai School of Medicine) for influenza A virus; Z.J. Chen (University of Texas Southwestern Medical Center) for MAVS-deficient MEFs; the Core Optical Imaging Facility (University of Texas Health Science Center at San Antonio) for confocal images; and K. Moncada Gorena and C. Thomas in the Flow Cytometry Core Facility (supported by the National Institutes of Health (P30 CA54174 to the San Antonio Cancer Institute; P30 AG013319 to the Nathan Shock Center; and P01AG19316)) for flow cytometry. Supported by National Institutes of Health (AI069062 to S.B., CA129246 to S.B. and T32-DE14318 to A.S. and AI067716 to P.H.D.) and the American Lung Association (RG-49629-N to S.B. and AI067716 to P.H.D.).

AUTHOR CONTRIBUTIONS

A.S. and S.B. designed the experiments and prepared the manuscript; A.S. and T.H.C. did the experiments; R.H. provided technical assistance and did several experiments; Y.X. did the experiments with vaccinia virus; V.F. did the immunofluorescence analysis; K.T. did the studies with mouse embryo fibroblasts; and P.H.D. did the MPO assay.

Published online at http://www.nature.com/natureimmunology/.
Reprints and permissions information is available online at http://npg.nature.com/reprintsandpermissions/.

1. Kawai, T. & Akira, S. Innate immune recognition of viral infection. *Nat. Immunol.* **7**, 131–137 (2006).
2. Bose, S. & Banerjee, A.K. Innate immune response against nonsegmented negative strand RNA viruses. *J. Interferon Cytokine Res.* **23**, 401–412 (2003).
3. Stark, G.R., Kerr, I.M., Williams, B.R.G., Silverman, R.H. & Schreiber, R.D. How cells respond to interferons. *Annu. Rev. Biochem.* **67**, 227–264 (1998).
4. Uematsu, S. & Akira, S. Toll-like receptors and type I interferons. *J. Biol. Chem.* **282**, 15319–15323 (2007).
5. O'Neill, L.A. How Toll-like receptors signal: what we know and what we don't know. *Curr. Opin. Immunol.* **18**, 3–9 (2006).
6. Basler, C.F. & Garcia-Sastre, A. Sensing RNA virus infections. *Nat. Chem. Biol.* **3**, 20–21 (2007).
7. Martinon, F. & Tschopp, J. NLRs join TLRs as innate sensors of pathogens. *Trends Immunol.* **26**, 447–454 (2005).
8. Fritz, J.H., Ferrero, R.L., Philpott, D.J. & Girardin, S.E. Nod-like proteins in immunity, inflammation and disease. *Nat. Immunol.* **7**, 1250–1257 (2006).
9. Kanneganti, T.D., Lamkanfi, M. & Núñez, G. Intracellular NOD-like receptors in host defense and disease. *Immunity* **27**, 549–559 (2007).
10. Franchi, L., Warner, N., Viani, K. & Nuñez, G. Function of Nod-like receptors in microbial recognition and host defense. *Immunol. Rev.* **227**, 106–128 (2009).
11. Moore, C.B. *et al.* NLRX1 is a regulator of mitochondrial antiviral immunity. *Nature* **451**, 573–577 (2008).
12. Tattoli, I. *et al.* NLRX1 is a mitochondrial NOD-like receptor that amplifies NF-κB and JNK pathways by inducing reactive oxygen species production. *EMBO Rep.* **9**, 293–300 (2008).
13. Kota, S. *et al.* Role of human β defensin-2 during tumor necrosis factor-α/NF-κB mediated innate anti-viral response against human respiratory syncytial virus. *J. Biol. Chem.* **283**, 22417–22429 (2008).
14. Voss, E. *et al.* NOD2/CARD15 mediates induction of the antimicrobial peptide human β-defensin-2. *J. Biol. Chem.* **281**, 2005–2011 (2006).
15. Hall, C.B. Respiratory syncytial virus and parainfluenza virus. *N. Engl. J. Med.* **344**, 1917–1928 (2001).
16. Falsey, A.R., Hennessey, P.A., Formica, M.A., Cox, C. & Walsh, E.E. Respiratory syncytial virus infection in elderly and high-risk adults. *N. Engl. J. Med.* **352**, 1749–1759 (2005).
17. Bose, S., Malur, A. & Banerjee, A.K. Polarity of human parainfluenza virus type 3 infection in polarized human lung epithelial A549 cells: Role of microfilament and microtubule. *J. Virol.* **75**, 1984–1989 (2001).

18. Bose, S., Kar, N., Maitra, R., DiDonato, J.A. & Banerjee, A.K. Temporal activation of NF-κB regulates an interferon-independent innate antiviral response against cytoplasmic RNA viruses. *Proc. Natl. Acad. Sci. USA* **100**, 10890–10895 (2003).
19. Jamaluddin, M. *et al.* IFN-β mediates coordinate expression of antigen-processing genes in RSV-infected pulmonary epithelial cells. *Am. J. Physiol. Lung Cell. Mol. Physiol.* **280**, L248–L257 (2001).
20. Liu, P. *et al.* Retinoic acid-inducible gene I mediates early antiviral response and Toll-like receptor 3 expression in respiratory syncytial virus-infected airway epithelial cells. *J. Virol.* **81**, 1401–1411 (2007).
21. Inohara, N., Ogura, Y. & Nuñez, G. Nods: a family of cytosolic proteins that regulate the host response to pathogens. *Curr. Opin. Microbiol.* **5**, 76–80 (2002).
22. Franchi, L. *et al.* Intracellular NOD-like receptors in innate immunity, infection and disease. *Cell. Microbiol.* **10**, 1–8 (2008).
23. Wathelet, M.G. *et al.* Virus infection induces the assembly of coordinately activated transcription factors on the IFN-β enhancer in vivo. *Mol. Cell* **1**, 507–518 (1998).
24. Jafri, H.S. *et al.* Respiratory syncytial virus induces pneumonia, cytokine response, airway obstruction, and chronic inflammatory infiltrates associated with long-term airway hyperresponsiveness in mice. *J. Infect. Dis.* **189**, 1856–1865 (2004).
25. Bolger, G. *et al.* Primary infection of mice with high titer inoculum respiratory syncytial virus: characterization and response to antiviral therapy. *Can. J. Physiol. Pharmacol.* **83**, 198–213 (2005).
26. Guerrero-Plata, A. *et al.* Activity and regulation of α interferon in respiratory syncytial virus and human metapneumovirus experimental infections. *J. Virol.* **79**, 10190–10199 (2005).
27. Guerrero-Plata, A., Casola, A. & Garofalo, R.P. Human metapneumovirus induces a profile of lung cytokines distinct from that of respiratory syncytial virus. *J. Virol.* **79**, 14992–14997 (2005).
28. Pletneva, L.M., Haller, O., Porter, D.D., Prince, G.A. & Blanco, J.C. Induction of type I interferons and interferon-inducible Mx genes during respiratory syncytial virus infection and reinfection in cotton rats. *J. Gen. Virol.* **89**, 261–270 (2008).
29. Chávez-Bueno, S. *et al.* Respiratory syncytial virus-induced acute and chronic airway disease is independent of genetic background: an experimental murine model. *Virol. J.* **2**, 46 (2005).
30. Castro, S.M. *et al.* Antioxidant treatment ameliorates respiratory syncytial virus-induced disease and lung inflammation. *Am. J. Respir. Crit. Care Med.* **174**, 1361–1369 (2006).
31. Hippenstiel, S., Opitz, B., Schmeck, B. & Suttorp, N. Lung epithelium as a sentinel and effector system in pneumonia--molecular mechanisms of pathogen recognition and signal transduction. *Respir. Res.* **7**, 97 (2006).
32. Yasui, K. *et al.* Neutrophil-mediated inflammation in respiratory syncytial viral bronchiolitis. *Pediatr. Int.* **47**, 190–195 (2005).
33. Wang, S.Z. & Forsyth, K.D. The interaction of neutrophils with respiratory epithelial cells in viral infection. *Respirology* **5**, 1–10 (2000).
34. Wang, S.Z. *et al.* Neutrophils induce damage to respiratory epithelial cells infected with respiratory syncytial virus. *Eur. Respir. J.* **12**, 612–618 (1998).
35. Bubeck, S.S., Cantwell, A.M. & Dube, P.H. Delayed inflammatory response to primary pneumonic plague occurs in both outbred and inbred mice. *Infect. Immun.* **75**, 697–705 (2007).
36. Wilmott, R.W., Kitzmiller, J.A., Fiedler, M.A. & Stark, J.M. Generation of a transgenic mouse with lung-specific overexpression of the human interleukin-1 receptor antagonist protein. *Am. J. Respir. Cell Mol. Biol.* **18**, 429–434 (1998).
37. Welliver, T.P. *et al.* Severe human lower respiratory tract illness caused by respiratory syncytial virus and influenza virus is characterized by the absence of pulmonary cytotoxic lymphocyte responses. *J. Infect. Dis.* **195**, 1126–1136 (2007).
38. Kato, H. *et al.* Differential roles of MDA5 and RIG-I helicases in the recognition of RNA viruses. *Nature* **441**, 101–105 (2006).
39. Opitz, B. *et al.* Nucleotide-binding oligomerization domain proteins are innate immune receptors for internalized *Streptococcus pneumoniae*. *J. Biol. Chem.* **279**, 36426–36432 (2004).
40. Matikainen, S. *et al.* Tumor necrosis factor alpha enhances influenza A virus-induced expression of antiviral cytokines by activating RIG-I gene expression. *J. Virol.* **80**, 3515–3522 (2006).
41. Le Goffic, R., Pothlichet, J., Vitour, D., Fujita, T., Meurs, E., Chignard, M. & Si-Tahar, M. Influenza A virus activates TLR3-dependent inflammatory and RIG-I-dependent antiviral responses in human lung epithelial cells. *J. Immunol.* **178**, 3368–3372 (2007).
42. Abbott, D.W. *et al.* Coordinated regulation of Toll-like receptor and NOD2 signaling by K63-linked polyubiquitin chains. *Mol. Cell. Biol.* **27**, 6012–6025 (2007).
43. Wang, J. *et al.* Retinoic acid-inducible gene-I mediates late phase induction of TNF-α by lipopolysaccharide. *J. Immunol.* **180**, 8011–8019 (2008).
44. Hornung, V. *et al.* 5′-Triphosphate RNA is the ligand for RIG-I. *Science* **314**, 994–997 (2006).
45. Pichlmair, A. *et al.* RIG-I-mediated antiviral responses to single-stranded RNA bearing 5′-phosphates. *Science* **314**, 997–1001 (2006).
46. Kanneganti, T.D. *et al.* Bacterial RNA and small antiviral compounds activate caspase-1 through cryopyrin/Nalp3. *Nature* **440**, 233–236 (2006).
47. Kanneganti, T.D. *et al.* Critical role for Cryopyrin/Nalp3 in activation of caspase-1 in response to viral infection and double-stranded RNA. *J. Biol. Chem.* **281**, 36560–36568 (2006).
48. Ichinohe, T., Lee, H.K., Ogura, Y., Flavell, R. & Iwasaki, A. Inflammasome recognition of influenza virus is essential for adaptive immune responses. *J. Exp. Med.* **206**, 79–87 (2009).
49. Kobayashi, K. *et al.* RICK/Rip2/CARDIAK mediates signalling for receptors of the innate and adaptive immune systems. *Nature* **416**, 194–199 (2002).

ONLINE METHODS

Viruses and cell culture. RSV (A2 strain) and VSV were propagated in HeLa and BHK cells, respectively[13,18]. Influenza A virus (A/PR/8/34 (H1N1)) was grown in the allantoic cavities of 10-day-old embryonated eggs. All viruses were purified by centrifugation (twice) on discontinuous sucrose gradients. A549 and 293 cells were maintained in DMEM supplemented with 10% (vol/vol) FBS, penicillin, streptomycin and glutamine. Primary NHBE cells (from Lonza) were maintained in bronchial epithelial growth medium according to the supplier's instruction.

Luciferase assay. First, 293 cells were transfected (Lipofectamine 2000; Invitrogen) with 1 μg of various plasmids (HA-Nod2, HA-Nod1, pcDNA6.1, IRF3-luciferase or IFN-β–luciferase) and 100 ng pRL-null–renilla luciferase. The cells were then infected or treated with RSV, ssRNA or CpG DNA. A549 cells were transfected (Lipofectamine 2000; Invitrogen) with 80 nM Nod2-specific siRNA or control siRNA. At 24 h after siRNA transfection, cells were cotransfected with pRL-null–renilla luciferase (100 ng), IRF3-luciferase (1 μg) or IFN-β–luciferase (1 μg). After 24 h, cells were infected with RSV (multiplicity of infection (MOI), 0.5) or were treated with ssRNA40-LyoVec (1 μg/ml; Invivogen) for various times. Luciferase activity was measured with the Dual-Luciferase Reporter Assay system according to the manufacturer's protocol (Promega). Transfection efficiency was normalized by comparison to expression of renilla luciferase. Luciferase units are presented as relative luciferase activity, which represents the 'fold induction' of luciferase activity after subtraction of the background (cells transfected with pRL-renilla-luciferase plasmid only).

RT-PCR. Primers for detecting the various genes by RT-PCR are in **Supplementary Table 1**.

Generation of siRNA. All siRNA was from Qiagen (sequences, **Supplementary Table 1**). AllStars Negative Control siRNA (proprietary sequence; 1027281; from Qiagen) was used as a negative control. A549 or 293 cells were transfected with siRNA using Lipofectamine 2000 (Invitrogen) and NHBE cells were transfected with siRNA using PrimeFect Primary Cell siRNA Transfection reagent according to the manufacturer's protocol (Lonza).

Viral infection. A549 or 293 cells were infected with purified RSV (MOI, 0.5) in serum-free antibiotic free Opti-MEM (Gibco). After adsorption for 1.5 h at 37 °C, cells were washed twice with serum containing DMEM and infection was continued for various times in the presence of serum-containing DMEM. MEFs were infected with purified RSV or influenza A (A/PR/8/34 virus) at an MOI of 1 in serum-free, antibiotic-free Opti-MEM.

Coimmunoprecipitation. After 293 cells were transfected with various tagged constructs, they were infected with RSV. Cell pellets were lysed (in TBS containing 1% (vol/vol) Triton X-100) and sonicated. All lysates were incubated for 12 h at 4 °C with monoclonal anti-HA agarose beads (HA-7; Sigma-Aldrich). Proteins bound to washed anti-HA–agarose were eluted at a pH of 2.8. Eluted proteins were analyzed by immunoblot with anti-GFP (sc-9996; Santa Cruz) or monoclonal anti-HA (HA-7; Sigma).

Immunofluorescence analysis. Cells plated on four-well glass chamber slides were transfected with various tagged constructs. Cells were then infected for 4 h or 6 h with RSV (MOI, 1). After infection, cells were fixed with 3.7% (wt/vol) formaldehyde and were made permeable and blocked in permeabilization buffer containing 0.2% (vol/vol) Triton X-100 and 3% (wt/vol) BSA and then were incubated for 1 h at 37 °C with monoclonal anti-HA (Sigma), monoclonal anti-Nod2 (2D9; Cayman Chemical) or anti-MAVS (3993; Cell Signaling Technology). The washed cells were then incubated with secondary antibody (Vector Laboratories). Finally, the washed cells were mounted and then imaged with an LSM510 META laser-scanning confocal microscopy (Zeiss).

Interaction of Nod2 with viral ssRNA. After 293 cells were transfected with HA-Nod2, they were infected with RSV. Lysates were immunoprecipitated for 4 h at 4 °C with anti-HA–agarose. After beads were washed with TBS, Tri reagent (TRIzol; Sigma-Aldrich) was added for isolation of bound RNA. Primers specific for RSV nucleocapsid protein or GAPDH were used for RT-PCR. For the cell-free interaction assay, lysates of 293 cells expressing HA-Nod2 were incubated with HA–agarose beads. HA-Nod2 bound to the beads was incubated for 45 min at 4 °C with RSV ssRNA or total cellular mRNA (isolated with an RNeasy Mini kit; Qiagen). Beads were washed and RNA isolated from the washed beads was amplified with primers described above.

Virus infection of mice. Animal studies were approved by the Institutional Animal Care and Use Committee of The University of Texas Health Science Center at San Antonio. Pathogen-free C57BL/6 mice and Nod2-deficient mice (C57BL/6J background) 6–8 weeks old were obtained from The Jackson Laboratory. These Nod2-deficient mice were further back-crossed to the C57BL/6 background for a total of eight generations. Genome-wide single-nucleotide polymorphism analysis of these mice (Harlan Laboratories) showed that wild-type and Nod2-deficient mice are genetically identical, except for the Nod2 deletion (data not shown). Mice were anesthetized with inhaled methoxyfluorane and were inoculated intranasally with RSV (5×10^6 PFU per mouse) in 100 μl low-serum Opti-MEM (Invitrogen). Uninfected control mice were 'sham inoculated' with 100 μl Opti-MEM. For another set of studies, mice were infected intranasally with RSV (5×10^8 PFU per mouse) and the survival of infected mice was monitored for 18 d.

TUNEL and MPO assay. Formalin-fixed lungs were stained with an *in situ* TUNEL assay kit Dead End Colorimetric TUNEL system (Promega). Lung neutrophil content was assessed by measurement of MPO activity[35,36].

Generation of Nod2 mutants. Nod2 cDNA was cloned into the pcDNA6-Myc-His vector (Invitrogen) and deletion mutants of Nod2 were constructed by PCR.

Treatment with synthetic and viral ssRNA. Cells were treated with synthetic ssRNA (1 μg/ml) already conjugated with the transfection reagent (ssRNA40-LyoVec; Invivogen). For isolation of viral ssRNA, purified RSV virion particles were centrifuged for 4 h at 28,000 r.p.m. with an SW32Ti rotor. The ssRNA genome was isolated from the viral pellet with the RNeasy Mini kit. Cells were transfected with viral ssRNA using Lipofectamine 2000 (Invitrogen).

Isolation of MEFs and macrophages. Alveolar macrophages were collected by centrifugation of BAL fluid at 1,300*g* for 10 min at 4 °C. After being washed, cell pellets were seeded in 24-well plates. MEFs were prepared as described[50]. BMMs were obtained from femurs and tibias of wild-type and Nod2-deficient mice and were cultured for 6–8 d.

ELISA. Human or mouse IFN-β-specific ELISA kits (PBL InterferonSource) were used for ELISA.

50. Tominaga, K. *et al.* MRG15 regulates embryonic development and cell proliferation. *Mol. Cell. Biol.* **25**, 2924–2937 (2005).

nature immunology

Recognition of RNA virus by RIG-I results in activation of CARD9 and inflammasome signaling for interleukin 1β production

Hendrik Poeck[1–3,9], Michael Bscheider[3,9], Olaf Gross[1,9,10], Katrin Finger[1], Susanne Roth[1,4], Manuele Rebsamen[5], Nicole Hannesschläger[1], Martin Schlee[2], Simon Rothenfusser[3], Winfried Barchet[2], Hiroki Kato[6], Shizuo Akira[6], Satoshi Inoue[7,8], Stefan Endres[3], Christian Peschel[1], Gunther Hartmann[2,9], Veit Hornung[2,9] & Jürgen Ruland[1,4,9]

Interleukin 1β (IL-1β) is a potent proinflammatory factor during viral infection. Its production is tightly controlled by transcription of *Il1b* dependent on the transcription factor NF-κB and subsequent processing of pro-IL-1β by an inflammasome. However, the sensors and mechanisms that facilitate RNA virus–induced production of IL-1β are not well defined. Here we report a dual role for the RNA helicase RIG-I in RNA virus–induced proinflammatory responses. Whereas RIG-I-mediated activation of NF-κB required the signaling adaptor MAVS and a complex of the adaptors CARD9 and Bcl-10, RIG-I also bound to the adaptor ASC to trigger caspase-1-dependent inflammasome activation by a mechanism independent of MAVS, CARD9 and the Nod-like receptor protein NLRP3. Our results identify the CARD9–Bcl-10 module as an essential component of the RIG-I-dependent proinflammatory response and establish RIG-I as a sensor able to activate the inflammasome in response to certain RNA viruses.

Viral infections are a constant threat to higher organisms, and early detection of viruses by the innate immune system is critical for host defense. Mammalian antiviral immunity is initiated by germline-encoded pattern-recognition receptors that recognize specific pathogen-associated molecular patterns such as viral nucleic acids. After recognizing viral RNA or DNA, pattern-recognition receptors activate signaling pathways that trigger the production of type I interferons and inflammatory cytokines to orchestrate immune responses for virus elimination and thereby produce the clinical symptoms of a viral infection[1]. The viral nucleic acid–recognition receptors include the transmembrane Toll-like receptors (TLRs) TLR3, TLR7, TLR8 and TLR9 (refs. 2–4), the HIN200 family member AIM2 (refs. 5–8) and the cytoplasmic RIG-I-like helicases (RLHs) RIG-I (encoded by *Ddx58*) and Mda5 (encoded by *Ifih1*)[9,10].

RLHs are responsible for the detection of viral RNA in the cytosol[1]. They are composed of an RNA-binding helicase domain, a regulatory domain and two caspase-recruitment domains (CARDs) for signal propagation to the interferon-regulatory factor (IRF) and transcription factor NF-κB signaling pathways. Despite such similarities, the RLHs RIG-I and Mda5 detect distinct RNA viruses. The viruses recognized by RIG-I include vesicular stomatitis virus (VSV) and influenza virus, whereas Mda5 controls responses to picornaviruses (encephalomyocarditis virus (EMCV) and poliovirus) and other viruses[11]. The selective ligand for RIG-I is a 5′ triphosphate on double-stranded RNA[12–15]. The natural ligand for Mda5 remains to be identified, but long stretches of polyinosinic-polycytidylic acid (poly(I:C)) can serve as an artificial agonist for this RLH[16].

To engage downstream pathways after recognizing a virus, RLHs form homotypic CARD-CARD interactions with the adaptor protein MAVS[17–19], which results in the recruitment and activation of further signaling molecules to mitochondria-associated complexes. The adaptors TRAF3, TANK and TRADD and the kinases TBK1 and IKKε are responsible for activation of the transcription factors IRF3 and IRF7 and subsequent synthesis of type I interferon[20]. RLHs additionally activate the proinflammatory NF-κB pathway for the production of cytokines such as interleukin 1β (IL-1β) and IL-6 (ref. 1), but the mechanisms that relay RLH signaling to NF-κB are not well defined.

The production of IL-1β requires, in addition to NF-κB-dependent new synthesis of pro-IL-1β, a second signal that triggers caspase-1 activation. Caspase-1 is responsible for the proteolytic processing of pro-IL-1β into mature, bioactive IL-1β. The activation of caspase-1 in response to many distinct danger signals depends on cytoplasmic multiprotein complexes called inflammasomes, which assemble

[1]III. Medizinische Klinik, Klinikum rechts der Isar, Technische Universität München, Munich, Germany. [2]Institute of Clinical Chemistry and Pharmacology, Universitätsklinikum Bonn, Bonn, Germany. [3]Center of Integrated Protein Science Munich and Division of Clinical Pharmacology, Department of Internal Medicine, University of Munich, Munich, Germany. [4]Laboratory of Signaling in the Immune System, Helmholtz-Zentrum München–Germany, Research Center for Environmental Health, Neuherberg, Germany. [5]Department of Biochemistry, University of Lausanne, Epalinges, Switzerland. [6]Department of Host Defense, Research Institute for Microbial Diseases, Osaka University, Japan. [7]Department of Geriatric Medicine, Graduate School of Medicine, The University of Tokyo, Tokyo, Japan. [8]Research Center for Genomic Medicine, Saitama Medical School, Saitama, Japan. [9]These authors contributed equally to this work. [10]Present address: Department of Biochemistry, University of Lausanne, Epalinges, Switzerland. Correspondence should be addressed to J.R. (jruland@lrz.tum.de).

Received 11 August; accepted 15 October; published online 15 November 2009; doi:10.1038/ni.1824

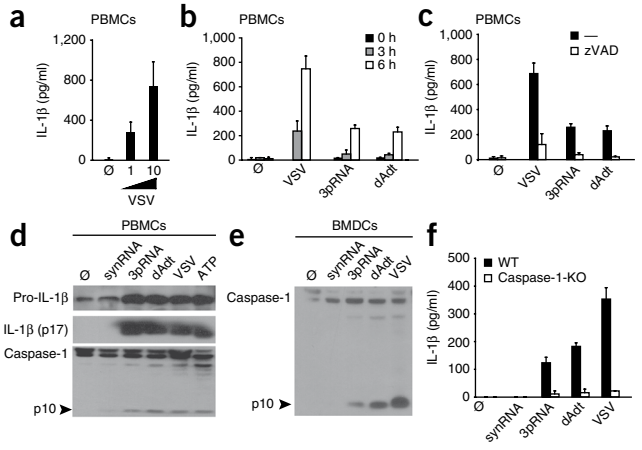

Figure 1 RIG-I signaling is required and sufficient for IL-1β production after infection with an RNA virus. (**a**,**b**) Enzyme-linked immunosorbent assay (ELISA) of IL-1β in supernatants of human PBMCs (2×10^6) left unstimulated (∅) or stimulated for 6 h with VSV at a multiplicity of infection of 1 or 10 (wedge; **a**) or for various times (key) with VSV (multiplicity of infection, 5) or 2 μg/ml of 3pRNA or poly(dA:dT) (dAdT; **b**). (**c**) ELISA of IL-1β production by PBMCs stimulated for 6 h as described in **b**, with (zVAD) or without (–) the addition of 0.05 μM z-VAD-fmk (pan-caspase inhibitor) 1 h before stimulation. (**d**) Immunoblot analysis of mature IL-1β (p17) and processed caspase-1 (p10 subunit) in supernatants of PBMCs stimulated with 2 μg/ml of synthetic dsRNA that lacks the 5′ triphosphate (synRNA), 3pRNA or poly(dA:dT), or with VSV (multiplicity of infection, 5). ATP (far right), LPS-primed PBMCs stimulated with 5 mM ATP (positive control). (**e**) Immunoblot analysis of caspase-1 processing (p10 subunit) in supernatants of BMDCs (1×10^6 cells per ml) stimulated for 6 h as described in **d**. (**f**) ELISA of IL-1β secretion by wild-type (WT) and caspase-1-deficient (Caspase-1-KO) BMDCs treated for 6 h with various stimuli (horizontal axis). Data are representative of three (**a**–**c**) or two (**f**) independent experiments (mean and s.e.m.) or are from one experiment representative of three (**d**) or at least three (**e**) experiments.

from various sensors and associated adaptor proteins in a context-dependent manner[21]. The best understood of these is the NLRP3 (also called NALP3) inflammasome, which activates caspase-1 indirectly via the inflammasome adaptor ASC (also called Pycard) in response to very diverse triggers, including crystals (such as uric acid, silica and asbestos), bacterial pore-forming toxins (such as nigericin), vaccine adjuvants, fungi, and certain DNA and RNA viruses[21–25]. However, the molecular interactions that engage the relatively non-specific NLRP3 inflammasome in response to such distinct stimuli are unclear at present. Another type of inflammasome that has been linked to viral recognition is the AIM2 inflammasome[5–8]. AIM2 is a cytoplasmic DNA receptor that directly interacts with ASC to trigger caspase-1 activation and subsequent IL-1β secretion after infection with a DNA virus. Here we demonstrate that RIG-I serves as a dual sensor that can trigger both NF-κB-dependent production of pro-IL-1β and inflammasome activation in response to certain RNA viruses. In this context, RIG-I engages the CARD9–Bcl-10 module for NF-κB activation and triggers ASC for inflammasome activation in an NLRP3-independent manner.

RESULTS

RIG-I in IL-1β production after VSV infection

To investigate the functions of RIG-I in RNA virus–induced production of IL-1β, we first infected human peripheral blood mononuclear cells (PBMCs) with VSV (**Fig. 1**). PBMCs exposed to VSV secreted mature IL-1β in a dose- and time-dependent manner (**Fig. 1a**,**b**). To selectively assess the role of RIG-I triggering in IL-1β production without considering the effects of viral RNA on other receptor systems, including TLRs, we transfected the cells with the selective RIG-I agonist 5′-triphosphate RNA (3pRNA). RIG-I ligation was sufficient to induce IL-1β production similar to that induced by transfected double-stranded DNA (poly(dA:dT)), which activates the AIM2 inflammasome[5–8] (**Fig. 1b**). Different 3pRNA species with distinct sequences resulted in similar IL-1β secretion (**Supplementary Fig. 1**), which indicated that the specific RNA sequence was not involved.

Next we pretreated PBMCs with the pan-caspase inhibitor z-VAD-fmk (**Fig. 1c**). Caspase inhibition abrogated IL-1β production after stimulation with 3pRNA and poly(dA:dT) and resulted in much less secretion of IL-1β induced by VSV (**Fig. 1c**). Then we analyzed the autocatalytic formation of the active caspase-1 subunit p10 (**Fig. 1d**). Consistent with the production of the mature (p17) form of IL-1β, caspase-1 was processed after activation of the NLRP3 inflammasome induced by ATP after priming with lipopolysaccharide (LPS) or after stimulation of cells with 3pRNA, poly(dA:dT) or VSV (**Fig. 1d**). In contrast, stimulation of cells with a synthetic double-stranded RNA (dsRNA) that lacks the 5′ triphosphate and triggers TLR7 but not RIG-I (ref. 26) did not induce IL-1β production or caspase-1 activation (**Fig. 1d**). Transfection of 3pRNA or poly(dA:dT) or infection with VSV also induced robust caspase-1 activation and IL-1β production in mouse bone marrow–derived dendritic cells (BMDCs), but transfection of the synthetic dsRNA lacking the 5′ triphosphate did not (**Fig. 1e**). As IL-1β production in response to these stimuli was defective in BMDCs from caspase-1-deficient mice (**Fig. 1f**), we conclude that caspase-1 activation is required for the 3pRNA- or VSV-induced proinflammatory responses. Together these results demonstrate that RIG-I engagement activates caspase-1 for IL-1β production.

To investigate whether RIG-I signaling is required for IL-1β production, we used DCs from RIG-I-deficient mice[16] (**Fig. 2**). Consistent with published data indicating that RIG-I ligation

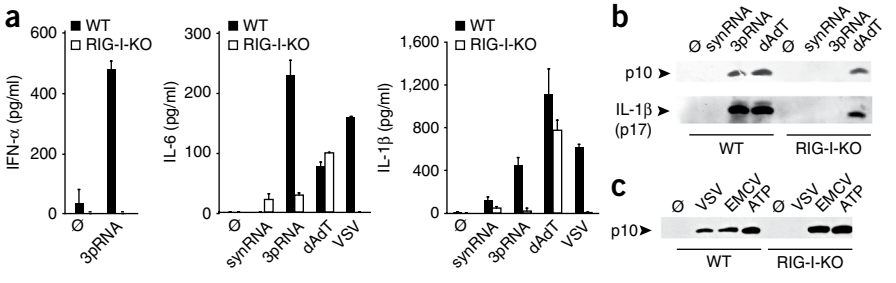

Figure 2 RIG-I controls IL-1β production and caspase-1 activation after detecting RNA viruses. (**a**) ELISA of IFN-α, IL-6 and IL-1β in supernatants of wild-type and RIG-I-deficient (RIG-I-KO) BMDCs treated for 6 h with various stimuli (horizontal axes). (**b**) Immunoblot analysis of caspase-1 processing (p10) and mature IL-1β (p17) in supernatants of the cells in **a**. (**c**) Immunoblot analysis of caspase-1 processing (p10) in wild-type and RIG-I-deficient BMDCs cells treated for 6 h with various stimuli (above lanes). ATP, LPS-primed BMDCs stimulated with 5 mM ATP (positive control). Data are representative of three independent experiments (mean and s.e.m.; **a**) or are from one experiment representative of three (**b**,**c**).

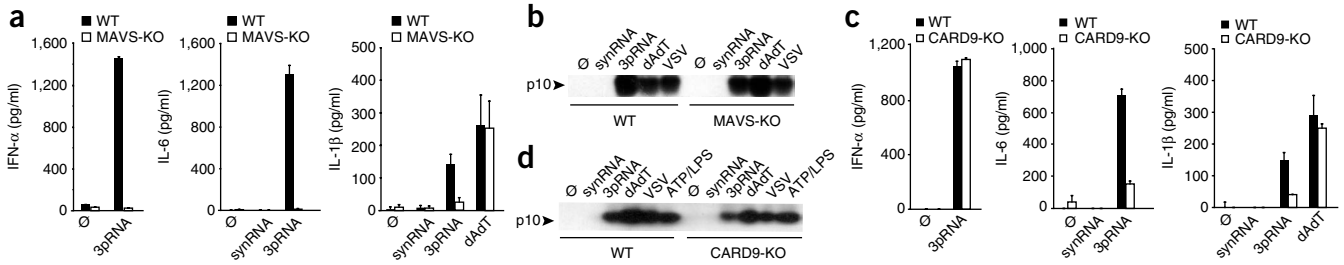

Figure 3 MAVS and CARD9 are essential for RIG-I-induced production of IL-1β but are dispensable for inflammasome activation. (**a**,**b**) ELISA of IFN-α, IL-6 and IL-1β in supernatants of wild-type and MAVS-deficient (MAVS-KO) BMDCs treated for 6 h with various stimuli (horizontal axes). (**b**) Immunoblot analysis of caspase-1 processing (p10) in supernatants of the cells in **a**. (**c**) ELISA of IFN-α, IL-6 and IL-1β in supernatants of wild-type and CARD9-deficient (CARD9-KO) BMDCs treated as described in **a**. (**d**) Immunoblot analysis of caspase-1 processing (p10) in supernatants of the cells in **c**. Data are representative of three (**a**) or at least four (**c**) independent experiments (mean and s.e.m.) or are from one experiment representative of three (**b**) or at least four (**d**) independent experiments.

activates the IRF and NF-κB transcription factors[10], RIG-I-deficient DCs were defective in IRF-controlled production of interferon-α (IFN-α) as well as in NF-κB-regulated secretion of IL-6 after stimulation with 3pRNA or VSV (**Fig. 2a**). RIG-I was required for VSV- or 3pRNA-triggered activation of caspase-1 and production of mature IL-1β p17, although poly(dA:dT) stimulation, exposure to EMCV or activation of NLRP3 with ATP and LPS induced normal activation of caspase-1 in RIG-I-deficient cells (**Fig. 2b**,**c**). Thus, RIG-I controls IRF- and NF-κB-dependent cytokine synthesis as well as inflammasome activation in response to certain RNA viruses.

RIG-I engages MAVS, CARD9 and Bcl-10

To understand the mechanisms that link RIG-I ligation to NF-κB-dependent synthesis of pro-IL-1β and to the activation of caspase-1 and inflammasomes, we investigated the role of the RIG-I effector MAVS in these pathways. Consistent with the essential role of MAVS in the activation of IRF and NF-κB[18,19], MAVS-deficient cells did not synthesize IFN-α or IL-6 after treatment with the RIG-I agonist 3pRNA (**Fig. 3a**). Moreover, MAVS-deficient cells did not secrete IL-1β after activation with RIG-I, although they produced normal amounts of IL-1β after stimulation with poly(dA:dT) (**Fig. 3a**). However, unlike RIG-I-deficient cells, MAVS-deficient BMDCs had normal activation of caspase-1 in response to stimulation with VSV or 3pRNA (**Fig. 3b**). These results indicate that although MAVS signaling is required for RIG-I-mediated production of IL-1β, MAVS engagement is not involved in RIG-I-mediated activation of caspase-1.

The E3 ubiquitin ligase TRIM25 catalyzes lysine 63–linked polyubiquitination of RIG-I to induce the recruitment of MAVS to RIG-I for the activation of effector pathways[27]. Consistent with the data reported above, TRIM25-deficient cells showed defects in IL-1β secretion after VSV infection (**Supplementary Fig. 2a**). However, caspase-1 was activated normally in VSV-infected or 3pRNA-stimulated TRIM25-deficient cells (**Supplementary Fig. 2b**).

Published work has identified the CARD coiled-coil protein CARD9 as a multifunctional adaptor that relays inputs from various pathogens to proinflammatory cascades[28]. We considered that CARD9 might also have a role in RIG-I signaling. To assess that possibility, we treated CARD9-deficient BMDCs with 3pRNA, synthetic dsRNA lacking the 5′ triphosphate, or poly(dA:dT). CARD9-deficient BMDCs showed much less of production IL-6 and IL-1β after stimulation with RIG-I, whereas the responses to poly(dA:dT) remained largely unchanged (**Fig. 3c**). Like MAVS, CARD9 was dispensable for caspase-1 activation (**Fig. 3d**). However, unlike MAVS, CARD9 was completely dispensable for IFN-α secretion (**Fig. 3c**). Thus, CARD9 selectively controls the RIG-I- and MAVS-induced proinflammatory response.

CARD9 is an upstream activator of the NF-κB pathway and of mitogen-activated protein kinases[29–31]. To define the role of CARD9 in RIG-I and MAVS signaling, we measured the activation of NF-κB in BMDCs stimulated with 3pRNA. RIG-I triggered a robust NF-κB response in wild-type BMDCs but not in cells lacking MAVS or CARD9 (**Fig. 4a**), which indicated that the two proteins act together to facilitate NF-κB activation. RIG-I engagement by 3pRNA or VSV also activated the kinases Jnk and p38, although in BMDCs this activation was independent of CARD9 (**Fig. 4b**). To determine the consequences of those findings for IL-1β production, we studied RIG-I-induced synthesis of pro-IL-1β. Consistent with the requirement for NF-κB activation in pro-IL-1β induction, both MAVS-deficient and CARD9-deficient BMDCs showed a defect in 3pRNA-induced synthesis of pro-IL-1β, although they responded normally to poly (dA:dT) (**Fig. 4c**). Accordingly, inhibition of canonical NF-κB signaling with a specific IKK kinase inhibitor, as well as CARD9 deletion, abrogated RIG-I-triggered upregulation of the secretion of pro-IL-1β mRNA and IL-1β protein after VSV infection (**Supplementary Fig. 3**). Thus, MAVS and CARD9 are essential for RIG-I-mediated activation of NF-κB and synthesis of pro-IL-1β. These findings explain why MAVS-deficient and CARD9-deficient cells fail to produce IL-1β although they regularly activate caspase-1 after RIG-I triggering.

CARD9-triggered activation of NF-κB depends on the CARD-containing adaptor Bcl-10 (refs. 28,30), which in turn can recruit the paracaspase MALT1 and use MALT1-dependent or MALT1-independent mechanisms for cell activation[32]. We next stimulated Bcl-10-deficient and MALT1-deficient cells with 3pRNA. BMDCs that lacked Bcl-10, like CARD9-deficient cells, showed severe defects in RIG-I-induced production of pro-IL-1β and secretion of IL-1β and IL-6 but had normal interferon responses (**Fig. 4d–f**) and caspase-1 activation (data not shown). The response to poly(dA:dT) remained unaffected by the Bcl-10 deletion (**Fig. 4e**,**f**). Notably, MALT1 was entirely dispensable for RIG-I-induced cytokine production (data not shown).

Together, the genetic experiments reported above demonstrated a signaling cascade downstream of RIG-I and MAVS that depended on CARD9 and Bcl-10 to control NF-κB-dependent cytokine production. To study the importance of this pathway *in vivo*, we infected wild-type and CARD9-deficient mice with VSV. Intravenous injection induced vigorous production of IFN-α, IL-6 and IL-1β in wild-type mice (**Fig. 4g**). Consistent with the *in vitro* results, the interferon responses were intact, but the concentrations of IL-6 and IL-1β were significantly lower in the serum of CARD9-deficient mice (**Fig. 4g**).

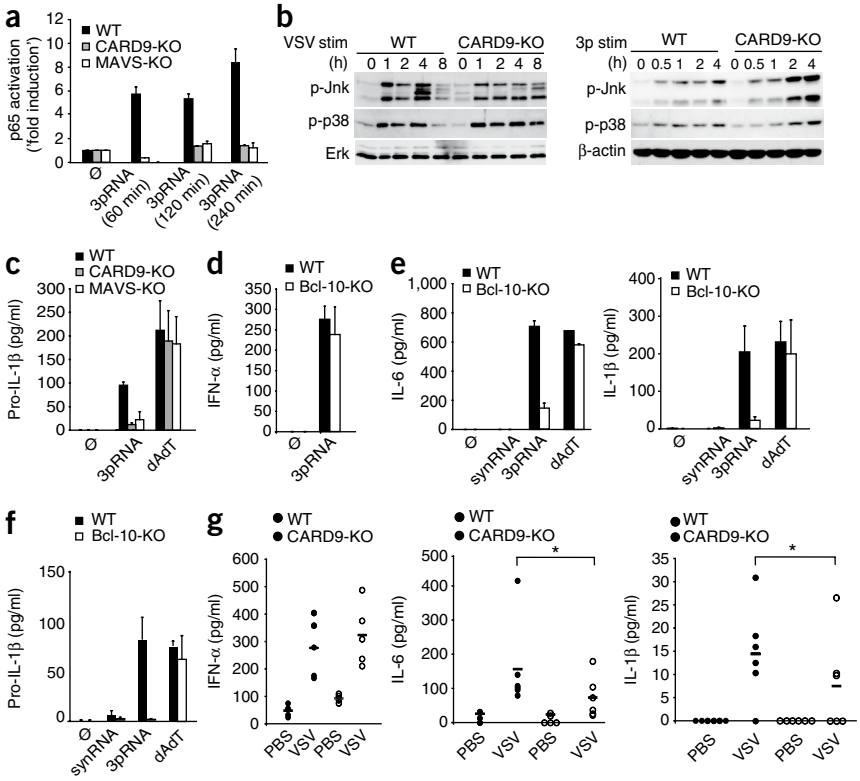

Figure 4 MAVS, CARD9 and Bcl-10 control pro-IL-1β production after RIG-I ligation. (**a**) Activation of the p65 subunit of NF-κB in nuclear protein extracts of wild-type, CARD9-deficient and MAVS-deficient BMDCs stimulated for 60, 120 or 240 min (horizontal axis) with 3pRNA, assessed by enhanced chemiluminescence and presented relative to activation in the unstimulated sample. (**b**) Immunoblot analysis of wild-type and CARD9-deficient BMDCs stimulated for various times (above lanes) with VSV (left) or 3pRNA (right), probed with antibodies specific for phosphorylated (p-) Jnk and p38. Bottom, immunoblot analysis of Erk and β-actin (loading control). (**c**) ELISA of intracellular pro-IL-1β in wild-type, CARD9-deficient and MAVS-deficient BMDCs stimulated for 6 h with 3pRNA or poly(dA:dT), assessed after cell lysis by repeated cycles of freezing and thawing. (**d–f**) ELISA of IFN-α (**d**), IL-6 and IL-1β (**e**), and intracellular pro-IL-1β (**f**) in supernatants of wild-type and Bcl-10-deficient (Bcl-10-KO) BMDCs treated with various stimuli (horizontal axes). (**g**) ELISA of IFN-α, IL-6 and IL-1β in serum collected from wild-type and CARD9-deficient mice 6 h after intravenous injection of 2×10^6 plaque-forming units of VSV or PBS (control). Each symbol represents an individual mouse; small horizontal lines indicate the mean. $^*P < 0.05$ (two-tailed Student's *t*-test). Data are representative of at least three (**a**,**c**) or three (**d–f**) independent experiments (mean and s.e.m.) or two experiments (**g**) or are from one experiment representative of at least four independent experiments (**b**).

RIG-I and ASC form an NLRP3-independent inflammasome

As the role of the MAVS–CARD9–Bcl-10 axis in RIG-I-induced production of IL-1β is restricted to the control of pro-IL-1β synthesis, it is still unclear how RIG-I activates caspase-1. Because the cytosolic bacterium *Francisella tularensis* induces a type I interferon response to indirectly activate caspase-1 (ref. 33), we considered possible indirect effects of interferon in RIG-I-mediated inflammasome activation. However, *Irf3*$^{-/-}$*Irf7*$^{-/-}$ BMDCs[34] which do not produce type I interferons, had normal production of IL-1β after stimulation with 3pRNA or DNA (**Fig. 5a**).

Many classical triggers of inflammasomes require a stimulus-induced potassium efflux for caspase-1 activation[21]. We therefore assessed RIG-I-induced production of IL-1β before and after pre-incubation with the potassium channel inhibitor glibenclamide. This treatment completely abrogated 3pRNA- or VSV-induced secretion of IL-1β, whereas IL-6 production was unaffected (**Fig. 5b**,**c**). We obtained similar results by adding excess extracellular potassium (130 mM) to the medium before RIG-I stimulation (data not shown).

Danger sensors of the NLRP family and the DNA sensor AIM2 activate caspase-1 by binding to ASC[35]. To determine whether RIG-I and ASC also form a caspase-1-activating signaling complex, we immunoprecipitated endogenous ASC from THP-1 human monocytic cells before and after infection with VSV and studied potential RIG-I interactions by immunoblot analysis. RIG-I precipitated together with ASC in uninfected and VSV-infected cells, but Mda5 did not (**Fig. 5d**), which indicated that RIG-I and ASC can form a complex.

To investigate the function of RIG-I–ASC interactions by genetic means, we studied IL-1β production in BMDCs from ASC-deficient mice. In parallel, we analyzed wild-type and NLRP3-deficient DCs. Wild-type DCs showed robust caspase-1 activation and mature IL-1β production in response to triggering of RIG-I with 3pRNA or VSV,

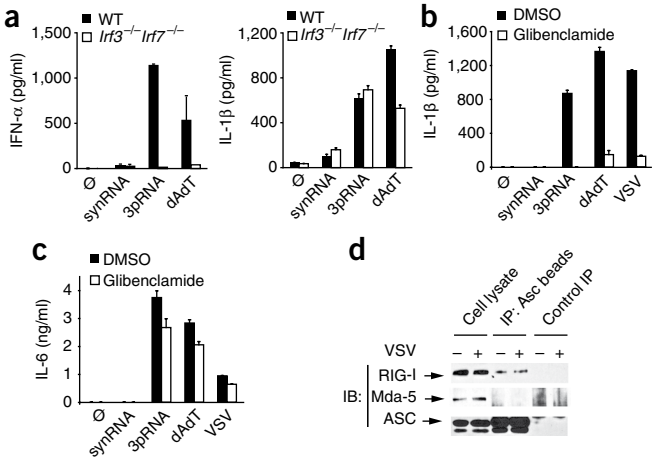

Figure 5 RIG-I engages ASC to induce inflammasome activation. (**a**) ELISA of IFN-α and IL-1β in supernatants of wild-type BMDCs and BMDCs doubly deficient in IRF3 and IRF-7 (*Irf3*$^{-/-}$*Irf7*$^{-/-}$) treated for 6 h with various stimuli (horizontal axes). (**b**,**c**) ELISA of IL-1β (**b**) and IL-6 (**c**) in supernatants of wild-type BMDCs treated for 6 h with various stimuli (horizontal axes) in the presence or absence (DMSO) of the potassium channel inhibitor glibenclamide. (**d**) Immunoassay of THP-1 cells infected with VSV (+) or left uninfected (–); immunoprecipitation of proteins from lysates with ASC-specific antibody (IP: Asc beads) or control antibody (Control IP) was followed by immunoblot analysis (IB) of immunoprecipitates (right four lanes) or total lysates (far left two lanes). Data are representative of two (**a**) or three (**b**,**c**) independent experiments (mean and s.e.m.) or are from one experiment representative of at least four independent experiments (**d**).

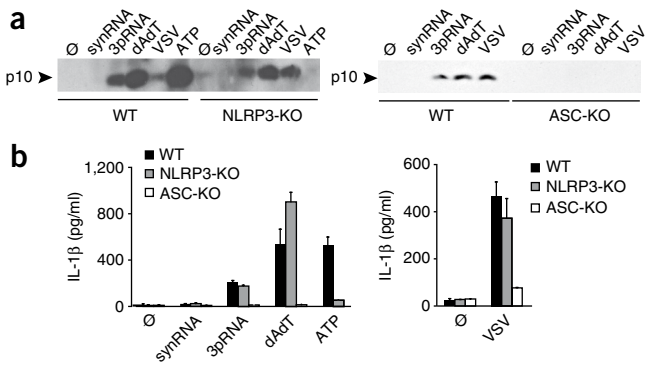

Figure 6 RIG-I-induced inflammasome activation is independent of NLRP3. (**a**) Immunoblot analysis of processed caspase-1 (p10) in supernatants of wild-type, NLRP3-deficient (NLRP3-KO) and ASC-deficient (ASC-KO) BMDCs treated with various stimuli (above lanes). ATP, cells pulsed with 5 mM ATP after 3 h of priming with ultrapure LPS (50 ng/ml). (**b**) ELISA of IL-1β in supernatants of the cells in **a**. Data are representative of at least three independent experiments (mean and s.e.m. in **b**).

after stimulation of AIM2 with poly(dA:dT) DNA, and after activation of NLRP3 with ATP after LPS priming (**Fig. 6a**). As expected, NLRP3-deficient DCs failed to activate caspase-1 (**Fig. 6a**) or to produce IL-1β (**Fig. 6b**) in response to ATP but responded normally to poly(dA:dT), as well as to triggering of RIG-I with 3pRNA or VSV. In contrast, ASC-deficient cells showed defective activation of caspase-1 and secretion of mature IL-1β after stimulation with ATP and LPS, poly(dA:dT), 3pRNA or VSV (**Fig. 6**). Thus, ASC is essential for coupling RIG-I-mediated recognition of RNA to NLRP3-independent caspase-1 activation for IL-1β production. We have proposed a model for the RIG-I-triggered proinflammatory responses and inflammasome activation (**Supplementary Fig. 4**).

Picornavirus engages Mda5, CARD9 and NLRP3

Finally, we investigated whether Mda5 engages similar mechanisms to induce IL-1β production. For this, we first infected Mda5-deficient or CARD9-deficient cells with the Mda5-engaging picornavirus EMCV[16]. Wild-type cells produced IL-1β robustly after EMCV infection (**Fig. 7a**,**b**). However, neither Mda5-deficient nor CARD9-deficient cells showed an IL-1β response (**Fig. 7b**), which indicates that CARD9 is an effector of Mda5 signaling. Further experiments demonstrated that CARD9 was required for EMCV-induced activation of NF-κB and was involved in pro-IL-1β synthesis (**Fig. 7c**,**d**). Next we assessed the role of Mda5 in inflammasome activation. In contrast to RIG-I activation in response to 3pRNA, transfection of poly(I:C) as an agonist for Mda5 (ref. 16) did not induce caspase-1 activation (**Fig. 7e**), which suggested that Mda5 activation by itself might not be sufficient for inflammasome activation. To study the requirement for Mda5 in inflammasome activation in response to the intact EMCV virus, we infected Mda5-deficient cells with EMCV (**Fig. 7f**). In parallel, we incubated the cells with the RIG-I-activating virus VSV and also infected NLRP3-deficient cells with the two viruses. Consistent with our results above (**Fig. 6a**,**b**), VSV strongly activated caspase-1 and led to potent IL-1β secretion in NLRP3-deficient cells. VSV also induced inflammasome activation in Mda5-deficient BMDCs (**Fig. 7f**). In contrast, EMCV infection required NLRP3 and Mda5 for caspase-1 activation and IL-1β production (**Fig. 7f–h**).

DISCUSSION

Here we have reported the identification of two RLH effector mechanisms that act together in the production of proinflammatory cytokines in response to recognition of RNA viruses. Although RLH-induced activation of NF-κB depended on the CARD9–Bcl-10 complex, RIG-I also activated the inflammasome by forming a signaling complex with ASC. Published work has demonstrated that RIG-I uses MAVS for activation of NF-κB and IRF[17–19]. We found that CARD9- and Bcl-10-deficient cells had profound defects in RIG-I-induced production of IL-6 and pro-IL-1β but had normal interferon responses, which provided genetic evidence that CARD9 and Bcl-10 act together downstream of MAVS to selectively control proinflammatory responses. Like RIG-I, Mda5 signals through MAVS[1]. We also observed a requirement for CARD9 in Mda5-induced production of proinflammatory cytokines. Thus, CARD9 represents a common and essential switch in RLH signaling that segregates the proinflammatory response from interferon production.

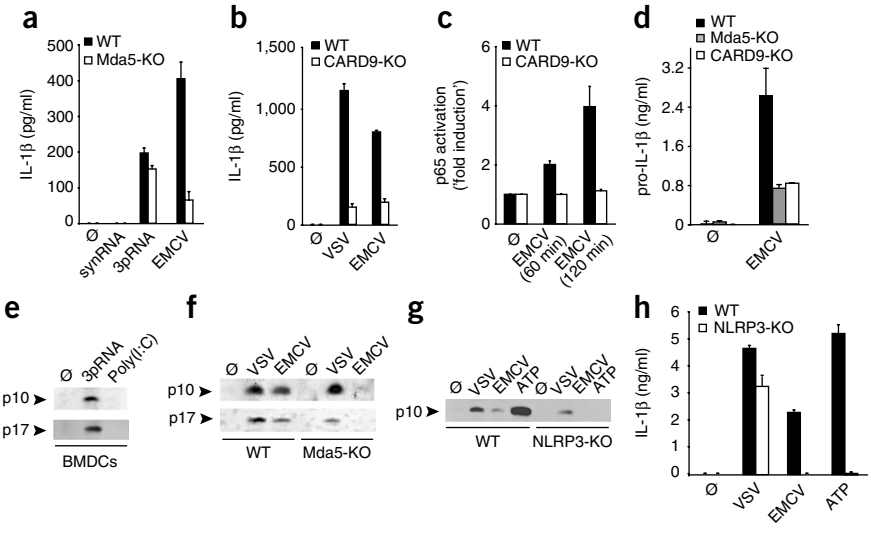

Figure 7 Mda5 requires NLRP3 for inflammasome activation. (**a**,**b**) ELISA of IL-1β in supernatants of wild-type, Mda5-deficient (Mda5-KO) and CARD9-deficient BMDCs treated for 6 h with various stimuli (horizontal axes). (**c**) Activation of the p65 subunit of NF-κB in nuclear protein extracts of wild-type and CARD9-deficient BMDCs stimulated for 60 or 120 min with EMCV, assessed by enhanced chemiluminescence and presented relative to activation in the unstimulated sample. (**d**) ELISA of intracellular pro-IL-1β in wild-type, Mda5-KO and CARD9-deficient cells, measured after cell lysis by repeated cycles of freezing and thawing. (**e**) Immunoblot analysis of caspase-1 processing (p10) and mature IL-1β (p17) in BMDCs stimulated for 6 h with 3pRNA or poly(I:C). (**f**) Immunoblot analysis of caspase-1 processing (p10) and mature IL-1β (p17) in wild-type and Mda5-deficient BMDCs infected for 6 h with VSV or EMCV. (**g**,**h**) Immunoblot analysis of caspase-1 processing (p10; **g**) and ELISA of IL-1β (**h**) in supernatants of wild-type and NLRP3-deficient BMDCs infected for 6 h with VSV or EMCV. ATP, LPS-primed BMDCs stimulated with 5 mM ATP (positive control). Data are representative of three (**a**,**b**,**d**), two (**c**) or at least three (**h**) independent experiments (mean and s.e.m.) or are from one experiment representative of QQ (**e**), three (**f**) or at least three (**g**) independent experiments.

CARD9 relays signals from various pattern-recognition receptors to proinflammatory pathways[28,36]. Together with its effector Bcl-10, CARD9 controls activation of the canonical NF-κB pathway after ligation of surface receptors containing or coupled to an immunoreceptor tyrosine-based activation motif, including dectin-1, FcγRIII, TREM-1 and Mincle[37]. This function of CARD9 is important for host defense against fungi and innate responses to certain bacteria, such as *Mycobacterium tuberculosis*[30,38]. Consistent with the function of CARD9–Bcl-10 complexes in NF-κB activation, we observed defective NF-κB signaling in CARD9-deficient and Bcl-10-deficient cells stimulated with agonists of RIG-I or Mda5. Those findings establish CARD9–Bcl-10 complexes as a missing link between RLHs and NF-κB. Previous work has shown that CARD9 can activate Jnk and p38, at least after macrophage infection with whole VSV particles[39]. However, we did not detect defects in Jnk or p38 signaling in CARD9-deficient DCs stimulated with 3pRNA. The fact that VSV triggers several innate signaling systems, including TLRs[40], and that CARD9 signaling to Jnk and p38 differs in DCs and macrophages[29] could explain why we did not observe Jnk or p38 signaling defects in our experiments, which focused specifically on the RLH-induced pathway.

Bcl-10 is also required for T cell and B cell antigen receptor signaling. In lymphocytes, Bcl-10 engages TRAF2 and TRAF6 to mediate lysine 63–linked polyubiquitinylation of IKKγ, which induces subsequent IKK activation[32]. It is therefore possible that a similar mechanism operates downstream of RLHs. Caspase-8 and FADD are also involved in antigen receptor–induced NF-κB activation[41], and a study has reported roles for caspase-8 and FADD downstream of MAVS[42]. Thus, several NF-κB activators seem to be shared by the RLH and antigen-receptor pathways.

Our work has additionally established RIG-I as a cytosolic RNA sensor for inflammasome activation. Selective RIG-I triggering was sufficient for caspase-1 activation and RIG-I was required for inflammasome activation in response to stimulation with 3pRNA or infection with VSV. In contrast to NF-κB signaling and pro-IL-1β production, this process was entirely independent of MAVS, TRIM25 and CARD9; it was also independent of NLRP3. To our knowledge, this represents the first example of MAVS-independent RIG-I signal transduction. RIG-I-induced inflammasome activation shows similarities to the activation of AIM2 inflammasomes by viral double-stranded DNA, which is also NLRP3 independent[35]. After binding double-stranded DNA, AIM2 interacts with ASC to induce ASC oligomerization and subsequent IL-1β production. Likewise, RIG-I can form a protein complex containing ASC, potentially with additional components, to induce IL-1β production in response to some RNA viruses. Thus, RIG-I and ASC can constitute a distinct inflammasome.

Influenza virus activates the NLRP3 inflammasome[22,24,25]. Influenza enters the cell via the lysosomal pathway, and lysosomal damage, which is a common NLRP3 activator, could trigger NLRP3 in this context. Consistent with that, lysosomal maturation is essential for influenza virus–induced NLRP3 activation[22]. We also observed a requirement for NLRP3 in IL-1β production after infection with EMCV. In contrast, VSV did not activate the NLRP3 inflammasome and instead relied on RIG-I and ASC. Our results and previously published data therefore indicate that inflammasome activation by RNA viruses can in principle use NLRP3-dependent or NLRP3-independent mechanisms. The precise viral ligands that trigger the NLRP3 inflammasome and the cellular sensors that detect these ligands remain to be identified. Although Mda5 was required for ECMV-induced inflammasome activation, ligation of Mda5 with poly(I:C) was not sufficient to induce inflammasome activation. In this context, the function of Mda5 might thus be restricted to priming of the NLRP3 inflammasome; that is, activation of Mda5 could potentially upregulate NLRP3, which is an essential step for activation of the NLRP3 inflammasome[43,44].

Together our findings have indicated that RLHs can trigger at least three different cellular responses: interferon production, NF-κB activation and inflammasome activation. RIG-I could in principle signal from one large signaling complex that 'fine tunes' interferon and proinflammatory responses. Alternatively, RIG-I might be a sensor in several distinct signalosomes: one may contain RIG-I together with MAVS, TRAF3 and TBK-1 for IRF activation; a second may involve MAVS, CARD and Bcl-10 for the activation of NF-κB; and a third might contain RIG-I together with ASC and potentially other factors for caspase-1 activation. Precisely how RIG-I integrates these cellular responses will be an important topic of future research, but our results offer one molecular explanation for the longstanding finding that RNA viruses are potent inducers of proinflammatory cytokines such as IL-1β and IL-6. In addition, as activation of the inflammatory responses forms a critical link to the induction of adaptive immunity, our results may have implications for the development of vaccines.

METHODS

Methods and any associated references are available in the online version of the paper at http://www.nature.com/natureimmunology/.

Note: Supplementary information is available on the Nature Immunology website.

ACKNOWLEDGMENTS

We thank J. Tschopp (University of Lausanne) for critical reading of the manuscript, discussions and NLRP3-deficient, ASC-deficient and MAVS-deficient mice and plasmids; and A. Krug (Technical University of Munich) for EMCV. This work includes parts of a thesis by M.B. at the University of Munich. Supported by Bundesministerium für Bildung und Forschung Biofuture (G.H.), Deutsche Forschungsgemeinschaft (SFB704, SFB670, SFB832 and KFO177 to G.H.; Sonderforschungsbereiche to S.E., V.H. and J.R.; Graduiertenkolleg 1202 to M.B.; and RO 2525/3–1 to S.R.), the Center for Integrated Protein Science Munich (S.E.), the European Research Council (V.H.) and Deutsche Krebshilfe (J.R.).

AUTHOR CONTRIBUTIONS

H.P., M.B., O.G., G.H., V.H. and J.R. designed the research; H.P., M.B., O.G., K.F., S.R., N.H., M.R. and M.S. did experiments; W.B., H.K., S.A. and S.I. contributed critical reagents; H.P., M.B., O.G., S.R., S.E., C.P., V.H., G.H. and J.R. analyzed results; H.P. and M.B. prepared the figures; and H.P., M.B., O.G., G.H. and J.R. wrote the paper.

Published online at http://www.nature.com/natureimmunology/.
Reprints and permissions information is available online at http://npg.nature.com/reprintsandpermissions/.

1. Kawai, T. & Akira, S. Toll-like receptor and RIG-I-like receptor signaling. *Ann. NY Acad. Sci.* **1143**, 1–20 (2008).
2. Alexopoulou, L., Holt, A.C., Medzhitov, R. & Flavell, R.A. Recognition of double-stranded RNA and activation of NF-κB by Toll-like receptor 3. *Nature* **413**, 732–738 (2001).
3. Heil, F. *et al.* Species-specific recognition of single-stranded RNA via toll-like receptor 7 and 8. *Science* **303**, 1526–1529 (2004).
4. Hemmi, H. *et al.* Toll-like receptor recognizes bacterial DNA. *Nature* **408**, 740–745 (2000).
5. Burckstummer, T. *et al.* An orthogonal proteomic-genomic screen identifies AIM2 as a cytoplasmic DNA sensor for the inflammasome. *Nat. Immunol.* **10**, 266–272 (2009).
6. Fernandes-Alnemri, T., Yu, J.W., Datta, P., Wu, J. & Alnemri, E.S. AIM2 activates the inflammasome and cell death in response to cytoplasmic DNA. *Nature* **458**, 509–513 (2009).
7. Hornung, V. *et al.* AIM2 recognizes cytosolic dsDNA and forms a caspase-1-activating inflammasome with ASC. *Nature* **458**, 514–518 (2009).
8. Roberts, T.L. *et al.* HIN-200 proteins regulate caspase activation in response to foreign cytoplasmic DNA. *Science* **323**, 1057–1060 (2009).
9. Andrejeva, J. *et al.* The V proteins of paramyxoviruses bind the IFN-inducible RNA helicase, mda-5, and inhibit its activation of the IFN-β promoter. *Proc. Natl. Acad. Sci. USA* **101**, 17264–17269 (2004).
10. Yoneyama, M. *et al.* The RNA helicase RIG-I has an essential function in double-stranded RNA-induced innate antiviral responses. *Nat. Immunol.* **5**, 730–737 (2004).
11. Pichlmair, A. & Reis e Sousa, C. Innate recognition of viruses. *Immunity* **27**, 370–383 (2007).

12. Hornung, V. *et al.* 5′-Triphosphate RNA is the ligand for RIG-I. *Science* **314**, 994–997 (2006).
13. Pichlmair, A. *et al.* RIG-I-mediated antiviral responses to single-stranded RNA bearing 5′-phosphates. *Science* **314**, 997–1001 (2006).
14. Schlee, M. *et al.* Recognition of 5′ triphosphate by RIG-I helicase requires short blunt double-stranded RNA as contained in panhandle of negative-strand virus. *Immunity* **31**, 25–34 (2009).
15. Schmidt, A. *et al.* 5′-triphosphate RNA requires base-paired structures to activate antiviral signaling via RIG-I. *Proc. Natl. Acad. Sci. USA* **106**, 12067–12072 (2009).
16. Kato, H. *et al.* Differential roles of MDA5 and RIG-I helicases in the recognition of RNA viruses. *Nature* **441**, 101–105 (2006).
17. Kawai, T. *et al.* IPS-1, an adaptor triggering RIG-I- and Mda5-mediated type I interferon induction. *Nat. Immunol.* **6**, 981–988 (2005).
18. Meylan, E. *et al.* Cardif is an adaptor protein in the RIG-I antiviral pathway and is targeted by hepatitis C virus. *Nature* **437**, 1167–1172 (2005).
19. Seth, R.B., Sun, L., Ea, C.K. & Chen, Z.J. Identification and characterization of MAVS, a mitochondrial antiviral signaling protein that activates NF-κB and IRF 3. *Cell* **122**, 669–682 (2005).
20. Nakhaei, P., Genin, P., Civas, A. & Hiscott, J. RIG-I-like receptors: Sensing and responding to RNA virus infection. *Semin. Immunol.* **21**, 215–222 (2009).
21. Yu, H.B. & Finlay, B.B. The caspase-1 inflammasome: a pilot of innate immune responses. *Cell Host Microbe* **4**, 198–208 (2008).
22. Allen, I.C. *et al.* The NLRP3 inflammasome mediates in vivo innate immunity to influenza a virus through recognition of viral RNA. *Immunity* **30**, 556–565 (2009).
23. Gross, O. *et al.* Syk kinase signalling couples to the Nlrp3 inflammasome for anti-fungal host defence. *Nature* **459**, 433–436 (2009).
24. Ichinohe, T., Lee, H.K., Ogura, Y., Flavell, R. & Iwasaki, A. Inflammasome recognition of influenza virus is essential for adaptive immune responses. *J. Exp. Med.* **206**, 79–87 (2009).
25. Thomas, P.G. *et al.* The intracellular sensor NLRP3 mediates key innate and healing responses to influenza A virus via the regulation of caspase-1. *Immunity* **30**, 566–575 (2009).
26. Poeck, H. *et al.* 5′-Triphosphate-siRNA: turning gene silencing and Rig-I activation against melanoma. *Nat. Med.* **14**, 1256–1263 (2008).
27. Gack, M.U. *et al.* TRIM25 RING-finger E3 ubiquitin ligase is essential for RIG-I-mediated antiviral activity. *Nature* **446**, 916–920 (2007).
28. Hara, H. & Saito, T. CARD9 versus CARMA1 in innate and adaptive immunity. *Trends Immunol.* **30**, 234–242 (2009).
29. Goodridge, H.S. *et al.* Differential use of CARD9 by dectin-1 in macrophages and dendritic cells. *J. Immunol.* **182**, 1146–1154 (2009).
30. Gross, O. *et al.* Card9 controls a non-TLR signalling pathway for innate anti-fungal immunity. *Nature* **442**, 651–656 (2006).
31. Wang, L. *et al.* Card10 is a novel caspase recruitment domain/membrane-associated guanylate kinase family member that interacts with BCL10 and activates NF-κB. *J. Biol. Chem.* **276**, 21405–21409 (2001).
32. Rawlings, D.J., Sommer, K. & Moreno-Garcia, M.E. The CARMA1 signalosome links the signalling machinery of adaptive and innate immunity in lymphocytes. *Nat. Rev. Immunol.* **6**, 799–812 (2006).
33. Henry, T., Brotcke, A., Weiss, D.S., Thompson, L.J. & Monack, D.M. Type I interferon signaling is required for activation of the inflammasome during Francisella infection. *J. Exp. Med.* **204**, 987–994 (2007).
34. Steinberg, C. *et al.* The IFN regulatory factor 7-dependent type I IFN response is not essential for early resistance against murine cytomegalovirus infection. *Eur. J. Immunol.* **39**, 1007–1018 (2009).
35. Schroder, K., Muruve, D.A. & Tschopp, J. Innate immunity: cytoplasmic DNA sensing by the AIM2 inflammasome. *Curr. Biol.* **19**, R262–R265 (2009).
36. Colonna, M. All roads lead to CARD9. *Nat. Immunol.* **8**, 554–555 (2007).
37. Geijtenbeek, T.B. & Gringhuis, S. I. Signalling through C-type lectin receptors: shaping immune responses. *Nat. Rev. Immunol.* **9**, 465–479 (2009).
38. Werninghaus, K. *et al.* Adjuvanticity of a synthetic cord factor analogue for subunit *Mycobacterium tuberculosis* vaccination requires FcRgamma-Syk-Card9-dependent innate immune activation. *J. Exp. Med.* **206**, 89–97 (2009).
39. Hsu, Y.M. *et al.* The adaptor protein CARD9 is required for innate immune responses to intracellular pathogens. *Nat. Immunol.* **8**, 198–205 (2007).
40. Hara, H. *et al.* The adaptor protein CARD9 is essential for the activation of myeloid cells through ITAM-associated and Toll-like receptors. *Nat. Immunol.* **8**, 619–629 (2007).
41. Su, H. *et al.* Requirement for caspase-8 in NF-κB activation by antigen receptor. *Science* **307**, 1465–1468 (2005).
42. Takahashi, K. *et al.* Roles of caspase-8 and caspase-10 in innate immune responses to double-stranded RNA. *J. Immunol.* **176**, 4520–4524 (2006).
43. Bauernfeind, F.G. *et al.* Cutting edge: NF-κB activating pattern recognition and cytokine receptors license NLRP3 inflammasome activation by regulating NLRP3 expression. *J. Immunol.* **183**, 787–791 (2009).
44. Franchi, L., Eigenbrod, T. & Nunez, G. Cutting edge: TNF-α mediates sensitization to ATP and silica via the NLRP3 inflammasome in the absence of microbial stimulation. *J. Immunol.* **183**, 792–796 (2009).

ONLINE METHODS

Mice. Mice genetically deficient in NLRP3, ASC, RIG-I, IRF3 and IRF7, CARD9, Bcl-10, MALT1, MAVS, Mda5, TRIM25 or caspase-1 have been described[16,27,30,34,45–48]. Mice were 6–12 weeks of age at the onset of experiments and were used according to local guidelines. Animal studies were approved by the local regulatory agency (Regierung von Oberbayern, Munich, Germany).

Media and reagents. RPMI-1640 medium (Invitrogen) and DMEM (Invitrogen) were supplemented with 10% (vol/vol) FCS (Hyclone), 3 mM L-glutamine, 100 U/ml of penicillin and 100 μg/ml of streptomycin (all from Sigma-Aldrich). ATP (A6419), poly(dA:dT) sodium salt (P9764), Glyburide (glibenclamide) and Bay11-7082 (specific IKK kinase inhibitor) were from Sigma-Aldrich. OptiMEM reduced-serum medium was from Invitrogen. Both poly(I:C) and ultrapure LPS (from *Escherichia coli* strain K12; used at a concentration of 50 ng/ml) were from Invivogen. The pan-caspase inhibitor z-VAD-fmk (benzyloxycarbonyl–Val-Ala-Asp–fluoromethylketone) was from Calbiochem. Chemically synthesized RNA oligonucleotides were from MWG-Biotech. Double-stranded *in vitro*–transcribed 3pRNA was generated as described[26]. Synthetic dsRNA lacking the 5′ triphosphate (sense, 5′-GCAUGCGACCUCUGUUUGA-3′) and 3pRNA1 (sense, 5′-GCAUGCGACCUCUGUUUGAC-3′) were used in most experiments; 3pRNA2 (sense, 5′-GCAUGCGAGGACUGUUUGAC-3′) was used to exclude sequence-specific effects on inflammasome activation.

Cells. Human PBMCs were isolated from whole human blood of healthy, voluntary donors by Ficoll-Hypaque density-gradient centrifugation (Biochrom). BMDCs were generated and grown as described[23]. Experiments involving human materials were in accordance with precepts established by the Helsinki Declaration and approved by the local ethics committee.

Cell culture and stimulation. All cells were stimulated in OptiMEM reduced-serum medium (Invitrogen) at a density of 1×10^6 cells per ml. Where not indicated otherwise, cells were incubated for 6–8 h with 2 μg/ml of synthetic RNA, 3pRNA or poly(dA:dT). Cells were transfected with RNA and DNA with Lipofectamine 2000 according to the manufacturer's protocol (Invitrogen). In some experiments, ultrapure LPS (50 ng/ml) and ATP (5 mM) were used as positive controls. For all conditions, cell-free supernatants were analyzed for cytokine secretion by ELISA or cells were lysed for immunoprecipitation and/or immunoblot analysis. Glibenclamide (25 μM) and z-VAD-fmk (0.05 μM) were used as described[23].

Cytokine measurement. Cell supernatants and serum were analyzed for cytokine secretion by ELISA (BD, R&D Systems or PBL Biomedical Laboratories). For analysis of intracellular pro-IL-1β, cells were lysed by repeated cycles of freezing and thawing in RPMI medium containing 10% (vol/vol) FCS, 3 mM L-glutamine, 100 U/ml of penicillin and 100 μg/ml of streptomycin and were analyzed by ELISA.

Immunoblot analysis. Precipitated media supernatants or cell extracts were analyzed by standard immunoblot techniques[49]. Primary antibodies were polyclonal goat antibody to mouse-IL-1β (anti–mouse IL-1β; BAF401; R&D Systems), polyclonal rabbit anti–human IL-1β (D116; Cell Signaling), monoclonal mouse anti-RIG-I (Alme-1; Alexis), polyclonal rabbit anti-Mda5 (AT113; Alexis), polyclonal rabbit anti-caspase-1 (sc-514 and sc-515; Santa Cruz), and polyclonal rabbit anti-Erk (9102), monoclonal rabbit antibody to phosphorylated p38 (12F8; 4631), polyclonal rabbit antibody to phosphorylated Jnk (9251) and polyclonal rabbit anti-β-actin (4967; all from Cell Signaling).

NF-κB activation. Nuclear extracts were prepared according to standard methods, and 1 μg nuclear protein was analyzed with a NF-κB p65 Transcription Factor Assay kit (Pierce) as described[50].

Coimmunoprecipitation. Endogenous RIG-I was immunoprecipitated from 5×10^6 THP-1 cells seeded in 10-cm dishes with or without 3 h of VSV stimulation (multiplicity of infection, 10). Cells were lysed in ice-cold lysis buffer (150 mM NaCl, 50 mM Tris pH 7.0, 1 mM EDTA, 1% (vol/vol) Nonidet P-40, 10% (vol/vol) glycerol, 1 mM Na_3VO_4, 1 mM phenylmethyl sulfonyl fluoride and a Protease Inhibitor Cocktail tablet (Roche)) and lysates were incubated overnight at 4 °C with 80 μl protein G Sepharose beads (GE Healthcare) and 2 μg antibody (polyclonal anti-ASC (AL177; Alexis Biochemicals) or polyclonal rabbit anti–Syrian hamster immunoglobulin G (307-005-003; Jackson ImmunoResearch)). Immunoprecipitates were analyzed by immunoblot.

RNA extraction and quantification. Total RNA was extracted from cells with a High Pure RNA Isolation kit as described by the manufacturer (Roche) and was analyzed by quantitative RT-PCR. RNA (1 μg) was reverse-transcribed with SuperScript II Reverse Transcriptase and oligo(dT) oligonucleotide according to the manufacturer's protocol (Invitrogen). The Universal ProbeLibrary and LightCycler 480 system (Roche) were used for quantitative PCR (primer sequences, **Supplementary Table 1**). Gene expression was calculated as a ratio of the expression of the gene of interest to that of *Hprt1* (encoding hypoxanthine guanine phosphoribosyl transferase) measured for the same sample.

Preparation of virus stock and plaque assay. Baby hamster kidney (BHK-21) cells were infected with VSV Indiana (Mudd-Summers strain) or EMCV (a gift from A. Krug) and cell culture supernatants were collected 20 h after infection. Virus yield in culture supernatants was determined by standard plaque assay. VSV and EMCV were used at a multiplicity of infection of 5–10.

***In vivo* viral infection.** For viral infection, mice were given intravenous injection of 2×10^6 plaque-forming units VSV per mouse in 200 μl medium or an equal amount of PBS (as a control). Serum was collected after 6 h. Cytokine concentrations were measured by ELISA.

Statistical analyses. The statistical significance of differences was determined by the paired two-tailed Student's *t*-test. Differences with a *P* value of less than 0.05 were considered statistically significant.

45. Dostert, C. *et al.* Innate immune activation through Nalp3 inflammasome sensing of asbestos and silica. *Science* **320**, 674–677 (2008).
46. Gitlin, L. *et al.* Essential role of mda-5 in type I IFN responses to polyriboinosinic: polyribocytidylic acid and encephalomyocarditis picornavirus. *Proc. Natl. Acad. Sci. USA* **103**, 8459–8464 (2006).
47. Mariathasan, S. *et al.* Differential activation of the inflammasome by caspase-1 adaptors ASC and Ipaf. *Nature* **430**, 213–218 (2004).
48. Michallet, M.C. *et al.* TRADD protein is an essential component of the RIG-like helicase antiviral pathway. *Immunity* **28**, 651–661 (2008).
49. Petrilli, V. *et al.* Activation of the NALP3 inflammasome is triggered by low intracellular potassium concentration. *Cell Death Differ.* **14**, 1583–1589 (2007).
50. LeibundGut-Landmann, S. *et al.* Syk- and CARD9-dependent coupling of innate immunity to the induction of T helper cells that produce interleukin 17. *Nat. Immunol.* **8**, 630–638 (2007).

doi:10.1038/ni.1824

nature immunology

PCBP2 mediates degradation of the adaptor MAVS via the HECT ubiquitin ligase AIP4

Fuping You, Hui Sun, Xiang Zhou, Wenxiang Sun, Shimin Liang, Zhonghe Zhai & Zhengfan Jiang

MAVS is critical in innate antiviral immunity as the sole adaptor for RIG-I-like helicases. MAVS regulation is essential for the prevention of excessive harmful immune responses. Here we identify PCBP2 as a negative regulator in MAVS-mediated signaling. Overexpression of PCBP2 abrogated cellular responses to viral infection, whereas knockdown of PCBP2 exerted the opposite effect. PCBP2 was induced after viral infection, and its interaction with MAVS led to proteasomal degradation of MAVS. PCBP2 recruited the HECT domain–containing E3 ligase AIP4 to polyubiquitinate and degrade MAVS. MAVS was degraded after viral infection in wild-type mouse embryonic fibroblasts but remained stable in AIP4-deficient (*Itch*$^{-/-}$) mouse embryonic fibroblasts, coupled with greatly exaggerated and prolonged antiviral responses. The PCBP2-AIP4 axis defines a new signaling cascade for MAVS degradation and 'fine tuning' of antiviral innate immunity.

Viral invasion triggers host antiviral innate immune responses, which lead to the production of various cytokines and chemokines. Cells use pattern-recognition receptors to detect viral infection by sensing viral nucleic acids[1]. RIG-I-like helicases (RLHs), including RIG-I and Mda5, function as cytoplasmic RNA sensors that recognize viral RNA released during virus replication. Although RIG-I and Mda5 sense distinct types of viruses[2–4], they share the common adaptor protein MAVS (also known as Cardif, IPS-1 or VISA) to transmit signals[5–8]. MAVS resides on the mitochondrial outer membrane, where it interacts with Mda5 or RIG-I and recruits 'downstream' signaling molecules, eventually leading to the production of type I interferons and proinflammatory cytokines.

Activation of innate immunity is necessary to prevent the spread of infection. Attenuation or termination of signaling, however, is also essential for preventing the detrimental effects of excessive responses on the host. Ubiquitination-mediated protein degradation has pivotal roles in this regulation[9]. This cascade initiates from the covalent attachment of ubiquitin moieties to proteins through the stepwise action of three enzymes: a ubiquitin-activating enzyme (E1), a ubiquitin-conjugating enzyme (E2) and a ubiquitin ligase (E3) that provides substrate specificity[10]. Ubiquitin ligases are broadly categorized into two families: HECT domain E3 ubiquitin ligases and RING-type E3 ubiquitin ligases[11]. Both HECT and RING domain E3 ubiquitin ligases have key roles in immune regulation. In RLH signaling, the RING-type E3 ligase RNF125 can ubiquitinate and trigger degradation of Mda5, RIG-I and MAVS to suppress RLH-mediated responses[12]. MAVS is the first mitochondrial protein linked to innate immunity. Mitochondrial localization is crucial for MAVS function[7]. It has been reported that in response to infection Sendai virus (SeV), MAVS undergoes lysine 63 (K63)- as well as K48-linked polyubiquitination. The K63-linked ubiquitination mediates recruitment of the kinase IKK to mitochondria[13]. The potential involvement of the ubiquitin system, however, as well as the E3 ligase specific to MAVS are unknown at present.

Studies have shown that PCBP2 ('poly(rC) binding protein 2') belongs to a class of proteins that bind to poly(C) stretches of both RNA and DNA. Apart from its roles in maintaining mRNA stability and regulating translation[14], PCBP2 can also participate in protein-protein interactions[15–17]. Although PCBP2 has been linked to the regulation of poliovirus replication[18], its functions in innate immunity have not been reported.

Here we identify PCBP2 as a negative regulator in MAVS-mediated antiviral signaling. Overexpression of PCBP2 abrogated cellular responses to viral infection, whereas knockdown of PCBP2 exerted the opposite effect. PCBP2 was induced after viral infection and interacted with MAVS, leading to proteasomal degradation of MAVS. PCBP2 recruited the HECT domain–containing E3 ligase AIP4 (A000959) to catalyze K48-linked polyubiquitination and degradation of MAVS. MAVS was degraded after viral infection in wild-type mouse embryonic fibroblasts (MEFs) but remained stable in AIP4-deficient (*Itch*$^{-/-}$) MEFs; the latter result was accompanied by a greatly exaggerated and prolonged antiviral responses. The PCBP2-AIP4 axis thus defines a previously unknown signaling cascade for MAVS degradation and 'fine tuning' of antiviral innate immunity.

RESULTS

PCBP2 associates with MAVS to regulate RLH signaling

In an attempt to identify proteins that interact with MAVS, we did yeast two-hybrid screens with full-length MAVS as the bait. We found that PCBP2 associated with MAVS, and we confirmed this

The Education Ministry Key Laboratory of Cell Proliferation and Differentiation, School of Life Sciences, Peking University, Beijing, China. Correspondence should be addressed to Z.J. (jiangzf@pku.edu.cn).

Received 20 July; accepted 23 September; published online 1 November 2009; doi:10.1038/ni.1815

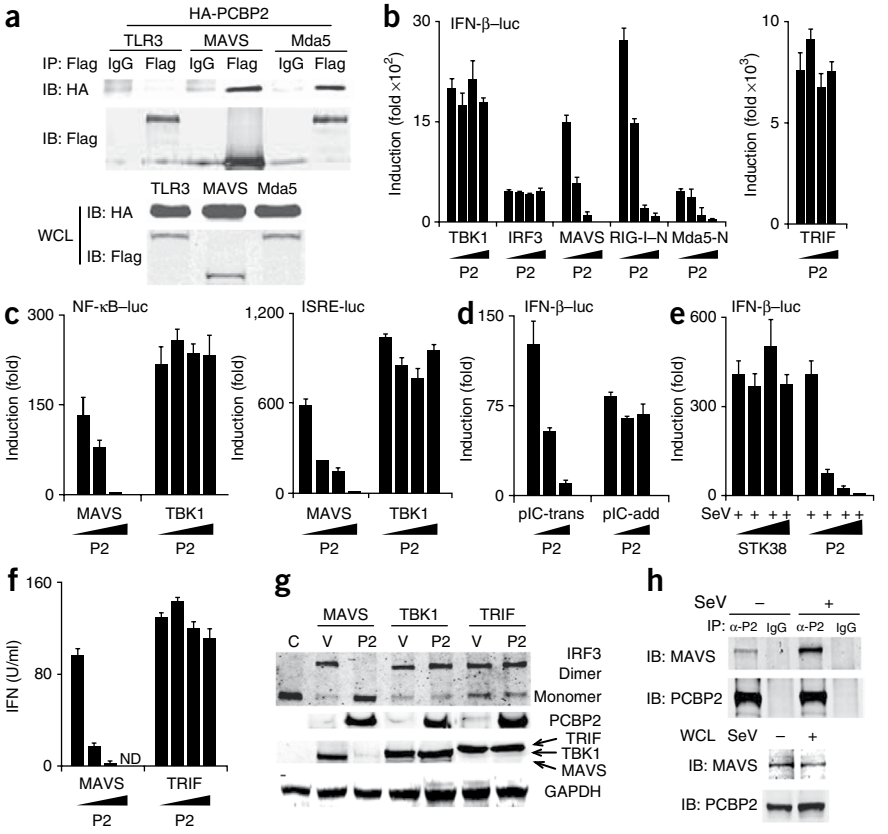

Figure 1 PCBP2 interacts with MAVS and negatively regulates MAVS-mediated signaling. (**a**) Immunoprecipitation (IP), with anti-Flag (Flag) or control mouse immunoglobulin G (IgG), of proteins from lysates of 293 cells transfected with plasmids encoding hemagglutinin (HA)-tagged PCBP2 and Flag-tagged Toll-like receptor 3 (TLR3), MAVS or Mda5, followed by immunoblot analysis (IB) with anti-HA (top) or anti-Flag (middle). WCL (bottom), expression of transfected proteins in whole-cell lysates (without immunoprecipitation). (**b**,**c**) Gene induction in 293 cells transfected with luciferase reporter constructs driven by promoters of genes encoding IFN-β (IFN-β–luc; **b**), or NF-κB (NF-κB–luc) or interferon-stimulated response element (ISRE-luc; **c**), plus 100 ng of various plasmids (horizontal axes) and 0, 50, 100 or 200 ng (wedges) of PCBP2 (P2), assessed as luciferase activity after 24 h; results are presented relative to the luciferase activity in control cells (transfected with luciferase reporter and empty vector). (**d**) Gene induction in 293 cells stably transfected with Toll-like receptor 3 and with IFN-β–luc and PCBP2, and treated for 5 h with poly(I:C) (pIC-add) or transfected for 18 h with poly(I:C) (pIC-trans), then assessed as in **b**,**c**. (**e**) Gene induction in 293 cells transfected for 24 h with IFN-β–luc plus STK38 (negative control) or PCBP2 and then infected for 18 h with SeV, followed by analysis as in **b**,**c**. (**f**) Bioassay of type I interferon in supernatants of 293 cells transfected for 24 h with 100 ng MAVS or TRIF and PCBP2 (0, 50, 100 or 200 ng; wedges). ND, not detectable. (**g**) IRF3 dimerization in 293 cells left untransfected (C) or transfected for 24 h with 1 μg plasmid (top) plus 2 μg empty vector (V) or PCBP2 (P2), detected by native gel electrophoresis with anti-IRF3 (top). Below, immunoblot analysis of the expression of transfected proteins. GAPDH, glyceraldehyde phosphate dehydrogenase (loading control). (**h**) Immunoprecipitation, with anti-PCBP2 (α-P2) or IgG (control), of proteins from lysates of HT1080 human fibrosarcoma cells left uninfected (–) or infected for 4 h with SeV (+), followed by immunoblot analysis with anti-MAVS or anti-PCBP2 (top). Below, immunoblot analysis of endogenous protein expression with anti-MAVS or anti-PCBP2. Data are from one representative of at least three independent experiments (**b**–**f**; mean and s.d. of triplicate or duplicate assays) or are representative of three independent experiments (**a**), three experiments (**g**) or three independent experiments with similar results (**h**).

interaction in human embryonic kidney (293) cells. Moreover, PCBP2 interacted with MAVS and Mda5 but not with Toll-like receptor 3 (**Fig. 1a**). Similarly, PCBP2 selectively interacted with RIG-I but not with the kinases TBK1 or IKKi, downstream components of RLH pathway (**Supplementary Fig. 1** and data not shown). The finding that PCBP2 interacted with MAVS prompted us to investigate whether PCBP2 is involved in MAVS-mediated RLH signaling. We initially tested the effect of PCBP2 on various components of the RLH pathway in their activation of relevant promoters in a reporter assay. We transfected 293 cells with expression plasmids encoding the adaptor protein TRIF, MAVS, RIG-I–N, Mda5-N (where 'N' indicates the amino-terminal CARD module of RIG-I or Mda5), TBK1 or the transcription factor IRF3, together with increasing amounts of PCBP2 and luciferase reporter constructs driven by promoters of genes encoding interferon-β (IFN-β; **Fig. 1b**) or IFN-α4 (**Supplementary Fig. 2a**) or the transcription factor NF-κB or interferon-stimulated response element (**Fig. 1c**). We found that PCBP2 strongly inhibited the activation of these promoters induced by MAVS, RIG-I or Mda5 in a dose-dependent manner, whereas activation of promoters by TRIF, TBK1 or IRF3 was unaffected. As RLHs are required for the innate immune antiviral response, we sought to see if these results were of physiological importance. We found that PCBP2 overexpression led to strong inhibition of the production of type I interferon after 293 cells were transfected with poly(I:C), which mimics the intracellular double-stranded RNA generated during viral replication, but not after cells were treated with poly(I:C) (**Fig. 1d**). We obtained results in cells infected with SeV similar to those obtained with poly(I:C)-transfected cells (**Fig. 1e**). After PCBP2 overexpression, type I interferon was much lower in supernatants of cells transfected with MAVS, but not those transfected with TRIF (**Fig. 1f**); we obtained similar results for other inflammatory mediators, including RANTES, tumor necrosis factor (TNF) and interleukin 28b (IL-28b; **Supplementary Fig. 2b**). Consistent with those findings, PCBP2 specifically inhibited the dimerization of IRF3 induced by overexpression of MAVS, but not that induced by overexpression of TRIF or TBK1 (**Fig. 1g**). To determine whether PCBP2 interacts with MAVS in physiological conditions, we did coimmunoprecipitation experiments with antibodies recognizing endogenous PCBP2 and MAVS. A PCBP2-MAVS interaction was induced after SeV infection (**Fig. 1h**). These data collectively demonstrate that PCBP2 is a MAVS-associated protein that negatively regulates RLH-mediated signaling downstream of MAVS but upstream of TBK1-IKKi.

PCBP2 is negatively involved in cellular antiviral responses

Feedback expression of negative regulators is usually upregulated after activation of the related signaling module. When we analyzed the expression pattern of PCBP2 at the level of mRNA (**Fig. 2a**, top) and protein (**Fig. 2a**, middle and bottom), we found that PCBP2

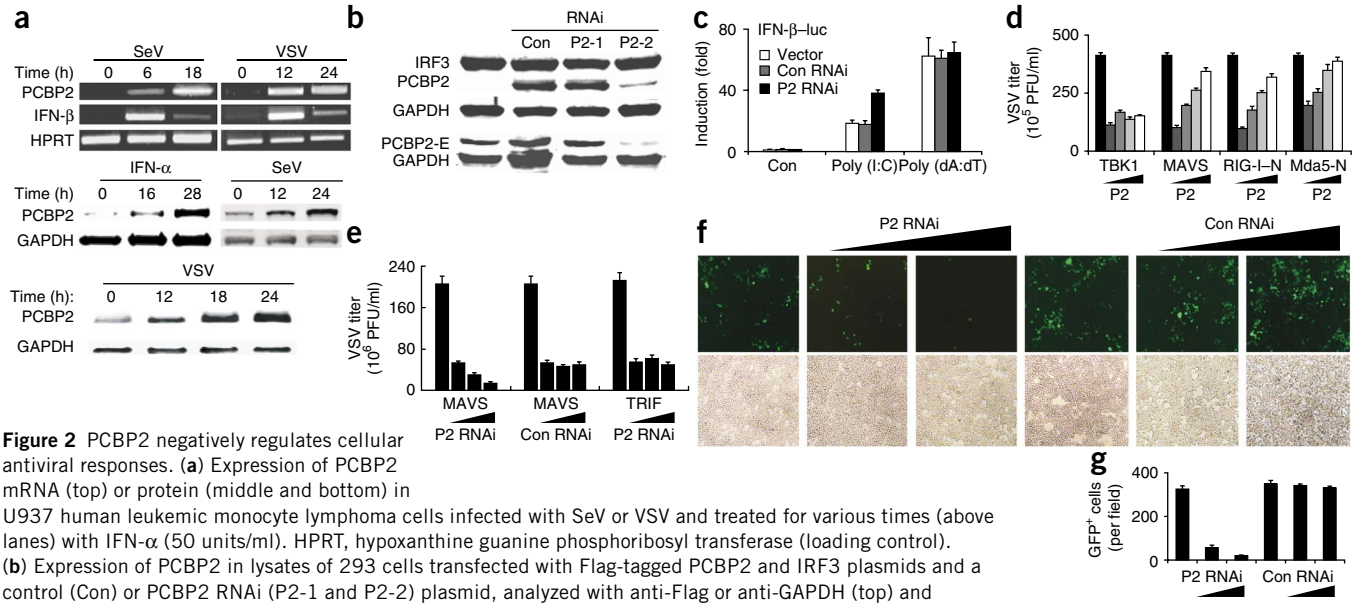

Figure 2 PCBP2 negatively regulates cellular antiviral responses. (**a**) Expression of PCBP2 mRNA (top) or protein (middle and bottom) in U937 human leukemic monocyte lymphoma cells infected with SeV or VSV and treated for various times (above lanes) with IFN-α (50 units/ml). HPRT, hypoxanthine guanine phosphoribosyl transferase (loading control). (**b**) Expression of PCBP2 in lysates of 293 cells transfected with Flag-tagged PCBP2 and IRF3 plasmids and a control (Con) or PCBP2 RNAi (P2-1 and P2-2) plasmid, analyzed with anti-Flag or anti-GAPDH (top) and expression of endogenous PCBP2 (PCBP2-E) in 293 cells transfected with control or PCBP2 RNAi plasmid alone (bottom). (**c**) Gene induction in 293 cells left untreated (Con) or transfected for 48 h with RNAi plasmid (key) and IFN-β–luc, then transfected for 18 h with poly(I:C) or poly(dA:dT) and assessed as described in **Figure 1b,c**. (**d**) Plaque assay of VSV in supernatants of 293 cells transfected for 24 h with 100 ng plasmid (horizontal axis) plus PCBP2 (0, 50, 100 or 200 ng; wedges), then infected with VSV (multiplicity of infection (MOI), 0.1) and assessed 12 h after infection. PFU, plaque-forming units. (**e**) Plaque assay (as described in **d**) of VSV in 293 cells transfected for 24 h with 100 ng plasmid (horizontal axis) plus control or PCBP2 RNAi plasmid (0, 50, 100 or 200 ng; wedges), then infected with VSV. (**f**) Fluorescence microscopy of 293 cells transfected for 48 h with control or PCBP2 RNAi plasmid (0, 50 or 200 ng; wedges), then infected for 48 h with GFP-tagged NDV (MOI, 0.05). Original magnification, ×200. (**g**) Quantification of GFP^+ cells in **f**. Data are representative of three (**a**,**b**,**e**) or four (**d**) experiments (error bars (**d**,**e**), s.d.) or three independent experiments with similar results (**f**,**g**; mean and s.d. of 30 randomly selected fields in **g**) or are from one representative of at least three independent experiments (**c**; mean and s.d. of triplicate or duplicate assays).

was highly inducible by viral infection or IFN-α treatment, which further suggested involvement of this protein in antiviral responses. To explore the physiological role of PCBP2, we made an RNA-mediated inhibition (RNAi) construct specific for PCBP2 that substantially diminished PCBP2 abundance (**Fig. 2b** and **Supplementary Fig. 3**). The elimination of PCBP2 enhanced *Ifnb* promoter activity triggered by cytoplasmic poly(I:C), but not activity triggered by poly(dA:dT), which mimics viral or bacterial double-stranded DNA (**Fig. 2c**). As PCBP2 inhibited RLH-mediated interferon signaling, we determined whether PCBP2 affects RLH-mediated antiviral responses. Plaque assay of 293 cells infected with vesicular stomatitis virus (VSV) showed that overexpression of PCBP2 completely abolished the inhibitory effect on viral replication mediated by overexpression of MAVS, Mda5-N or RIG-I–N, but not that mediated by TBK1 (**Fig. 2d**). Consistent with that finding, elimination of PCBP2 expression by RNAi enhanced the inhibitory effect on VSV replication by MAVS overexpression (**Fig. 2e**). We also observed lower susceptibility to infection with Newcastle disease virus (NDV) in 293 cells in which PCBP2 expression was eliminated by RNAi (**Fig. 2f,g**). These data suggest that PCBP2 is a physiological suppressor of RLH-mediated cellular antiviral responses.

Characterization of the PCBP2-MAVS interaction

The ubiquitous RNA-binding protein PCBP2 had its highest expression in brain, thymus and spleen (**Supplementary Fig. 4**). PCBP2 is characterized by three heterogenous nuclear ribonucleoprotein K-homology (KH) domains and a linker region (amino acids 169–278) between KH2 and KH3. The linker region of this protein accounts for about one third of its size, but no obvious structural motifs have been described[19]. To study domains responsible for the PCBP2-MAVS interaction, we generated deletions and truncations of these two proteins and analyzed them by coimmunoprecipitation experiments. We found that the linker region of PCBP2 was absolutely required for its interaction with MAVS. Deletion of the linker alone totally abolished its binding to MAVS, whereas deletion of any KH domain did not show effect (**Fig. 3a**). *Ifnb* luciferase reporter assays confirmed the functionality of this interaction in that only PCBP2 deletion constructs with binding ability demonstrated the inhibitory effect on MAVS-induced reporter activation (**Fig. 3b**). The MAVS carboxy-terminal domain was required for interaction with PCBP2 (**Fig. 3c**). We found that a very short region in the carboxyl terminus of MAVS (amino acids 460–540) interacted with PCBP2 (**Fig. 3d**, left). MAVS contains a carboxy-terminal transmembrane domain; we determined if this domain was required for its interaction with PCBP2. We found that although a MAVS recombinant protein lacking the transmembrane domain (MAVS-ΔTM) interacted with RIG-I (**Fig. 3d**, right), it did not interact with PCBP2. Notably, when amino acids 460–510 of MAVS were deleted, PCBP2 binding was abolished (data not shown), which suggested that this part of MAVS was also required for the interaction. We further analyzed the intracellular localization of endogenous MAVS and PCBP2 in HeLa human cervical cancer cells. PCBP2 was retained mainly in the nuclei of uninfected control cells, but it translocated to cytosol and localized together with MAVS and COX IV (a mitochondrial marker) in a punctuate perinuclear pattern after SeV infection (**Fig. 3e**). MAVS overexpression also led to the translocation of PCBP2 and localization together with full-length MAVS but not with MAVS-ΔTM, which showed a dispersed pattern

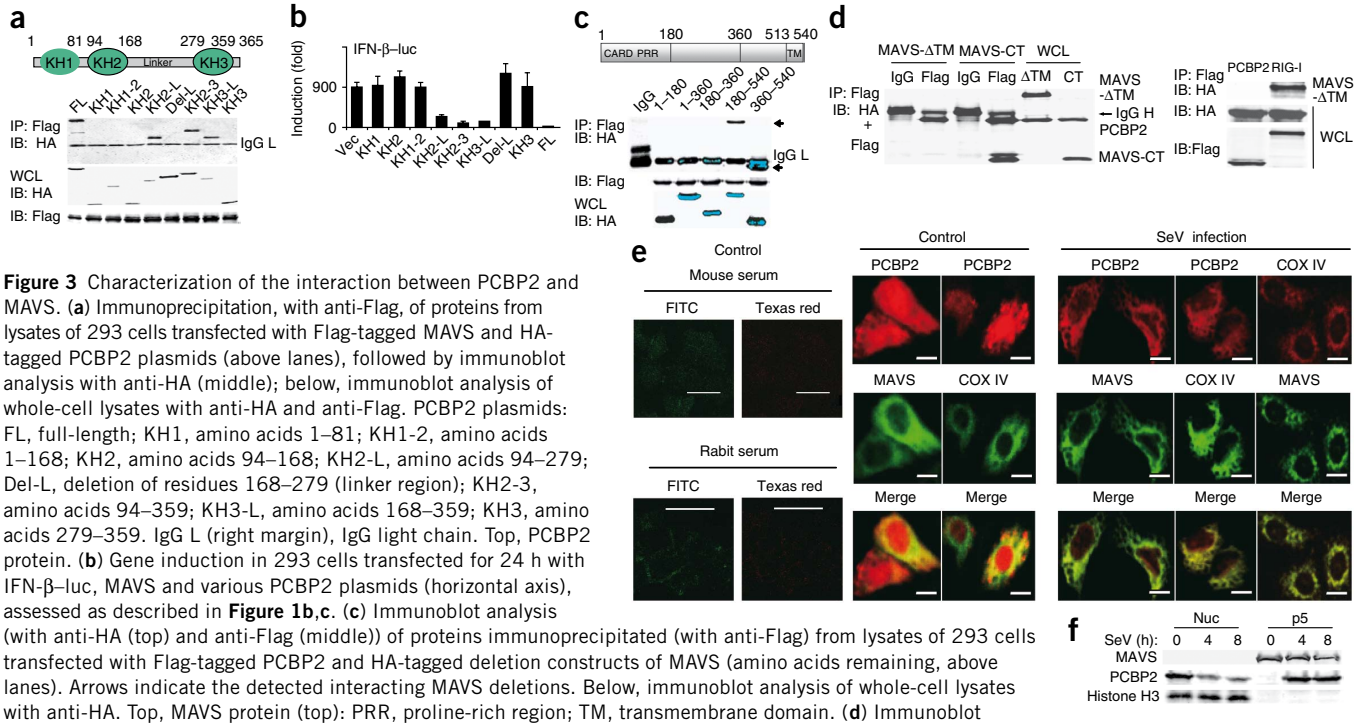

Figure 3 Characterization of the interaction between PCBP2 and MAVS. (**a**) Immunoprecipitation, with anti-Flag, of proteins from lysates of 293 cells transfected with Flag-tagged MAVS and HA-tagged PCBP2 plasmids (above lanes), followed by immunoblot analysis with anti-HA (middle); below, immunoblot analysis of whole-cell lysates with anti-HA and anti-Flag. PCBP2 plasmids: FL, full-length; KH1, amino acids 1–81; KH1-2, amino acids 1–168; KH2, amino acids 94–168; KH2-L, amino acids 94–279; Del-L, deletion of residues 168–279 (linker region); KH2-3, amino acids 94–359; KH3-L, amino acids 168–359; KH3, amino acids 279–359. IgG L (right margin), IgG light chain. Top, PCBP2 protein. (**b**) Gene induction in 293 cells transfected for 24 h with IFN-β–luc, MAVS and various PCBP2 plasmids (horizontal axis), assessed as described in **Figure 1b**,**c**. (**c**) Immunoblot analysis (with anti-HA (top) and anti-Flag (middle)) of proteins immunoprecipitated (with anti-Flag) from lysates of 293 cells transfected with Flag-tagged PCBP2 and HA-tagged deletion constructs of MAVS (amino acids remaining, above lanes). Arrows indicate the detected interacting MAVS deletions. Below, immunoblot analysis of whole-cell lysates with anti-HA. Top, MAVS protein (top): PRR, proline-rich region; TM, transmembrane domain. (**d**) Immunoblot analysis (with anti-HA and anti-Flag) of proteins immunoprecipitated (with anti-Flag) from lysates of 293 cells transfected with plasmids encoding Flag-tagged PCBP2 (left) or Flag-tagged RIG-I (right) and MAVS-ΔTM or the MAVS carboxyl terminus (MAVS-CT; residues 460–540). (**e**) Confocal microscopy of HeLa cells labeled with antibodies to various molecules (above images (right)) or control preimmune serum (left), followed by fluorescein isothiocyanate (FITC)- or Texas red–conjugated secondary antibody. Scale bars, 10 μm (right) or 50 μm (left). (**f**) Subcellular fractionation of HeLa cells infected for 0, 4 or 8 h with SeV (MOI, 0.01), then homogenized in a hypotonic buffer and separated into nuclear pellet (Nuc) and supernatant by centrifugation at 700*g*, followed by further centrifugation of the post-nuclear supernatant at 5,000*g* to obtain the mitochondrial fraction (p5); fractions were analyzed with anti-MAVS, anti-PCBP2 and antibody to the nuclear protein histone H3. Results are representative of three (**a**,**b**,**d**), four (**c**), two (**f**) or at least three (**e**) independent experiments (mean and s.d. of triplicate assays in **b**).

in the cytoplasm (**Supplementary Fig. 5**). Subcellular fractionation demonstrated rapid translocation of PCBP2 from nuclei to the mitochondrial fraction after SeV infection (**Fig. 3f**). Together these data suggest that PCBP2 interacts with MAVS in cellular conditions.

PCBP2 induces MAVS degradation

During the coimmunoprecipitation experiments, we repeatedly observed that MAVS expression was much lower after cotransfection with PCBP2. That finding prompted us to investigate the effect of PCBP2 on MAVS expression. We found that overexpression of PCBP2 led to considerable loss of overexpressed MAVS (**Supplementary Fig. 6a**,**b**), as well as endogenous MAVS (**Fig. 4a**), but not of any other proteins tested (**Supplementary Fig. 6a**). RT-PCR data showed that MAVS mRNA abundance was not altered with PCBP2 expression (**Fig. 4b**), which suggested that the decrease in MAVS occurred at the protein level. Elimination of PCBP2 expression by RNAi reversed this effect (**Fig. 4c**). The MAVS loss induced by PCBP2 overexpression was blocked by the proteasome inhibitor MG-132 (**Fig. 4d**); thus, we concluded that PCBP2 might trigger proteasomal degradation of MAVS. Notably, MAVS-ΔTM was not degraded in the same conditions (**Fig. 4e**). Those data correlated with our previous findings that MAVS-ΔTM did not interact with PCBP2. To elucidate the function of the transmembrane domain in this process, we used chimeric MAVS proteins in which the transmembrane domain was replaced with the transmembrane domain from peptides that targeted MAVS to the endoplasmic reticulum (VAMP-2–TM), to both the endoplasmic reticulum and mitochondria (Bcl-2–TM), or to the mitochondrial outer membrane (Bcl-x_L–TM)[7]. Chimeras with the transmembrane domain of Bcl-2 (Bcl-2–TM) or Bcl-x_L (Bcl-x_L–TM) did not affect MAVS degradation. In contrast, mislocalization of MAVS to the endoplasmic reticulum (VAMP-2–TM) markedly impaired MAVS degradation (**Fig. 4f**). In reporter assays, PCBP2 considerably inhibited *Ifnb* activation induced by Bcl-2–TM or Bcl-x_L–TM but not that induced by VAMP-2–TM (**Fig. 4g**). These data suggest that mitochondrial localization of MAVS is a prerequisite for PCBP2 interaction and subsequent MAVS degradation.

Next we studied the degradation of various MAVS truncation constructs. Whereas MAVS with amino-terminal truncation, containing amino acids 180–540 or 360–540, was degraded in presence of PCBP2, MAVS containing carboxy-terminal amino acids 460–540 was not (**Fig. 4h**, left). Because the last protein fragment could still bind PCBP2, we reasoned that MAVS amino acids 360–460 might contain a lysine residue (or residues) responsible for the ubiquitination and degradation of MAVS. There are three lysine residues in this region: K362, K371 and K420. We generated single substitutions (K362A, K371A or K420A) and combined point substitutions of MAVS and tested their degradation. K371A or K420A MAVS showed partial resistance to PCBP2-induced degradation (data not shown), whereas MAVS with the combined substitutions K371A and K420A (KK-AA) completely withstood the degradation (**Fig. 4h**, right). To exclude the possibility of any artifacts, we reverted the double mutant to the wild-type version (AA-KK), which had the same degradation pattern as wild-type MAVS (**Fig. 4h**, right). PCBP2 overexpression led to more polyubiquitination of wild-type MAVS but not of the KK-AA mutant (**Fig. 4i**). A cycloheximide 'chase' assay of 293 cells

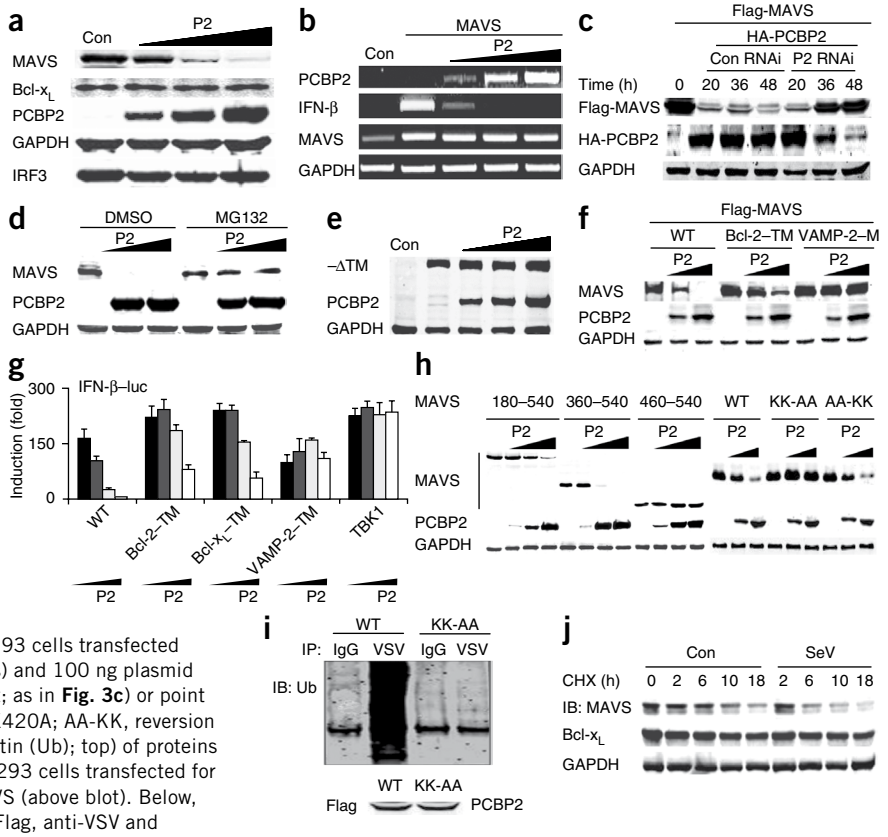

Figure 4 PCBP2 induces the degradation of MAVS. (**a**) Immunoblot analysis (with anti-MAVS, anti-IRF3 or anti-GAPDH) of lysates of 293 cells left untransfected (Con) or transfected with PCBP2 (1, 2 or 4 μg; wedge). (**b**) RT-PCR analysis of total RNA from 293 cells transfected for 24 h with plasmids encoding MAVS and PCBP2 (1, 2 or 4 μg; wedge). (**c**) Immunoblot analysis of 293 cells transfected for various times (above lanes) with plasmids encoding Flag-tagged MAVS and HA-tagged PCBP2 plus PCBP2 or control RNAi plasmid. (**d**) Immunoblot analysis of 293 cells transfected with PCBP2 (0, 2 or 4 μg; wedges) pretreated with MG132 or DMSO. (**e**) Immunoblot analysis of 293 cells transfected with MAVS-ΔTM (1 μg) and PCBP2 (1, 2 or 4 μg; wedges). (**f**) Immunoblot analysis of 293 cells transfected with Flag-tagged MAVS chimera plasmid (above lanes; 2 μg) and PCBP2 plasmid (0, 1, 2 μg; wedges). WT, wild-type. (**g**) Gene induction in 293 cells transfected for 24 h with IFN-β–luc, 100 ng MAVS chimera plasmid or TBK1 (horizontal axis) and PCBP2 plasmid (0, 50, 100 or 200 ng; wedges), assessed as described in **Figure 1b,c**. (**h**) Immunoblot analysis of 293 cells transfected for 24 h with PCBP2 (0, 50, 100 or 200 ng; wedges) and 100 ng plasmid encoding Flag-tagged MAVS deletion constructs (left; as in **Fig. 3c**) or point substitution constructs (right: KK-AA, K371A plus K420A; AA-KK, reversion of KK-AA). (**i**) Immunoblot analysis (with anti-ubiquitin (Ub); top) of proteins immunoprecipitated (with anti-VSV) from lysates of 293 cells transfected for 24 h with plasmid encoding wild-type or KK-AA MAVS (above blot). Below, immunoblot analysis of whole-cell lysates with anti-Flag, anti-VSV and anti-HA to assess the expression of PCBP2, MAVS and ubiquitin. (**j**) Immunoblot analysis of MAVS degradation (top) in lysates of 293 cells left untreated or infected for 2 h with SeV, then treated for various times (above lanes) with cycloheximide (CHX). Below, immunoblot analysis with anti-GAPDH and anti-Bcl-x_L to demonstrate specific degradation of MAVS and equal loading. Results are representative of three independent experiments (error bars (**g**), s.d.).

infected with SeV showed that viral infection caused rapid degradation of endogenous MAVS (**Fig. 4j**), which suggested that MAVS degradation occurred in physiological conditions. Together these results demonstrate that PCBP2 induces proteosomal degradation of MAVS.

PCBP2 WB sequence is critical for MAVS degradation

Deletion of the linker region of PCBP2 not only blocked its interaction with MAVS but also impaired its ability to induce MAVS degradation (**Fig. 5a**). That finding prompted us to investigate this region more closely. The Eukaryotic Linear Motif website

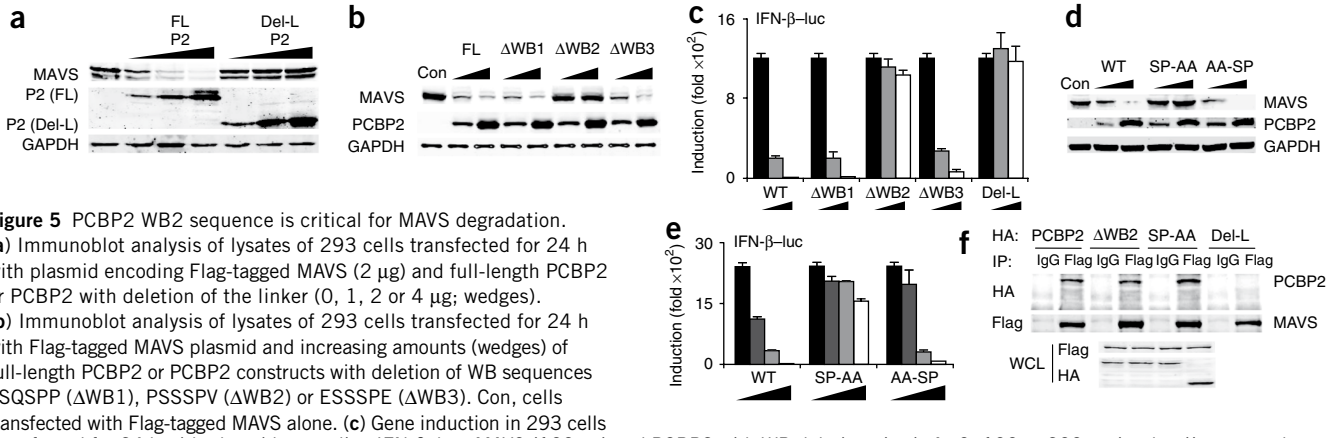

Figure 5 PCBP2 WB2 sequence is critical for MAVS degradation. (**a**) Immunoblot analysis of lysates of 293 cells transfected for 24 h with plasmid encoding Flag-tagged MAVS (2 μg) and full-length PCBP2 or PCBP2 with deletion of the linker (0, 1, 2 or 4 μg; wedges). (**b**) Immunoblot analysis of lysates of 293 cells transfected for 24 h with Flag-tagged MAVS plasmid and increasing amounts (wedges) of full-length PCBP2 or PCBP2 constructs with deletion of WB sequences LSQSPP (ΔWB1), PSSSPV (ΔWB2) or ESSSPE (ΔWB3). Con, cells transfected with Flag-tagged MAVS alone. (**c**) Gene induction in 293 cells transfected for 24 h with plasmids encoding IFN-β–luc, MAVS (100 ng) and PCBP2 with WB deletions (as in **b**; 0, 100 or 200 ng (wedges)), assessed as described in **Figure 1b,c**. (**d**) Immunoblot analysis of lysates of 293 cells transfected for 24 h with plasmids encoding Flag-tagged MAVS and PCBP2 with point substitutions of WB2 (SP-AA, PSSSPV to PSSAAV; AA-SP, reversion of SP-AA to wild-type sequence). Con, cells transfected with Flag-tagged MAVS alone. (**e**) Gene induction in 293 cells transfected for 24 h with plasmids encoding IFN-β–luc, MAVS (100 ng) and the PCBP2 WB2 point substitutions in **d** (0, 50, 100 or 200 ng; wedges), assessed as described in **Figure 1b,c**. (**f**) Immunoblot analysis (with anti-HA (top) or anti-Flag (middle)) of proteins immunoprecipitated (with anti-Flag or control mouse IgG) from lysates of 293 cells transfected with plasmids for Flag-tagged MAVS and HA-tagged wild-type or PCBP2 WB2 mutants. Below, immunoblot analysis of expression of the transfected proteins. Data are representative of three independent experiments (**a**,**b**,**d**,**f**) or are from one representative of at least three independent experiments (mean and s.d. of triplicate or duplicate assays; **c**,**e**).

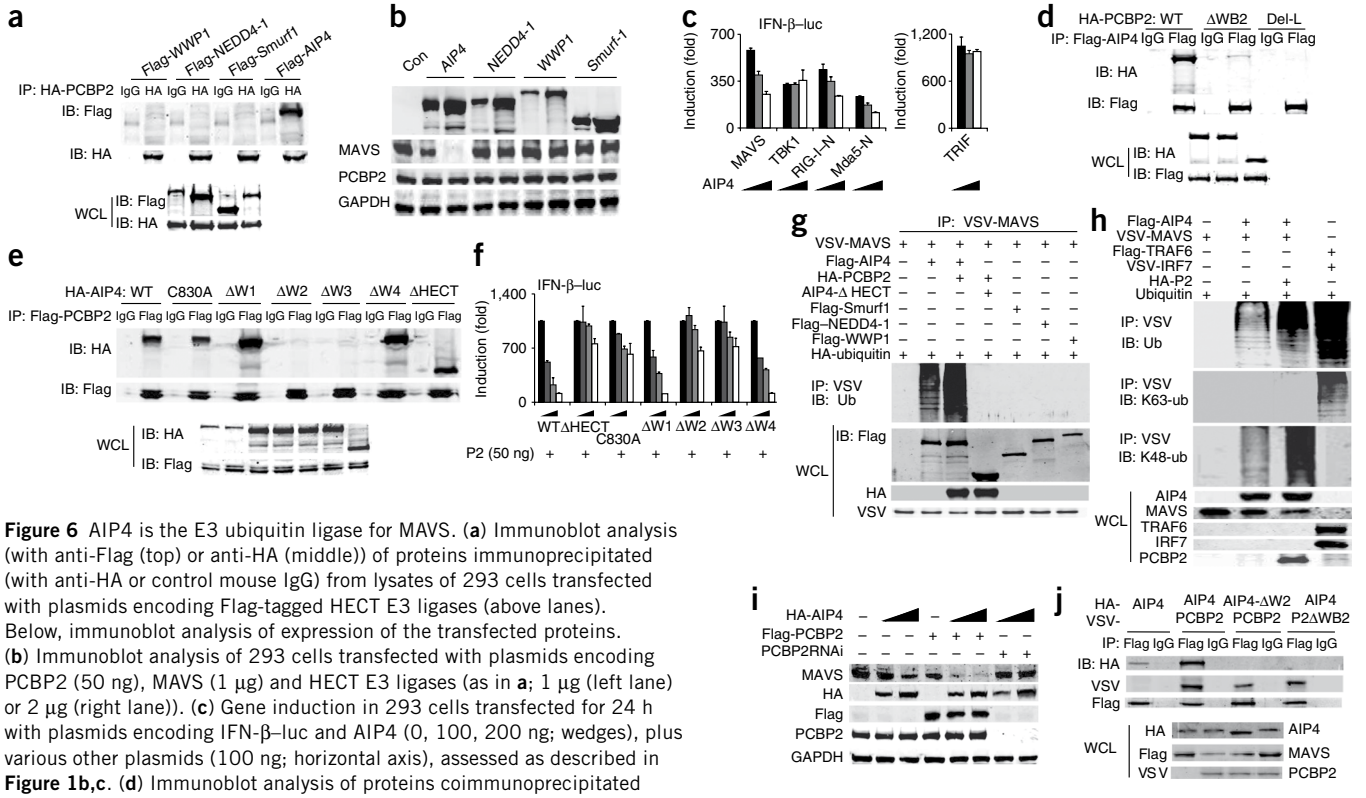

Figure 6 AIP4 is the E3 ubiquitin ligase for MAVS. (**a**) Immunoblot analysis (with anti-Flag (top) or anti-HA (middle)) of proteins immunoprecipitated (with anti-HA or control mouse IgG) from lysates of 293 cells transfected with plasmids encoding Flag-tagged HECT E3 ligases (above lanes). Below, immunoblot analysis of expression of the transfected proteins. (**b**) Immunoblot analysis of 293 cells transfected with plasmids encoding PCBP2 (50 ng), MAVS (1 μg) and HECT E3 ligases (as in **a**; 1 μg (left lane) or 2 μg (right lane)). (**c**) Gene induction in 293 cells transfected for 24 h with plasmids encoding IFN-β–luc and AIP4 (0, 100, 200 ng; wedges), plus various other plasmids (100 ng; horizontal axis), assessed as described in **Figure 1b,c**. (**d**) Immunoblot analysis of proteins coimmunoprecipitated (as described in **a**) from 293 cells transfected with plasmids encoding Flag-tagged AIP4 and HA-tagged PCBP2 (wild type or with deletion of WB2 (ΔWB2) or the linker region (Del-L)). (**e**) Immunoblot analysis of proteins coimmunoprecipitated (as described in **a**) from 293 cells transfected with plasmids encoding HA-tagged AIP4 (above blot): wild type; C830A mutant; deletion of residues 281–323 (ΔW1), 319–355 (ΔW2), 393–435 (ΔW3) or 437–475 (ΔW4); or containing residues 1-523 (ΔHECT). (**f**) Gene induction in 293 cells transfected with plasmids encoding IFN-β–luc, MAVS (100 ng), PCBP2 (50 ng) and the AIP4 constructs in **e** (0, 50, 100 or 200 ng; wedges), assessed as described in **Figure 1b,c**. (**g**) Immunoblot analysis (with anti-ubiquitin; top) of proteins immunoprecipitated (with anti-VSV) from lysates of 293 cells transfected for 20 h with various combinations of plasmids (above lanes). Below, immunoblot analysis of expression of the expression of HECT domain E3 ligases, ubiquitin and MAVS in whole-cell lysates, analyzed with anti-Flag, anti-HA and anti-VSV. (**h**) Immunoblot analysis (with anti-ubiquitin or antibody to K63-linked or K48-linked polyubiquitin (K63-ub or K48-ub, respectively); top) of proteins immunoprecipitated (with anti-VSV) from lysates of 293 cells transfected for 24 h with various combinations of plasmids (above lanes). Below, immunoblot analysis of the expression of Flag-tagged AIP4, TRAF6, PCBP2 and VSV-MAVS, or VSV-IRF7 in whole-cell lysates, analyzed with anti-Flag, anti-HA or anti-VSV. (**i**) Immunoblot analysis of 293 cells transfected for 24 h with control or PCBP2 RNAi plasmid, then transfected with various combinations of plasmids (above lanes). (**j**) Immunoblot analysis of the AIP4-MAVS interaction in 293 cells transfected with various plasmids (above lanes); after precipitation of MAVS with anti-Flag, its interaction with AIP4 was detected with anti-HA. Below, immunoblot analysis of the expression of AIP4, MAVS and PCBP2 in whole-cell lysates, analyzed with anti-HA, anti-Flag or anti-VSV. Data are representative of three independent experiments (**a**,**b**,**d**,**e**,**g**–**i**) or are from one representative of at least three independent experiments (mean and s.d. of triplicate or duplicate assays; **c**,**f**).

showed that there are three conserved WW domain–binding (WB) sequences in PCBP2 (WB1, WB2 and WB3), all located in the linker region (amino acid sequences: WB1, LSQSPP; WB2, PSSSPV; WB3, ESSSPE). WW domains are small modular domains that mediate protein-protein interactions through the binding of short proline-rich regions[20]; thus, they are involved in many cellular processes, including ubiquitin-mediated protein degradation[21]. Therefore, we wanted to determine if these WB sequences were important for PCBP2-induced degradation of MAVS. We found that deletion of WB2 alone abolished the ability of PCBP2 to induce MAVS degradation (**Fig. 5b**) and its ability to inhibit MAVS-driven activation of *Ifnb* (**Fig. 5c**). To confirm those findings, we generated a point substitution that replaced the amino acids serine-proline, which were critical for WW domain recognition, with alanine-alanine (SP-AA; PSSSPV to PSSAAV) and found that this mutant had features similar to those of the WB2 deletion mutant (**Fig. 5d**,**e**). Consistent with that, the reverse substitution (AA-SP) supported the full capacity of MAVS degradation. Notably, whereas deletion of the linker abolished the PCBP2-MAVS interaction, deletion of WB2 or the substitution SP-AA did not (**Fig. 5f**), which indicates the potential of this sequence to recruit some unknown protein(s) responsible for MAVS degradation.

Identification of AIP4 as the E3 ligase for MAVS

HECT domain–containing E3 ubiquitin ligases are a family of proteins composed of a catalytic carboxy-terminal HECT domain, an amino-terminal C2 domain and WW domains responsible for cellular localization and substrate recognition[22]. These proteins regulate diverse biological processes through the degradation of targeted proteins by WW domain recognition[21]. The mouse and human genomes encode five HECT E3 ligases that can be expressed as differently spliced isoforms: NEDD4-1/2, AIP4 (Itch in mice), WWP1/2, Smurf1/2 and BUL1/2. In a search of which HECT E3 ligase was involved in PCBP2-mediated degradation of MAVS, we cloned the genes encoding these proteins, except for BUL1, and tested their ability to interact with PCBP2 and degrade MAVS. Only AIP4 associated with PCBP2 (**Fig. 6a**) and

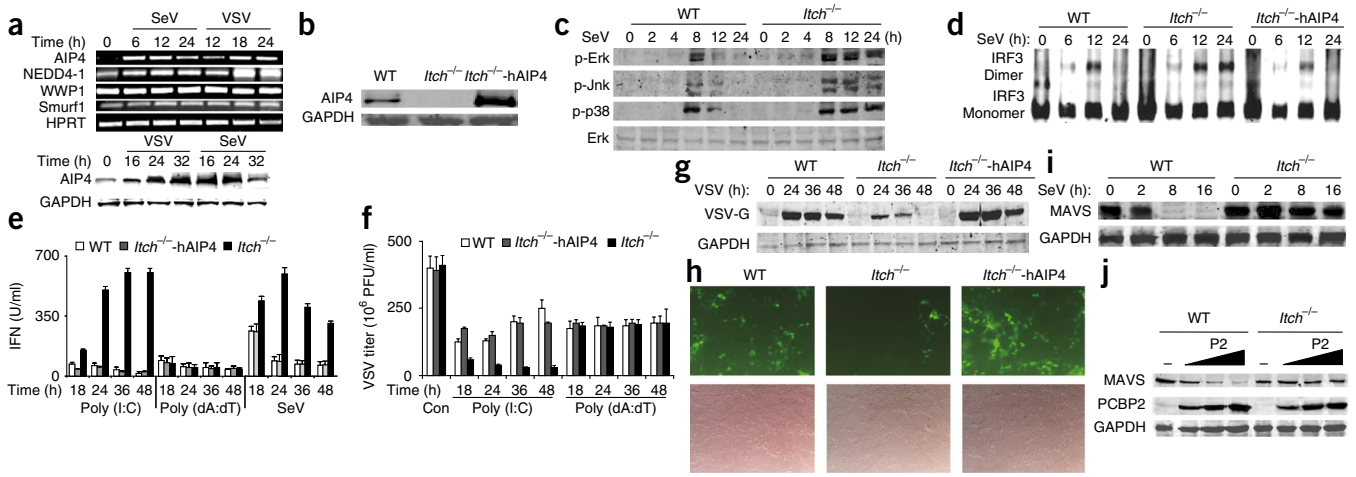

Figure 7 AIP4 negatively regulates RLH-mediated signaling. (**a**) RT-PCR analysis (top) and immunoblot analysis (bottom) of the expression of HECT domain E3 ligases in U937 cells infected for various times (above lanes) with SeV or VSV. (**b**) Immunoblot analysis of the expression of AIP4 in wild-type MEFs, *Itch*$^{-/-}$ MEFs and *Itch*$^{-/-}$ MEFs reconstituted with human AIP4 (*Itch*$^{-/-}$ hAIP4). (**c**) Immunoblot analysis of the phosphorylation (p-) of Jnk, p38 and Erk in lysates of wild-type and *Itch*$^{-/-}$ MEFs infected for various times (above lanes) with SeV. (**d**) IRF3 dimerization in MEFs infected for various times (above lanes) with SeV, detected by native gel electrophoresis with anti-IRF3. (**e**) Bioassay of type I interferon in supernatants of MEFs transfected with poly(I:C) or poly(dA:dT) or infected with SeV for various times (horizontal axis). (**f**) Plaque assay of VSV titers in MEFs transfected for various times (horizontal axis) with poly(I:C) or poly(dA:dT), then infected with VSV. (**g**) Immunoblot analysis of lysates of MEFs infected for various times (above lanes) with VSV (MOI, 0.1), probed with anti–VSV G protein. (**h**) Fluorescence microscopy of MEFs infected for 48 h with GFP-tagged NDV (MOI, 0.5). Original magnification, ×200. (**i**) Immunoblot analysis of lysates of MEFs infected for various times (above lanes) with SeV in the presence of cycloheximide, probed with anti-MAVS. (**j**) Immunoblot analysis (as in **i**) of MEFs transfected for 36 h with increasing amounts (wedges) of PCBP2. Data are representative of three independent experiments (**a**–**d**,**f**–**i**; error bars (**f**), s.d.) or are from one representative of at least four independent experiments (mean and s.d. of triplicate or duplicate assays; **e**).

caused MAVS degradation (**Fig. 6b**). Moreover, overexpression of AIP4 specifically inhibited *Ifnb* activation induced by RIG-I–Mda5–MAVS (**Fig. 6c**), which suggested a function for AIP4 in RLH-mediated signaling. The interaction between PCBP2 and AIP4 was abrogated when the linker region or WB2 of PCBP2 was deleted (**Fig. 6d**), which confirmed our previous data indicating that this region was critical for PCBP2-mediated degradation of MAVS. To determine which of the four WW domains (WW1–WW4) in AIP4 is important for the AIP4-PCBP2 interaction, we deleted individual WW domains and found that deletion of WW2 or WW3 completely abolished the interaction (**Fig. 6e**), as well as the ability of AIP4 to suppress *Ifnb* activation (**Fig. 6f**). It has been reported that the active site Cys830 in the HECT domain of AIP4 is vital for its E3 ligase function as docking site for ubiquitin transfer[23]. We generated the point substitution C830A in AIP4 and an AIP4 truncation lacking the HECT domain. These mutant proteins interacted with PCBP2 but lost the ability to inhibit MAVS-induced activation of *Ifnb* (**Fig. 6e**,**f**), which suggested that the E3 ligase activity of AIP4 was required for this function. Overexpression of AIP4 caused substantial polyubiquitination of MAVS, but overexpression of AIP4 lacking the HECT domain and PCBP2 did not (**Fig. 6g**). *In vitro* ubiquitination assays confirmed that AIP4 (E3 ligase), but not AIP4 with the C830A substitution, together with E1 ubiquitin-activating enzyme and UbcH5b or UbcH5c (E2 ubiquitin-conjugating enzyme), effectively delivered ubiquitin to MAVS, and incorporation of PCBP2 into the reaction greatly enhanced MAVS ubiquitination (**Supplementary Fig. 7**). Finally, we found that PCBP2-AIP4 catalyzed the ubiquitination of MAVS with wild-type ubiquitin and ubiquitin with a lysine residue only at position 48 (all others substituted with arginine) but not with ubiquitin with a lysine residue only at position 63 (**Supplementary Fig. 8**). Consistent with that, we detected AIP4-catalyzed ubiquitination of MAVS by antibodies specific for ubiquitin or K48-linked polyubiquitin, but not by antibodies specific for K63-linked polyubiquitin (**Fig. 6h**), which indicated that MAVS was ubiquitinated by K48-linked conjugation. These data collectively indicate that AIP4 is the E3 ligase for MAVS.

PCBP2 functions as an adaptor between MAVS and AIP4

We found that AIP4 (1, 2 or 4 μg) caused only partial MAVS degradation and inhibition of IFN-β expression (**Fig. 6i**). However, when we cotransfected a small amount of PCBP2 (50 ng), we observed greatly enhanced MAVS degradation (**Fig. 6i**) and IFN-β inhibition (**Supplementary Fig. 9**). Elimination of PCBP2 expression by RNAi abrogated AIP4-induced MAVS degradation (**Fig. 6i**), which indicated that AIP4-mediated MAVS degradation depended on PCBP2. Given those data, together with our data reported above, we hypothesized that PCBP2 functions as an adaptor, recruiting AIP4 to interact and degrade MAVS. To test that hypothesis, we did coimmunoprecipitation to analyze the interaction of MAVS and AIP4 in the presence or absence of PCBP2 and found that the interaction between MAVS and AIP4 became obvious only in the presence of wild-type PCBP2, but not in the presence of PCBP2 lacking WB2, whereas AIP4 lacking WW2 impaired its interaction with MAVS, even in the presence of wild-type PCBP2 (**Fig. 6j**). We further confirmed that effect by demonstrating that the interaction between the endogenous proteins MAVS and AIP4 was induced by PCBP2 but not by PCBP2 lacking WB2 (**Supplementary Fig. 10**). These data indicated that PCBP2 functions as an adaptor between MAVS and AIP4 through its WB sequence.

AIP4 negatively regulates cellular antiviral responses

Similar to PCBP2 expression, AIP4 expression was also induced after viral infection (**Fig. 7a**). Elimination of AIP4 by RNAi (**Supplementary Fig. 11a**) enhanced the inhibitory effect on VSV replication induced by transfection of poly(I:C) (**Supplementary Fig. 11b**) and the IRF3 dimerization induced by MAVS overexpression

(**Supplementary Fig. 11c**). Consistent with that, we observed greater resistance to NDV infection in cells in which AIP4 was eliminated by RNAi (**Supplementary Fig. 11d**). These data suggest that AIP4 is a suppressor of RLH-mediated antiviral responses.

To further test the function of AIP4 in RLH-mediated cellular antiviral responses, we used *Itch*$^{-/-}$ MEFs, which are deficient in mouse AIP4. We generated pools of *Itch*$^{-/-}$ MEFs that stably expressed Flag-tagged human AIP4, using a retroviral vector to avoid cloning variations (**Fig. 7b**). We found that *Itch*$^{-/-}$ MEFs had persistent activation of the kinases Erk, p38 and Jnk after infection with SeV (**Fig. 7c**) and also had persistent activation of IRF3 (**Fig. 7d**). Consistent with that, type I interferon bioassay and TNF bioassay showed that *Itch*$^{-/-}$ MEFs had greatly enhanced and sustained cytokine production after transfection of poly(I:C) or infection with SeV but not after transfection of poly(dA:dT) (**Fig. 7e** and data not shown). VSV plaque assay confirmed that result, showing that *Itch*$^{-/-}$ MEFs had much greater and sustained production of type I interferons in response to poly(I:C) transfection than did wild-type or *Itch*$^{-/-}$ MEFs stably expressing human AIP4 (**Fig. 7f**). We obtained similar results for the production of other cytokines, including IL-6 and ISG15 (**Supplementary Fig. 12**). VSV replication in *Itch*$^{-/-}$ MEFs was considerably suppressed as well, as indicated by less VSV G protein (**Fig. 7g**). We also observed resistance to NDV infection in *Itch*$^{-/-}$ MEFs (**Fig. 7h**). Notably, although MAVS in wild-type MEFs was degraded after viral infection or PCBP2 overexpression, MAVS in *Itch*$^{-/-}$ MEFs remained constant (**Fig. 7i,j**). These data collectively indicate AIP4 is a vital component that negatively regulates RLH-mediated antiviral responses.

DISCUSSION

Studies have demonstrated many functions for PCBP2 as either a nucleic acid–associating protein[24] or a protein-interacting molecule, 'preferably' for RNA-binding proteins[15–17]. In our study here, using yeast two-hybrid screening, we have identified PCBP2 as a MAVS-associating protein. It also interacted with RIG-I and Mda5, probably through MAVS–RIG-I and MAVS-Mda5 interactions. Several lines of evidence showed that PCBP2 has a negative role in this pathway. First, like many other negative regulators, PCBP2 was rapidly upregulated after viral infection or treatment with type I interferon. Second, endogenous PCBP2 bound to MAVS in a stimulus-dependent manner, which led to the attenuation of RLH-mediated antiviral effects. Third, whereas exogenous PCBP2 abolished the inhibitory effect on viral replication mediated by RLHs, elimination of PCBP2 expression by siRNA greatly enhanced the antiviral response. We further found that the attenuation caused by PCBP2 was mediated by MAVS degradation via the ubiquitin-proteasome pathway. Notably, the linker region of PCBP2 was absolutely necessary for its binding to and subsequent degradation of MAVS. Two lysine residues in MAVS were critical for the ubiquitination and degradation. However, as PCBP2 itself is not an E3 ubiquitin ligase, additional E3 ligases not yet identified must be involved in this process.

Among all WW domain–containing HECT E3 ligases, we regard AIP4 as the enzyme that regulates MAVS turnover *in vivo*. First, it specifically interacted with PCBP2 via interaction between the WW domain and the WB sequence. Second, it formed a complex with MAVS-PCBP2 and contributed to K48-linked ubiquitination and degradation of MAVS. Third, knockdown of AIP4 by siRNA specifically resulted in an increase in MAVS protein abundance (data not shown). Fourth, substitution of the conserved cysteine residue in the HECT domain of AIP4 abolished its E3 ligase activity in MAVS ubiquitination. Fifth, AIP4-deficient (*Itch*$^{-/-}$) MEFs had a markedly enhanced response to viral infection and poly(I:C) transfection relative to that of wild-type cells, which was suppressed by restoration of functional AIP4. Finally, MAVS in *Itch*$^{-/-}$ MEFs was not degraded after viral infection or PCBP2 overexpression. These data indicate that AIP4, but not other HECT E3 ligases, was indeed responsible for the degradation of MAVS.

Although the involvement of AIP4 in many signaling pathways and pathological conditions has been studied extensively[25], its functions in innate immunity have rarely been reported. Studies have identified several AIP4 substrates as central participants in the immune response, such as Jun family members[26–28]; PLC-γ and PKC-θ[29,30]; Notch receptors[31,32]; and c-FLIP[33] and RIP1 (ref. 34). Although Itch is involved in various signaling pathways, the enhanced antiviral responses in *Itch*$^{-/-}$ cells were probably not due to mechanisms other than AIP4-mediated MAVS degradation for several reasons. First, there were no differences among MEFs (wild-type MEFs, *Itch*$^{-/-}$ MEFs and *Itch*$^{-/-}$ MEFs expressing human AIP4) transfected with poly(dA:dT), despite the considerable differences between those cells and cells transfected with poly(I:C) or infected with SeV. These data support the fact that poly(dA:dT)-induced pathway activation and type I interferon production are MAVS independent, whereas poly(I:C)- or SeV-triggered responses are MAVS dependent. Moreover, we obtained similar results in 293 cells with elimination of AIP4 by RNAi. Second, thus far, RIG-I–Mda5–MAVS–TBK1–IKKi is the only known pathway activated by cytoplasmic viral nucleic acids to mount an antiviral response[1], and defects in the degradation of components in this pathway are reported to induce enhanced antiviral responses[12]. Finally, production of type I interferon induced by transfection of poly(dA:dT) was normal in *Itch*$^{-/-}$ MEFs, which indicated an intact amplification loop regulated by the pathway consisting of the kinase Jak and transcription factor STAT; thus, the enhanced production of type I interferon in response to poly(I:C) transfection or SeV infection was probably not due to the autologous Jak-STAT pathway, which is known to amplify antiviral responses.

Our designation of MAVS as another substrate of AIP4 further expands the biological functions of AIP4 in immune regulation, indicating that AIP4 controls cellular antiviral responses by regulating the abundance of MAVS. More notably, as *Itch*$^{-/-}$ mice have characteristic autoimmunity and chronic multiorgan inflammation, our results raise the possibility that *Itch*$^{-/-}$ mice may experience these immune disorders in part because of dysregulated RLHs signaling. This results in the uncontrolled activation of inflammatory molecules and in particular greater production of type I interferon, which is a hallmark of autoimmune disease.

PCBP2 overexpression enhanced the interaction between MAVS and AIP4 and led to more degradation of MAVS. Elimination of PCBP2 abrogated the ability of AIP4 to interact with and degrade MAVS. These data suggest that PCBP2 functions as an adaptor that recruits AIP4 to MAVS. It has been reported that the HECT E3 ubiquitin ligases can act together with a variety of accessory and adaptor proteins, which contribute to their substrate recruitment, subcellular localization and enzymatic activity[35,36]. For example, Numb recruits the carboxy-terminal intracellular domain of Notch to AIP4 through its phosphorylated tyrosine–binding domain, which promotes the degradation of the intracellular domain[31]. Moreover, TAX1BP1 is reported to function as an adaptor that recruits RIP1 to AIP4 (ref. 34). Thus, our data add PCBP2 as another member of this growing list of AIP4 adaptors.

Our data have shown that the AIP4-PCBP2-MAVS axis defines a regulating mechanism previously unreported in RLH-mediated signaling. Viral invasion stimulates cellular RLH pathways, activates MAVS as well as other signaling molecules, and results in secretion of type I interferon that would induce a set of interferon-stimulated

genes, including the gene encoding PCBP2. PCBP2 then associates with MAVS on the mitochondrial membrane through its linker region and recruits AIP4 through interactions between the WW domain and WB sequences, forming the AIP4-PCBP2-MAVS complex, which leads to ubiquitination and degradation of MAVS, promptly terminating the antiviral activities.

As it is a mitochondrial transmembrane protein, the proper localization of MAVS has been shown to be vital for its antiviral functions, which was also the case for the interaction with PCBP2 and subsequent degradation of MAVS as well. The transmembrane domain of MAVS is about 20 amino acids in length, so it is difficult to conceive that this domain physically mediates the interaction of MAVS with PCBP2. More probably the function of the transmembrane domain is to ensure the proper localization of MAVS for interaction with PCBP2. We confirmed that hypothesis using MAVS chimeras. Chimeras targeted for endoplasmic reticulum localization were not degraded, whereas chimeras targeted to the mitochondria were degraded like the wild-type protein.

In summary, our data have introduced a HECT E3 ligase that regulates activity of the RLH pathway. We have provided evidence that PCBP2 is another member of the AIP4 adaptors. Proper mitochondrial localization of MAVS and specific stimuli were both required for MAVS targeting and the MAVS-degradation process mediated by ubiquitin with lysine at position 48 only, demonstrating 'fine tuning' of spatiotemporal regulation of the innate immune response.

METHODS

Methods and any associated references are available in the online version of the paper at http://www.nature.com/natureimmunology/.

Accession codes. UCSD-Nature Signaling Gateway (http://www.signaling-gateway.org): A000959.

Note: Supplementary information is available on the Nature Immunology website.

ACKNOWLEDGMENTS

We thank D. Chen and D. Gao (Peking University) for technical assistance and the 293 cDNA library for yeast two-hybrid screening; Z. Chen (University of Texas Southwestern Medical Center) for MAVS chimera expression vectors; E. Harhaj (University of Miami) for *Itch*$^{-/-}$ MEFs; Q. Chen (Nankai University) for antibody to Bcl-x_L (anti-Bcl-x_L); H. Shu (Wuhan University) for HA-UB(K48) and HA-UB(K63) (plasmids encoding ubiquitin-K48 and ubiquitin-K63); C. Zheng (Wuhan University) for SeV; and C. Wang (Shanghai Institutes for Biological Sciences) for green fluorescent protein (GFP)-tagged NDV. Supported by the National Natural Science Foundation of China (30772024, 30721064), the National Basic Research Program of China (2007CB914502) and the Key Project of the Chinese Ministry of Education (108002).

AUTHOR CONTRIBUTIONS

Z.J. designed research; F.Y., H.S., X.Z., W.S. and S.L. did research; Z.Z. contributed new reagents and analytical tools; F.Y., H.S., X.Z., W.S. and Z.J. analyzed data; and F.Y., X.Z. and Z.J. wrote the paper.

Published online at http://www.nature.com/natureimmunology/.
Reprints and permissions information is available online at http://npg.nature.com/reprintsandpermissions/.

1. Kumagai, Y., Takeuchi, O. & Akira, S. Pathogen recognition by innate receptors. *J. Infect. Chemother.* **14**, 86–92 (2008).
2. Gitlin, L. *et al.* Essential role of mda-5 in type I IFN responses to polyriboinosinic: polyribocytidylic acid and encephalomyocarditis picornavirus. *Proc. Natl. Acad. Sci. USA* **103**, 8459–8464 (2006).
3. Kato, H. *et al.* Cell type-specific involvement of RIG-I in antiviral response. *Immunity* **23**, 19–28 (2005).
4. Kato, H. *et al.* Differential roles of MDA5 and RIG-I helicases in the recognition of RNA viruses. *Nature* **441**, 101–105 (2006).
5. Kawai, T. *et al.* IPS-1, an adaptor triggering RIG-I- and Mda5-mediated type I interferon induction. *Nat. Immunol.* **6**, 981–988 (2005).
6. Meylan, E. *et al.* Cardif is an adaptor protein in the RIG-I antiviral pathway and is targeted by hepatitis C virus. *Nature* **437**, 1167–1172 (2005).
7. Seth, R.B., Sun, L., Ea, C.K. & Chen, Z.J. Identification and characterization of MAVS, a mitochondrial antiviral signaling protein that activates NF-κB and IRF3. *Cell* **122**, 669–682 (2005).
8. Xu, L.G. *et al.* VISA is an adapter protein required for virus-triggered IFN-β signaling. *Mol. Cell* **19**, 727–740 (2005).
9. Bhoj, V.G. & Chen, Z.J. Ubiquitylation in innate and adaptive immunity. *Nature* **458**, 430–437 (2009).
10. Pickart, C.M. Mechanisms underlying ubiquitination. *Annu. Rev. Biochem.* **70**, 503–533 (2001).
11. Glickman, M.H. & Ciechanover, A. The ubiquitin-proteasome proteolytic pathway: destruction for the sake of construction. *Physiol. Rev.* **82**, 373–428 (2002).
12. Arimoto, K. *et al.* Negative regulation of the RIG-I signaling by the ubiquitin ligase RNF125. *Proc. Natl. Acad. Sci. USA* **104**, 7500–7505 (2007).
13. Paz, S. *et al.* Ubiquitin-regulated recruitment of IκB kinase ε to the MAVS interferon signaling adapter. *Mol. Cell. Biol.* **29**, 3401–3412 (2009).
14. Makeyev, A.V. & Liebhaber, S.A. The poly(C)-binding proteins: a multiplicity of functions and a search for mechanisms. *RNA* **8**, 265–278 (2002).
15. Funke, B. *et al.* The mouse poly(C)-binding protein exists in multiple isoforms and interacts with several RNA-binding proteins. *Nucleic Acids Res.* **24**, 3821–3828 (1996).
16. Wang, Z., Day, N., Trifillis, P. & Kiledjian, M. An mRNA stability complex functions with poly(A)-binding protein to stabilize mRNA in vitro. *Mol. Cell. Biol.* **19**, 4552–4560 (1999).
17. Bedard, K.M., Daijogo, S. & Semler, B.L. A nucleo-cytoplasmic SR protein functions in viral IRES-mediated translation initiation. *EMBO J.* **26**, 459–467 (2007).
18. Blyn, L.B. *et al.* Poly(rC) binding protein 2 binds to stem-loop IV of the poliovirus RNA 5′ noncoding region: identification by automated liquid chromatography-tandem mass spectrometry. *Proc. Natl. Acad. Sci. USA* **93**, 11115–11120 (1996).
19. Sean, P., Nguyen, J.H. & Semler, B.L. The linker domain of poly(rC) binding protein 2 is a major determinant in poliovirus cap-independent translation. *Virology* **378**, 243–253 (2008).
20. Chen, H.I. & Sudol, M. The WW domain of Yes-associated protein binds a proline-rich ligand that differs from the consensus established for Src homology 3-binding modules. *Proc. Natl. Acad. Sci. USA* **92**, 7819–7823 (1995).
21. Ingham, R.J., Gish, G. & Pawson, T. The Nedd4 family of E3 ubiquitin ligases: functional diversity within a common modular architecture. *Oncogene* **23**, 1972–1984 (2004).
22. Lu, P.J., Zhou, X.Z., Shen, M. & Lu, K.P. Function of WW domains as phosphoserine- or phosphothreonine-binding modules. *Science* **283**, 1325–1328 (1999).
23. Scheffner, M., Nuber, U. & Huibregtse, J.M. Protein ubiquitination involving an E1–E2-E3 enzyme ubiquitin thioester cascade. *Nature* **373**, 81–83 (1995).
24. Dejgaard, K. & Leffers, H. Characterisation of the nucleic-acid-binding activity of KH domains. Different properties of different domains. *Eur. J. Biochem.* **241**, 425–431 (1996).
25. Hustad, C.M. *et al.* Molecular genetic characterization of six recessive viable alleles of the mouse agouti locus. *Genetics* **140**, 255–265 (1995).
26. Oberst, A. *et al.* The Nedd4-binding partner 1 (N4BP1) protein is an inhibitor of the E3 ligase Itch. *Proc. Natl. Acad. Sci. USA* **104**, 11280–11285 (2007).
27. Fang, D. *et al.* Dysregulation of T lymphocyte function in itchy mice: a role for Itch in T_H2 differentiation. *Nat. Immunol.* **3**, 281–287 (2002).
28. Gao, M. *et al.* Jun turnover is controlled through JNK-dependent phosphorylation of the E3 ligase Itch. *Science* **306**, 271–275 (2004).
29. Mueller, D.L. E3 ubiquitin ligases as T cell anergy factors. *Nat. Immunol.* **5**, 883–890 (2004).
30. Heissmeyer, V. *et al.* Calcineurin imposes T cell unresponsiveness through targeted proteolysis of signaling proteins. *Nat. Immunol.* **5**, 255–265 (2004).
31. McGill, M.A. & McGlade, C.J. Mammalian numb proteins promote Notch1 receptor ubiquitination and degradation of the Notch1 intracellular domain. *J. Biol. Chem.* **278**, 23196–23203 (2003).
32. Matesic, L.E., Haines, D.C., Copeland, N.G. & Jenkins, N.A. Itch genetically interacts with Notch1 in a mouse autoimmune disease model. *Hum. Mol. Genet.* **15**, 3485–3497 (2006).
33. Chang, L. *et al.* The E3 ubiquitin ligase itch couples JNK activation to TNFα-induced cell death by inducing c-FLIP(L) turnover. *Cell* **124**, 601–613 (2006).
34. Shembade, N. *et al.* The E3 ligase Itch negatively regulates inflammatory signaling pathways by controlling the function of the ubiquitin-editing enzyme A20. *Nat. Immunol.* **9**, 254–262 (2008).
35. Melino, G. *et al.* Itch: a HECT-type E3 ligase regulating immunity, skin and cancer. *Cell Death Differ.* **15**, 1103–1112 (2008).
36. Shearwin-Whyatt, L., Dalton, H.E., Foot, N. & Kumar, S. Regulation of functional diversity within the Nedd4 family by accessory and adaptor proteins. *Bioessays* **28**, 617–628 (2006).

ONLINE METHODS

Cells, viruses, antibodies and reagents. The 293 cells HeLa cells, HT1080 cells, L929 cells (mouse fibroblast cells), 2fTGH-ISRE (human fibrosarcoma cells expressing an interferon-stimulated responsive element), L929-ISRE cells, Vero cells and wild-type and *Itch*$^{-/-}$ MEFs were cultured in DMEM; U937 cells were cultured in RPMI-1640 medium supplemented with 10% (vol/vol) FBS, 5 μg/ml of penicillin and 10 μg/ml of streptomycin. VSV (Indiana strain) was propagated and amplified by infection of a monolayer of Vero cells. At 24 h after infection, the supernatant was collected and was clarified by centrifugation. Viral titers were determined by plaque assay on Vero cells. SeV was from C. Zheng and GFP-tagged NDV was from C. Wang. Poly(I:C) was from Amersham. Poly(dA-dT)·poly(dT-dA) was synthesized as 5′-d$(AT)_{30}$-3′ and was annealed by heating to 95 °C and cooling to 25 °C. Lipofectamine 2000 (Wisegen) was used for lipid transfection. For the generation of mouse polyclonal anti–human PCBP2, cDNA containing full-length PCBP2 was cloned into the vector pET30c (Novagen) and protein was purified from *Escherichia coli* by nickel-column chromatography. Recombinant protein was injected into mice to produce antiserum. Other antibodies used were as follows: anti-Flag (F3165), anti-HA (H9658) and anti-VSV (A5977; all from Sigma); anti-ubiquitin (sc-8017), anti-GAPDH (sc-25778), anti-IRF3 (sc-9082) and anti-AIP4 (sc-11890; all from Santa Cruz); anti-MAVS (sc-68881 (Santa Cruz) and 3993 (Cell Signaling)); antibody to phosphorylated p42/44 (9101), Jnk (9251) or p38 (9211; all from Cell Signaling); anti-ubiquitin (K48 specific (05-1307) and K63 specific (05-1308); both from Millipore); anti–COX IV (ab16056; Abcam); and anti–histone H3 (31560; Upstate). Polyclonal anti-Bcl-x_L was provided by Q. Chen.

Plasmids. After cDNA encoding human PCBP2, MAVS, RIG-I, Mda5, TBK1, IRF3, AIP4, Smurf1, NEDD4-1, WWP1 or STK38 was amplified from cDNA made from 293 or U937 cells, it was cloned into plasmid p3xFLAG-CMV-7.1 (Sigma), pCMV-3XHA or pcDNA3.1(+)-3′VSV (Invitrogen) to generate Flag-tagged, HA-tagged or VSV-tagged protein, respectively. Flag-tagged MAVS constructs VAMP-TM, Bcl-2–TM and Bcl-x_L–TM were provided by Z. Chen. HA-UB(K48) and HA-UB(K63) were provided by H. Shu.

Deleted, truncated and point mutants were generated by the QuickChange site-directed mutagenesis kits with PfuUltra as the polymerase (Stratagene) and the construct encoding wild-type protein as the template (**Supplementary Table 1**). Each mutation was confirmed by sequencing. For reporter assays, pISRE-Luc (Stratagene) and pNifty-Luc (Invivogen), an NF-κB-dependent E-selectin luciferase reporter plasmid, were used. Other promoters were cloned into pGL3-Basic vector (Promega) with the following promoter regions: −1 to −155 for mouse IFN-β, and −1 to −476 for mouse IFN-α4. All constructs were verified by sequencing.

Yeast two-hybrid screening. A 293 cell cDNA library was screened with full-length MAVS as bait, according to protocols recommended by the manufacturer (Clontech).

Luciferase reporter assay. These assays were done as described[37].

Restoration of AIP4 expression in *Itch*$^{-/-}$ MEFs. Human AIP4 cDNA was cloned into the vector pBabe-puro with a Flag tag to produce retrovirus encoding AIP4, with PLAT-E as the packaging cells. *Itch*$^{-/-}$ MEFs were infected for 48 h with retrovirus in the presence of polybrene (8 μg/ml) and were selected by puromycin (2 μg/ml). Cells resistant to puromycin were pooled together and expression of AIP4 was examined by immunoblot analysis with anti-Flag.

RT-PCR. Total RNA was extracted with TRIzol reagent (TianGen) and was reversed-transcribed with a Reverse Transcription system (Promega). Induction of type I interferon was analyzed by RT-PCR with 28–30 cycles of 94 °C for 30 s, 58 °C for 30 s and 72 °C for 40 s (primers, **Supplementary Table 2**).

Type I interferon bioassay and TNF bioassay. The activity of type I interferon and TNF was measured as described[38], with reference to recombinant human or mouse IFN-β (R&D Systems) as a standard with 2fTGH cells (for human assays) or L929 cells (for mouse assays; 1×10^5 cells per ml) stably transfected with an interferon-sensitive (ISRE) luciferase construct.

Cycloheximide chase assays. Cells were treated with cycloheximide (100 mg/ml) for various periods of time at 24 h after transfection, then were lysed and analyzed by immunoblot.

RNAi. Double-stranded oligonucleotides corresponding to the target sequences were cloned into the pSuper.Retro RNAi plasmid (Oligoengine). The sequences targeting human PCBP2 were 5′-ATACGAGAGAGTACAGGGG-3′ (1#) and 5′-GGACAGTATGCCATTCCAC-3′ (2#); the sequence targeting human AIP4 was 5′-CCAGTTGGACTCAAGGATTTA-3′ (ref. 39).

Fraction isolation. Nuclear fractions and mitochondrial membranes were purified as described[37]. Cells in hypotonic buffer (10 mM HEPES, pH 7.4, 10 mM KCl, 1.5 mM $MgCl_2$, 0.2 mM phenylmethylsulfonyl fluoride and 0.5 mM dithiothreitol) were homogenized on ice with 40 strokes, cell homogenates were centrifuged at 700*g* for 10 min at 4 °C to obtain the nuclear fractions, and the post-nuclear supernatant was centrifuged at 5,000*g* for 10 min to obtain the pellet (p5). Nuclear fractions and p5 pellets were resuspended in lysis buffer and analyzed by immunoblot.

Immunofluorescence microscopy. These experiments were done as described[37]. Cells were imaged with an Olympus BX51 microscope or a Leica TCS SP2 confocal system under a 100× oil objective.

Coimmunoprecipitation, immunoblot analysis and native PAGE. These procedures were done as described[37]. For endogenous coimmunoprecipitation, cells (2×10^7) were lysed in 1 ml lysis buffer and subsequent procedures were done as described[37].

***In vitro* ubiquitination assay.** Proteins were expressed *in vitro* with TNT Quick Coupled Transcription/Translation systems (Promega) and ubiquitination was assayed with a ubiquitination kit according to protocols recommended by the manufacturer (ENZO Life Sciences).

VSV plaque assay. First, 293 cells (~1×10^5) were transfected with plasmids for 24 h before VSV infection. Then, 1 h later, cells were washed with PBS and then fresh medium was added. Supernatants were collected and used to infect confluent BHK21 cells. Then, 1 h later, supernatants were removed and culture medium containing 2% (wt/vol) methylcellulose was overlaid for 60 h, cells were fixed for 30 min with 0.5% (vol/vol) glutaraldehyde and were stained with 1% (wt/vol) crystal violet dissolved in 70% ethanol. Plaques were counted and average counts were multiplied by the dilution factor to determine the viral titer as plaque-forming units per ml.

37. Sun, W. *et al.* ERIS, an endoplasmic reticulum IFN stimulator, activates innate immune signaling through dimerization. *Proc. Natl. Acad. Sci. USA* **106**, 8653–8658 (2009).
38. Jiang, Z. *et al.* CD14 is required for MyD88-independent LPS signaling. *Nat. Immunol.* **6**, 565–570 (2005).
39. Wegierski, T., Hill, K., Schaefer, M. & Walz, G. The HECT ubiquitin ligase AIP4 regulates the cell surface expression of select TRP channels. *EMBO J.* **25**, 5659–5669 (2006).